

High Permeability/High Diffusivity Mixed Matrix Membranes For Gas Separations

By

Sangil Kim

Dissertation submitted to the faculty of the Virginia Polytechnic Institute and State
University in partial fulfillment of the requirements for the degree of

Doctor of Philosophy

In

Chemical Engineering

Dr. Eva Marand, Chair

Dr. S. Ted Oyama

Dr. Richey M. Davis

Dr. Vadim V. Guliants

March 22, 2007

Blacksburg, VA

Keywords: Mixed Matrix Membrane, Carbon Nanotube, Mesoporous Silica, Poly(imide siloxane), Polysulfone, Gas Permeation, Gas Adsorption

Copyright 2007

High Permeability/High Diffusivity Mixed Matrix Membranes For Gas Separations

Sangil Kim
(Abstract)

The vast majority of commercial gas separation membrane systems are polymeric because of processing feasibility and cost. However, polymeric membranes designed for gas separations have been known to have a trade-off between permeability and selectivity as shown in Robeson's upper bound curves. The search for membrane materials that transcend Robeson's upper bound has been the critical issue in research focused on membranes for gas separation in the past decade. To that end, many researchers have explored the idea of mixed matrix membranes (MMMs). These membranes combine a polymer matrix with inorganic molecular sieves such as zeolites. The ideal filler material in MMMs should have excellent properties as a gas adsorbent or a molecular sieve, good dispersion properties in the polymer matrix of submicron thickness, and should form high quality interfaces with the polymer matrix.

In order to increase gas permeance and selectivity of polymeric membranes by fabricating MMMs, we have fabricated mixed matrix membranes using carbon nanotubes (CNTs) and nano-sized mesoporous silica. Mixed matrix membranes containing randomly oriented CNTs showed that addition of nanotubes to a polymer matrix could improve its selectivity properties as well as permeability by increasing diffusivity. Overall increases in permeance and diffusivity for all tested gases suggested that carbon nanotubes can provide high diffusivity tunnels in the CNT within the polymer matrix. This result agreed well with molecular simulation estimations. In order to prepare ordered CNTs membranes, we have developed a simple, fast, commercially attractive, and scalable orientation method. The oriented CNT membrane sample showed higher permeability by one order of magnitude than the value predicted by a Knudsen model. This CNT membrane showed higher selectivities for CO₂ over other gas molecules because of preferential interaction of CO₂ with the amine functionalized nanotubes, demonstrating practical applications in gas separations.

Recently, mesoporous molecular sieves have been used in MMMs to enhance permeability or selectivity. However, due to their micrometer scale in particle size, the composite membrane was extremely brittle and tended to crack at higher silica loading. In this study, we have developed fabrication techniques to prepare MMMs containing mesoporous MCM-41 nanoparticles on the order of ~50 nm in size. This smaller nanoparticle lead to higher polymer/particle interfacial area and provides opportunity to synthesize higher loading of molecular sieves in polymer matrix up to ~80 vol%. At 80 vol% of nano-sized MCM-41 silica loading, the permeability of the membrane increased dramatically by 300 %. Despite these increases in permeability, the separation factor of the MMMs changed only slightly. Therefore, these nanoscale molecular sieves are more suitable for commercialization of MMMs with very thin selective layers than are micro-sized zeolites or molecular sieves.

Acknowledgements

The education and success of an individual are influenced and supported by many persons including professional peers, friends, and family. Although it is impossible to list all persons that helped me thorough three years at Virginia Tech., I owe special thanks to several individuals that strongly influenced my graduate studies.

First, I would like to show my best gratitude to my adviser, Dr. Eva Marand for her guidance, suggestions and help throughout this study. Her willingness to help me and the support she provided made the completion of my studies. She always seemed to know what I was feeling, and she helped me understand not only the data, but also myself and my family.

Sincere appreciation and gratitude go to Dr. Ted Oyama and Dr. Richey Davis for their participation on my committee. I am very grateful to Dr. Vaidm Guliants, my former adviser, for useful advice in studying for mesoporous silica/PSF MMMs system, as well as his help in characterizing pore structure of my materials. My thanks also go to Dr. Junichi Ida for his idea for mesoporous silica/PSF MMMs.

I would like to thank Steve McCartney (SEM), and Dr. Joerg Jinscheck (HRTEM) for their efforts in training me and characterizing some of my materials.

I wish to offer my sincere gratitude to Dr. Karl Johnson and Dr. David Sholl for providing the atomistic simulation data and their helpful input concerning the result of this study.

Another important group to thank would be all of the group members. I would like to thank Todd Pechar for providing the copolymer used in this study. I thank Will

James, Ben Vaughan, and Jose Herrera-Alonso for being supportive lab mates and good friends.

I'd also like to thank all of my family and friends who have endured my conversations about research. Especially I would like to thank my wife, Dr. Hyang Seol for her helpful discussion and constant encouragement behind scenes.

Table of Contents

Abstract	ii
List of Figures	vi
List of Tables	viii
Chapter 1 Introduction	1
1.1 Problem Statement.....	1
1.2 Research Studies.....	2
1.3 Outline of Chapters.....	4
1.4 References.....	6
Chapter 2 Literature Review	7
2.1 Introduction.....	7
2.2 Polymeric Membrane for Gas Separation.....	8
2.3 Fundamental Transport Mechanism in Gas Separation Membrane.....	9
2.3.1 Porous Membrane.....	9
2.3.2 Nonporous (dense) Membrane.....	10
2.4 Fundamental Transport Parameters of Membrane.....	11
2.5 Gas Sorption.....	14
2.5.1 Gas Sorption in Rubbery Polymers.....	14
2.5.2 Gas Sorption in Glassy Polymers.....	16
2.5.3 Transient Sorption and Diffusivity.....	19
2.6 History of Gas Separation Membranes.....	21
2.7 Mixed Matrix Membrane.....	23
2.8 Carbon Nanotube.....	26
2.8.1 Structure of CNTs.....	26
2.8.2 Diffusion in CNTs.....	28
2.9 Ordered Mesoporous Silica.....	29
2.10 References.....	31
Chapter 3 Poly(imide siloxane) and CNT Mixed Matrix Membranes for Gas Separation	34
3.1 Introduction.....	34
3.2 Experimental and Characterization Method.....	36
3.2.1 6FDA-6FpDA-PDMS Copolymer.....	36
3.2.2 Preparation of CNTs.....	36
3.2.3 Fabrication 6FDA-6FpDA-PDMS Copolymer Membranes.....	38
3.2.4 Fabrication of Poly(imide siloxane)-CNT Mixed Matrix Membranes	38
3.2.5 Gas Permeation Measurement.....	40
3.3 Results and Discussion.....	40
3.4 Conclusion.....	49
3.5 References.....	50

Chapter 4	Polysulfone and Functionalized Carbon Nanotube Mixed Matrix Membranes for Gas Separation: Theory and Experiment	51
4.1	Introduction.....	51
4.2	Experimental and Characterization Method.....	54
4.2.1	Functionalization of Carbon Nanotubes.....	54
4.2.2	Fabrication of PSF membrane.....	55
4.2.3	Fabrication of Functionalized Carbon Nanotube-Polysulfone MMMs.....	56
4.2.2	Characterization.....	56
4.3	Molecular Simulation.....	58
4.4	Results and Discussion.....	59
4.5	Conclusions.....	81
4.6	References.....	83
Chapter 5	Carbon Nanotube/Polymer Nanocomposites for Large Surface Area Membrane Applications	88
5.1	Introduction.....	88
5.2	Experimental and Characterization Method.....	90
5.2.1	Purification and Functionalization of CNTs.....	90
5.2.2	CNT/Polymer Nanocomposite Membrane Fabrication.....	90
5.2.3	CNT/polymer Nanocomposite Sample Preparation for High- resolution TEM Experiments.....	91
5.2.4	Calculation of Knudsen Diffusion Flow.....	91
5.3	Results and Discussion.....	92
5.4	Conclusion.....	103
5.5	References.....	104
Chapter 6	Polysulfone and Mesoporous Molecular Sieve MCM-48 Mixed Matrix Membranes for Gas Separation	106
6.1	Introduction.....	106
6.2	Experimental and Characterization Method.....	108
6.2.1	Synthesis of MCM-48 Silica.....	108
6.2.2	Fabrication of PSF Membrane.....	108
6.2.3	Fabrication of MCM-48/PSF MMMs.....	109
6.2.4	Characterization.....	109
6.3	Results and Discussion.....	111
6.4	Conclusions.....	125
6.5	References.....	126
Chapter 7	Mesoporous Nanoparticles and Polymer Nano-composite Membranes: High Flux and High Permeability	128
7.1	Introduction.....	128

7.2	Experimental and Characterization Method.....	129
7.2.1	Synthesis and Functionalization of Nano-sized MCM-41.....	129
7.2.2	Fabrication of Membranes.....	130
7.2.3	Characterization.....	131
7.3	Results and Discussion.....	133
7.4	Conclusions.....	150
7.5	References.....	151
Chapter 8	Conclusions and Future Work.....	153

List of Figures

Chapter 1		
Figure 1-1	Trade off curve between selectivity and permeability for O ₂ /N ₂ mixtures.....	1
Chapter 2		
Figure 2-1	Schematic representation of membrane separation.....	7
Figure 2-2	Schematic representation of membrane-based gas separations.....	10
Figure 2-3	Schematic representation of the relationship between the polymer specific volume and temperature	18
Figure 2-4	Schematic representation of a dual-mode sorption analysis.....	18
Figure 2-5	(a) CO ₂ Sorption isotherm on mesoporous silica at 308 K, and (b) CO ₂ mass uptake curve of mesoporous silica at 398 K and 0.1 bar.....	20
Figure 2-6	Trade-off curve of O ₂ /N ₂ selectivity and O ₂ permeability.....	24
Figure 2-7	Predicted zeolite 4A-polysulfone MMM performance.....	25
Figure 2-8	The grapheme lattice vectors of CNT.....	28
Chapter 3		
Figure 3-1	Synthesis of 6FDA-6FpDA-PDMS.....	37
Figure 3-2	Schematic of the system used to perform permeation experiments.....	39
Figure 3-3	FESEM images of CNTs (a) before (b) after purification, and (c) cut CNTs.....	42
Figure 3-4	FESEM cross-sectional images of MMMs (a) 2 wt% CNTs (arrows indicated CNTs in copolymer matrix) ,(b) and (c) 10 wt% CNTs.....	43
Chapter 4		
Figure 4-1	FT-IR spectrum of SWNTs samples. (a) carboxylated, and (b) ODA-functionalized.....	60
Figure 4-2	Cross-sectional FESEM images of 10 wt % unmodified SWNT/PSF MMMs.....	62
Figure 4-3	Cross-sectional FESEM images of 10 wt % functionalized SWNT/PSF MMMs.....	63
Figure 4-4	FESEM images of 15 wt % functionalized SWNT/PSF MMMs XRD pattern of MCM-48 silica.....	64
Figure 4-5	DMTA results for pure polysulfone and functionalized SWNT/PSF MMMs.....	67
Figure 4-6	Adsorption isotherms for various gases from experiments, (a) and (b), and from simulations.....	69
Figure 4-7	Comparison of closed and open nanotubes for adsorption of CO ₂ at 308 K.....	71
Figure 4-8	Adsorption isotherms on 0 wt%, 2.5 wt%, 5 wt%, 10 wt% functionalized SWNT/PSF MMMs, and SWNT.....	73
Figure 4-9	CO ₂ kinetic uptake curves curves in SWNT/PSF MMMs at 308 K and 0.1 bar.....	77
Figure 4-10	CO ₂ diffusion coefficients in SWNT/PSF MMMs at 308 K.....	77

Figure 4-11	Solubility coefficients of SWNT/PSF MMMs at 308 K and 4 bar.....	79
Chapter 5		
Figure 5-1	SWNT pore structure.....	93
Figure 5-2	CNT nanocomposite membrane process.....	95
Figure 5-3	HRTEM images in plan-view orientation of CNTs in a polymer matrix..	97
Figure 5-4	Effect of the pressure drop on the permeance of helium through CNTs/PSF membrane.....	99
Figure 5-5	Single gas transport properties of CNT nanocomposite membrane.....	100
Figure 5-6	Gas transport properties of CNT nanocomposite membrane.....	101
Figure 5-7	Mixed gas selectivity (CO ₂ /CH ₄) of CNTs/PSF membrane.....	102
Chapter 6		
Figure 6-1	XRD pattern of MCM-48 silica.....	111
Figure 6-2	The N ₂ adsorption-desorption isotherms of MCM-48 silica at 77 K.....	112
Figure 6-3	FESEM images of MCM-48 at (a) lower and (b) higher magnification...	113
Figure 6-4	Cross-sectional FESEM images of 10 wt % as-synthesized MCM-48/PSF MMMs	114
Figure 6-5	Cross-sectional FESEM images of 10 wt % calcined MCM-48/PSF MMMs	116
Figure 6-6	FESEM images of 20 wt % calcined MCM-48/PSF MMMs.....	117
Figure 6-7	Simple illustration for (a) discontinuous pathway through MCM-48 (10 wt % of MCM-48 loading), and (b) continuous pathway through MCM-48 (20 wt % of MCM-48 loading).....	120
Figure 6-8	Gas adsorption isotherms for (a) PSF, (b) MCM-48 silica, and (c) 20 wt % MCM-48/PSF MMMs for N ₂	124
Chapter 7		
Figure 7-1	XRD pattern of MCM-41 silica.....	133
Figure 7-2	The N ₂ adsorption-desorption isotherms of MCM-48 silica at 77 K.....	135
Figure 7-3	TEM images of MCM-41 silica.....	135
Figure 7-4	FESEM images of (a) unmodified MCM-41/PSF and (b) modified MCM-41/PSF	137
Figure 7-5	Cross-sectional FESEM images of 80 vol % functionalized MCM-41/PSF MMMs.....	139
Figure 7-6	Gas adsorption isotherms for (a) N ₂ and (b) CO ₂ on MMMs and additive model for 80 vol% MCM41.....	143
Figure 7-7	Solubility coefficient of 0 wt%, 60 vol%, and 80 vol% MCM41/PSF MMMs at 308 K and 4 bar.....	145
Figure 7-8	CO ₂ kinetic uptake curves curves in 0 wt%, 60 vol%, and 80 vol% MCM41/PSF MMMs at 308 K and 0.1 bar.....	147
Figure 7-9	CO ₂ diffusion coefficients in 0 wt%, 60 vol%, and 80 vol% MCM41/PSF MMMs at 308 K and 0.1 bar.....	149

List of Tables

Chapter 3

Table 3-1	Kinetic diameter of various gases.....	44
Table 3-2	Gas permeabilities of the pure PDMS poly(imide siloxane) and close-ended CNT MMMs	45
Table 3-3	Diffusivity and solubility (N ₂) of the pure PDMS poly(imide siloxane) and close-ended CNT MMM.....	45
Table 3-4	Gas permeabilities (Barrer) of various gases in the pure PDMS poly(imide siloxane) and CNT MMMs.....	47
Table 3-5	Diffusivity (10 ⁻⁸ , cm ² /sec) of various gases in the pure PDMS poly(imide siloxane) and CNT MMMs.....	47
Table 3-6	Solubility (cm ³ @ STP cm ⁻³ _{polymer} atm) of various gases in the pure PDMS poly(imide siloxane) and CNT MMMs.....	48

Chapter 4

Table 4-1	Pore properties of SWNTs.....	55
Table 4-2	Gas permeabilities (Barrer) of various gases in the pure polysulfone and functionalized SWNT MMMs.....	75
Table 4-3	Diffusivity (10 ⁻⁸ , cm ² /sec) of various gases in the pure polysulfone and SWNT MMMs.....	75
Table 4-4	Selectivity for polysulfone and functionalized SWNT MMMs.....	80

Chapter 6

Table 6-1	Gas permeabilities of the pure polysulfone and as-synthesized MCM-48 MMMs.....	114
Table 6-2	Gas permeabilities (Barrer) of various gases in the pure polysulfone and MCM-48 MMMs.....	118
Table 6-3	Selectivity for polysulfone and MCM-48 MMMs.....	119
Table 6-4	Diffusivity (D) and solubility (S) of various gases in the pure polysulfone and MCM-48 MMMs.....	121

Chapter 7

Table 7-1	Gas permeabilities (Barrer) of various gases in the pure polysulfone and MCM-41 MMMs.....	141
Table 7-2	Selectivity for polysulfone and MCM-41 MMMs.....	141

Chapter 1. Introduction

1.1. Problem Statement

Membrane gas separation is a dynamic and rapidly growing field due to the high selectivity and fluxes achievable by membranes, low energy requirements, and simple, easy to operate modules. As a result, membranes have the potential of acquiring a significant industrial role in the gas separation area, particularly if they can compete economically with traditional separation methods such as cryogenic distillation and pressure-swing absorption. Since hydrogen-separating membranes have been launched in 1980, membrane based gas separation has grown into a \$150 million/year industry and the future membrane market has been anticipated to reach \$ 760 million/year by 2020.¹ The vast majority of commercial membrane systems are polymeric because of processing feasibility and cost.^{2,3} However, polymeric membranes designed for gas separations have been known to have a trade-off between permeability and selectivity as shown in Robeson's upper bound curves.⁴ In 1991, Robeson analyzed all available permeation data for polymeric membranes, and plotted each membrane's permeability against selectivity

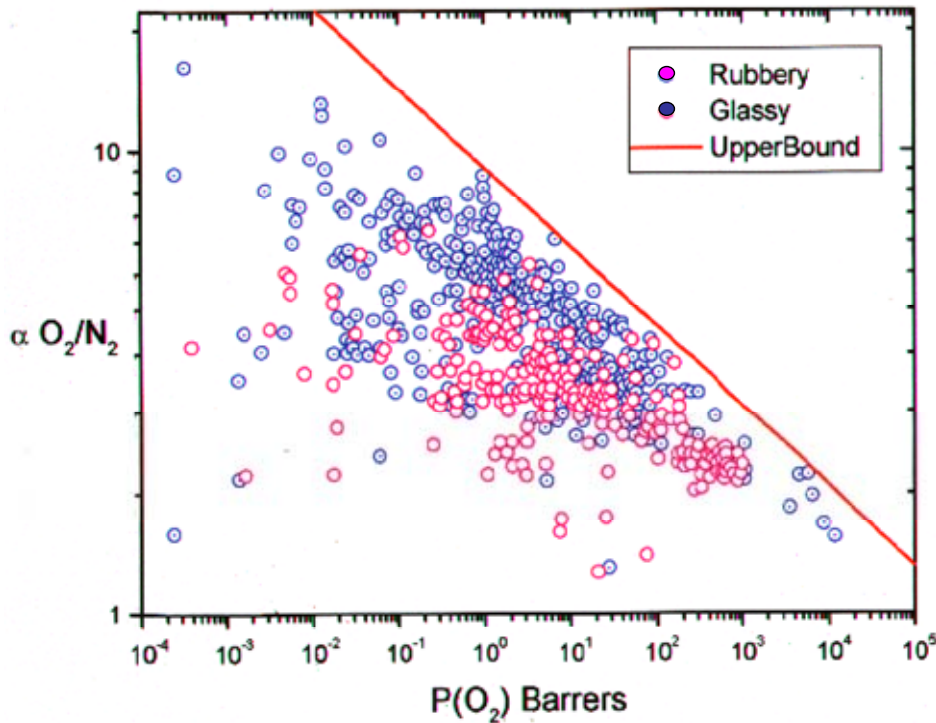


Figure 1-1. Trade off curve between selectivity and permeability for O₂/N₂ mixtures.

on a log-log scale. The plot revealed that there is an upper bound for selectivity, such that the selectivity decreases linearly with increasing permeability. In Figure 1-1 (taken from Reference 4), the trade-off of permeability of O₂ versus O₂/N₂ selectivity is shown for air separation. Since then, the search for polymeric membrane materials that transcend Robeson's upper bound has been the critical issue in membrane research for gas separation.^{5,6} Many research efforts have been aimed at modifying the backbone and side-chain of polymers experimentally in order to make stiffer and more open structures that could surpass the permeability-selectivity tradeoff.^{2,7} This has been difficult to achieve and in fact, as shown by Freeman, theoretically improbable.⁵ Thus, the application of polymeric materials as membranes remains with technical limitations. Therefore, there is a critical need for new membrane materials that have fundamentally different properties from polymeric membrane materials. Many efforts have focused on mixed matrix membranes (MMMs) to develop new membranes. These membranes combine polymers with inorganic molecular sieves such as zeolites or carbon molecular sieves.⁸⁻¹² However, commercialization of this approach has been interrupted by poor adhesion between zeolite and polymer as well as inadequate particle dispersion causing losses in selectivity.⁹ Therefore, the ideal filler materials in MMMs should have excellent properties as gas adsorbents or a molecular sieves, good dispersion properties in a polymer matrix of submicron thickness, and should form high quality interfaces with the polymer matrix.

The addition of inorganic fillers such as carbon nanotubes (CNTs) or nano-sized mesoporous silica into polymers appears to offer a unique solution to the deficiencies of conventional polymeric membrane systems. This is the primary motivation of this research. These MMM membranes can be utilized as a separation system for small molecules. For example, separation of hydrogen from contaminants such as CO and CO₂ is critical in coal gasification, water-gas-shift reactions, and in providing high-purity hydrogen for use in fuel cells. The focus of this research is to establish these oriented CNTs and nano-sized mesoporous silica/MMMs as a new viable technology for separating small molecules from gas mixtures.

1.2. Research Studies

A summary of the various research efforts encompassing this thesis is presented below.

1. **CNTs/poly(imide)-siloxane copolymer mixed matrix membranes** – The fabrication and characterization of randomly mixed CNTs/poly(imide)-siloxane copolymer MMMs is studied. The goals of this investigation are to determine if the copolymer has good compatibility with CNTs, to determine if defect free MMMs can be fabricated using these two components, and to determine the permeation properties of the prepared CNT/copolymer MMMs.
2. **Functionalized CNTs/polysulfone mixed matrix membranes** - The fabrication and characterization of randomly mixed functionalized CNTs/polysulfone MMMs is studied. The goals of this investigation are to determine if the functionalized CNTs are well dispersed throughout polymer matrix without agglomeration, and to determine the permeation properties of the functionalized CNTs/polysulfone MMMs.
3. **Vertically aligned CNTs/polymer nanocomposite membranes** - The fabrication and characterization of vertically aligned CNTs contained by a polymer matrix is investigated. This study presents a simple, fast, and practical route to vertically align CNTs membrane using filtration methods. The gas permeation properties of the aligned CNTs membrane are studied using single- and mixed-gas systems.
4. **Mesoporous MCM-48 silica/polysulfone mixed matrix membranes** – The fabrication and characterization of a mesoporous MCM-48 silica and polysulfone is studied. This investigation looks at developing MMMs without the need for any modification of the inorganic particles. The permeation properties of the MMMs are studied as function of wt % of mesoporous silica in the polymer matrix.
5. **Nanosized mesoporous MCM-41 silica/polysulfone mixed matrix membranes** - The fabrication and characterization of a mesoporous MCM-41 silica, particle size ~50 nm and polysulfone is studied. The purpose of this investigation is to determine the feasibility of fabricating MMMs containing higher loading of mesoporous silica.

1.3. Outline of Chapters

Chapter 2 is devoted to literature review for gas separation membranes. The first part of the literature review focuses on the fundamental gas transport mechanism and parameters describing the performance of gas separation membranes. The second part reviews history of gas separation membrane and mixed matrix membranes. Finally, a brief section on inorganic fillers employed in this research (carbon nanotubes and mesoporous silica) and their properties is included.

Chapter 3 describes the nano-composite membranes consisting of single-walled carbon nanotubes embedded in a poly(imide siloxane) copolymer and evaluates their transport properties. We designed poly(imide siloxane) copolymer because the siloxane segment can provide good wetting properties with nanotubes while the polyimide component can impart mechanical integrity. A poly(imide siloxane) was synthesized using an aromatic dianhydride, an aromatic diamine and amine-terminated PDMS for the siloxane block. The weight percent of PDMS was determined to be 41 using $^1\text{H-NMR}$. Permeability measurements of helium showed drops in permeability with the addition on close-ended CNTs. This large drop in permeability of helium suggests that the copolymer adhered well to the CNTs and that the prepared CNT MMMs were defect free. However, the permeability of O_2 , N_2 and CH_4 increased in proportion to the amount of open-ended CNTs in the polymer matrix. The results suggested that CNTs can be an attractive additive for universally enhancing the gas permeabilities of polymers.

Chapter 4 describes novel nano-composite membranes containing single walled carbon nanotubes inside a commercial polymeric membrane material, polysulfone. The carbon nanotubes were functionalized with long chain alkyl amines to facilitate dispersion in the polymer solution. Both permeabilities and diffusivities of the membranes increased with increasing weight fraction of carbon nanotubes at 4 atm. Experimental sorption isotherms of H_2 , O_2 , CH_4 and CO_2 were consistent with isotherms predicted by atomistic simulations conducted by Prof. Karl Johnson at University of Pittsburgh. Overall increases in permeance and diffusivity for all tested gases suggested that carbon nanotubes can provide high diffusivity tunnels in the SWNTs within the PSF matrix.

Chapter 5 presents a simple, fast, and practical route to vertically align carbon nanotubes on a porous support using a combination of self-assembly and filtration methods. The advantage of this approach is that it can be easily scaled up to large surface areas, allowing for fabrication of membranes for practical gas separation applications. The gas transport properties of the constructed carbon nanotube/polymer nanocomposite membranes are analogous to those of carbon nanotube membranes grown by chemical vapor deposition. As a result of functionalization, the high gas permeation rates through the carbon nanotubes are coupled with a “gatekeeper” mechanism which leads to an enhancement of selectivity observed when separating gas mixtures.

Chapter 6 describes mesoporous MCM-48 silica and polysulfone (PSF) mixed matrix membranes. Helium permeation data and SEM images of as-synthesized MCM-48/PSF MMMs suggest that MCM-48 silica particles adhered well to the PSF matrix and the MMMs were defect free. Gas permeation tests indicated that the increase in permeability resulted from an increase in solubility as well as diffusivity. The increase in transport properties for all gases tested makes mesoporous MCM-48 silica an attractive additive for enhancing the gas permeability of MMMs without sacrificing selectivity.

Chapter 7 describes MMMs containing mesoporous MCM-41 nanoparticles with particle size around 50 nm. These smaller nanoparticles lead to a higher polymer/particle interfacial area and provide opportunity to synthesize composites containing up to 80 vol% of molecular sieve loading in the polymer matrix. We show that 80 vol% of nano-sized MCM-41 silica loading in the polymer matrix increases gas permeability of the membranes by 300 %. Despite these increases in permeability, the separation factor of the MMMs remains really constant. Therefore, these nanoscale molecular sieves are more suitable for commercialization of MMMs with very thin selective layers than micro-sized zeolite or molecular sieves.

Finally, **Chapter 8** discusses future work based on the conclusions reached from our research efforts.

1.4. References

- [1] R. W. Baker, Future directions of membrane gas separation technology, *Ind. Eng. Chem. Res.*, 41 (2002) 1393.
- [2] W. J. Koros and G. K. Fleming, Membrane-based gas separation *J. Membr. Sci.*, 83 (1993) 1.
- [3] K. Ghosal and B. D. Freeman, Gas separation using polymer membranes: an overview, *Polymers for advanced technologies*, 5 (1994) 673.
- [4] L. M. Robeson, Correlation of separation factor versus permeability for polymeric membranes, *J. Membr. Sci.*, 62 (1991) 165.
- [5] B. D. Freeman, Basis of permeability/selectivity tradeoff relations in polymeric gas separation membranes, *Macromolecules*, 32 (1999) 375
- [6] T. C. Merkel, B. D. Freeman, R. J. Spontak, Z. He, I. Pinnau, P. Meakin and A. J. Hill, Ultrapermeable, Reverse-selective nanocomposite membranes, *Science*, 296 (2002) 519.
- [7] S. A. Stern, Polymers for gas separations: The next decade, *J. Membr. Sci.*, 94 (1994) 1.
- [8] R. Mahajan and W. J. Koros, Factors controlling successful formation of mixed-matrix gas separation materials, *Ind. Eng. Chem. Res.*, 39 (2000) 2692
- [9] R. Mahajan and W. J. Koros, Mixed matrix membrane materials with glassy polymers. Part 1, *Polym. Eng. Sci.*, 42 (2002) 1420
- [10] R. Mahajan and W. J. Koros, Mixed matrix membrane materials with glassy polymers. Part 2, *Polym. Eng. Sci.*, 42 (2002) 1432
- [11] D. Q. Vu, W. J. Koros and S. J. Miller, High pressure CO₂/CH₄ separation using carbon molecular sieve hollow fiber membranes, *Ind. Eng. Chem. Res.*, 41 (2002) 367.
- [12] K. M. Steel and W. J. Koros, Investigation of porosity of carbon materials and related effects on gas separation properties, *Carbon*, 41 (2003) 253.

Chapter 2. Literature Review

2.1. Introduction

A membrane can be defined as a selective barrier between two phases, the “selective” being inherent to a membrane or a membrane processes. The membrane gas separation technology is over 15 years old and is proving to be one of the most significant unit operations. The technology inherits certain advantages over other methods. These advantages include compactness and light weight, low labor intensity, modular design that allows for easy expansion or operation at partial capacity, low maintenance, low energy requirements, low cost, and environmentally friendly operations.¹ A schematic representation of a simple gas separation membrane process is shown in Figure 2-1. A pressurized feed stream containing A and B comes in contact with the membrane surface. The membrane helps to produce a permeate containing pure A and a retentate containing pure B.

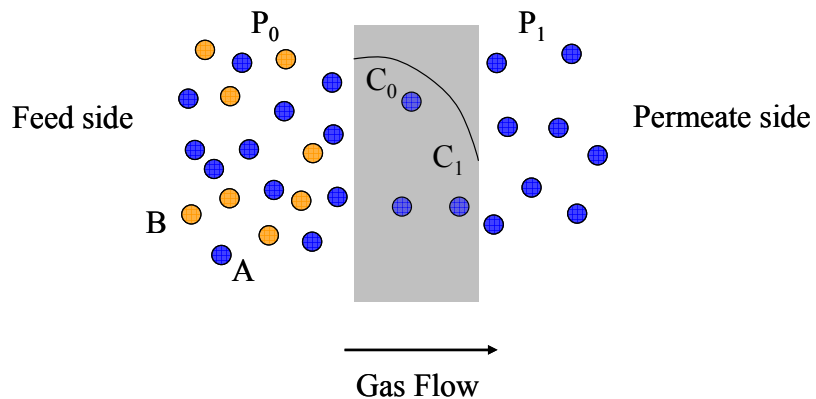


Figure 2-1. Schematic representation of membrane separation

Today, membrane processes are used in a wide range of applications and the number of such applications is still growing. From an economic point of view, the present time is

intermediate between the development of first generation membrane processes such as microfiltration (MF), ultrafiltration (UF), nanofiltration (NF), reverse osmosis (RO), electrodialysis (ED), membrane electrolysis (ME), diffusion dialysis (DD), and dialysis and second generation membrane processes such as gas separation (GS), vapour permeation (VP), pervaporation (PV), membrane distillation (MD), membrane contactors (MC) and carrier mediated processes.²

The permeation of gas molecules through polymers and the gas separation ability of polymers were observed and described over a century ago. In 1866, Thomas Graham demonstrated gas separation processes by showing that air can be enriched in O₂ by permeation through natural rubber polymeric membranes. He suggested that permeation of a penetrant molecule through a polymer membrane proceeded by the solution of the gas in the upstream surface of the membrane, diffusion across the membrane, and then the evaporation from the downstream membrane surface. Membrane materials currently used in gas separation application are understood to permeate and separate small molecules based on this mechanism.³

2.2. Polymeric Membranes for Gas Separation

The polymeric membranes used for gas separation can be classified into two classes based on flux density and selectivity: porous and non-porous.

A porous membrane has highly voided structure with randomly distributed interconnected pores through out the polymer matrix. The gas separation process in porous membranes is mainly a function of the permeate and polymer membrane properties such as the permeate molecular size, pore size and pore-size distribution of polymer. Porous

membranes used for gas separation can exhibit high fluxes but still provide low selectivity.⁴

Nonporous membranes have been mainly used in gas separation. This type of membrane provides high selectivity or separation of gases from gas mixtures but the permeate flux is usually low. An important property of a nonporous membrane is that even gases of similar size may be separated if their solubility in the polymer differs significantly.^{2,4}

2.3. Fundamental Transport Mechanism in Gas Separation Membrane

For gas separation, the selectivity and permeability of the membrane determines the efficiency of the gas separation process and porosity is an important characteristic of such membranes. Various mechanisms including Knudsen diffusion, surface diffusion, capillary condensation, molecular sieving diffusion, and solution-diffusion mechanism for gas transport thorough membranes have been proposed as shown in Figure 2-2.⁴

2.3.1. Porous Membrane

In Knudsen diffusion (Figure 2-2a), the pore size forces the penetrant molecules to collide more frequently with the pore wall than with other penetrant species.⁵ Except for some special applications as membrane reactors, Knudsen-selective membranes are not commercially attractive because of their low selectivities.⁶ In surface diffusion mechanism (Figure 2-2b), the penetrant molecules adsorb on the surface of the pores and subsequently move from one site to another of lower concentration.⁷ Capillary condensation (Figure 2-2c) occurs when the pore size and the interactions of the penetrant with the pore walls induce penetrant condensation in the pore, thus influencing

the rate of diffusion across the membrane.⁸ Molecular-sieve membranes in Figure 2-2d have received increasing attention recently because they may offer higher productivities and selectivities than solution-diffusion membranes. Molecular sieving membranes are an alternative to polymeric membranes. They have ultramicroporous ($< 7 \text{ \AA}$) with sufficiently small pores to exclude some molecules, while allowing others to pass through. Although they have extremely attractive permeation performance, chemical and thermal stability, these membranes are still difficult to process, are fragile, and are expensive to fabricate.⁹

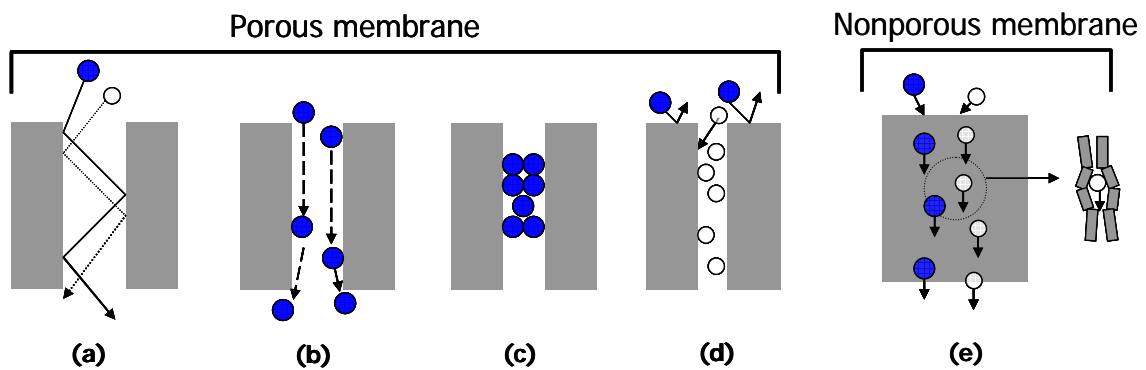


Figure 2-2. Schematic representation of membrane-based gas separations. (a) Knudsen-flow separation, (b) surface-diffusion, (c) capillary condensation, (d) molecular-sieving separation, and (e) solution-diffusion mechanism.

2.3.2. Nonporous (dense) Membrane

The mechanism for gas separation by non-porous membranes is different from that of porous membranes. The transport of gases through a nonporous polymeric membranes is usually described by a solution–diffusion mechanism (Figure 2-2e). The most current commercial polymeric membranes operate according to the solution–diffusion mechanism. The solution–diffusion mechanism is considered to consist of three steps: (1)

the absorption or adsorption at the upstream boundary, (2) activated diffusion through the membrane, and (3) desorption or evaporation on the other side. This solution–diffusion mechanism is driven by a difference in the thermodynamic activities existing at the upstream and downstream faces of the membrane as well as the intermolecular forces acting between the permeating molecules and those making up the membrane material. The concentration gradient leads to diffusion in the direction of decreasing activity. Differences in the permeability in dense membranes are caused not only by diffusivity differences of the various gas species but also by differences in the physicochemical interactions of the gas species within the polymer. The solution–diffusion model assumes that the pressure within a membrane is uniform and that the chemical potential gradient across the membrane is expressed only as a concentration gradient. Because this mechanism controls permeation in polymeric membranes for gas separations, it will be further discussed in the following section.

2.4. Fundamental Transport Parameters of Membrane

A schematic diagram of a gas transport through a membrane is shown in Figure 2-1.

The permeability of a pure gas A (P_A) across a membrane is defined by

$$P_A = \frac{N_A}{(p_0 - p_1)/l} \quad (2-1)$$

where,

p_0 = the pressure at the feed side

p_1 = the pressure at the permeate side

N_A = the steady state gas flux

L = membrane thickness

If a pressure gradient is applied across a membrane in the x direction (Figure 2.1), the one-dimensional flux of gas A through the membrane in the x direction (N_A) at steady state is given by

$$N_A = -\frac{D}{(1-w_A)} \frac{dC}{dx} \quad (2-2)$$

where,

C = the component A concentration

D = the gas diffusivity

dC/dx = the gas concentration in the polymer

w_A = the weight fraction of A in the system

Combining Equations (2-1) and (2-2), then gives

$$P = \frac{D}{1-w_A} \frac{1}{(p_0 - p_1)/l} \frac{dC}{dx} \quad (2-3)$$

Integrating both sides of Equation from $x = 0$ ($C = C_0$) to $x = l$ ($C = C_1$),

$$P = -\frac{1}{(p_0 - p_1)} \int_{C_1}^{C_0} \frac{D}{1-w_A} dC = [D] \frac{C_0 - C_1}{p_0 - p_1} \quad (2-4)$$

where, $[D]$ is a concentration averaged diffusivity defined as follows

$$[D] = \frac{1}{(C_0 - C_1)} \int_{C_1}^{C_0} \frac{D}{1-w_A} dC \quad (2-5)$$

When the pressure at permeate side is low, the permeability can be expressed by

$$P = [D][S] \quad (2-6)$$

where $[S] = C_0/P_0$ is the secant slope of the sorption isotherm, which is called the apparent solubility coefficient. Therefore, the gas permeability can be expressed as a product of $[D]$, a kinetic parameter, and $[S]$, a thermodynamic parameter.

For a binary gas mixture, the separation factor for component A relative to component B, α_{AB}^* , is defined by

$$\alpha_{AB}^* = \frac{y_A/(1-y_A)}{x_A/(1-x_A)} = \frac{y_A/y_B}{x_A/x_B} \quad (2-7)$$

where x_i and y_i refer to the mole fraction of component i in the gas phase at the feed side and permeate side, respectively. For a binary gas mixture, the composition of gas can be expressed with the gas flux as follows:

$$y_A = \frac{N_A}{N_A + N_B} \quad (2-8a)$$

and

$$y_B = \frac{N_B}{N_A + N_B} \quad (2-8b)$$

Then, Equation (2-7) can be written as

$$\alpha_{AB}^* = \frac{N_A/N_B}{x_A/x_B} \quad (2-9)$$

Using equation (2-1) and (2-9), following expression can be obtained.

$$\alpha_{AB}^* = \left(\frac{P_A}{P_B} \right) \left(\frac{\Delta p_A/x_A}{\Delta p_B/x_B} \right) \quad (2-10)$$

where P_i is the permeability of pure component i , and Δp_i is the partial pressure differences of component i . When the downstream pressure is negligible relative to the upstream pressure, the separation factor can be expressed as the term of permeabilities.

$$\alpha_{AB} \equiv \frac{P_A}{P_B} \quad (2-11)$$

where α_{AB} is the ideal selectivity. In typical separation applications, the downstream pressure is not negligible. However, the ideal selectivity has been used for providing a useful idea for assessing the relative ability of various polymers to separate gas mixtures.³

Factoring the permeability into the diffusivity and solubility terms, the ideal selectivity can be expressed in terms of the diffusivity selectivity and the solubility selectivity:

$$\alpha_{AB}^* = \left[\frac{D_A}{D_B} \right] \left[\frac{S_A}{S_B} \right] \quad (2-12)$$

Gas solubility depends on operating the conditions (i.e. temperature, pressure and composition), penetrant condensability, polymer-penetrant interactions, and polymer morphology. Gas diffusivity depends on the ability of small gas molecules to undergo diffusive jumps, which occur when thermally driven, random, cooperative polymer segmental dynamics from transient gaps, large enough to accommodate penetrants, in the immediate vicinity of the gas molecules. Like solubility, diffusivity depends on the membrane operating conditions. Moreover, gas diffusivity is also sensitive to properties such as penetrant size, polymer morphology and polymer segmental motions.³

2.5. Gas Sorption

2.5.1. Gas Sorption in Rubbery Polymers.

For polymers above their glass transition temperature (T_g), the permeation behavior is relatively simple phenomenologically. Henry's law is generally assumed to apply to describe the solubility of the gas in the rubbery polymers:

$$C = k_D p \quad (2-13)$$

where C is the concentration of gas in the polymer in cc(STP)/cc_{polymer}, k_D is the Henry's solubility constant for the particular polymer-gas pair in cc(STP)/(cc_{polymer} cmHg), and p is the gas penetrant pressure.

Gas diffusion through rubbery polymers normally is described by Fick's first law:

$$Q = -D \left(\frac{dC}{dx} \right) \quad (2-14)$$

where, Q = the permeation flux

D = the diffusion coefficient

C = the concentration of gas in the membrane

x = the coordinate direction of permeation in the membrane

At steady-state condition (constant Q) for a constant diffusivity, above equation can be integrated from the feed side (x_0 and C_0) to the permeate side (x_1 and C_1),

$$Q = -D \frac{[C_0 - C_1]}{[x_0 - x_1]} \quad (2-15a)$$

or

$$Q = D \frac{[C_0 - C_1]}{l} \quad (2-15b)$$

where l is the membrane thickness. Substituting Equation (2-13) into Equation (2-15b) gives

$$Q = k_D D \frac{(p_0 - p_1)}{l} = P \frac{(p_0 - p_1)}{l} \quad (2-16)$$

where p_0 and p_1 are the partial pressure of the gas on the feed and permeate side. Therefore, the permeability in rubbery polymers can be expressed by

$$P = D \cdot S \quad (2-17)$$

2.5.2. Gas Sorption in Glassy Polymers.

Rubbery polymers are in a hypothetical thermodynamic equilibrium state and their gas solubility follows Henry's law. On the other hand, glassy polymers are typically assumed to be in a non-equilibrium state which is closely related to the existence of non-equilibrium excess volume.^{3,10-12} As shown in Figure 2-3, a glassy polymer exhibits a specific volume, V_g , which is greater than the specific volume of an equivalent hypothetical rubber, V_l , obtained by extrapolating the specific volume data above glass transition temperature, T_g . This non-equilibrium excess free volume results from the inability of the polymer chains to undergo conformation rearrangement sufficiently to attain equilibrium once the temperature is below T_g .

A gas sorption isotherm in a glassy polymer generally exhibits nonlinear pressure dependence. This behavior is characteristic for dual-mode sorption composed of Henry's law sorption in an equilibrium region and Langmuir-type sorption in a non-equilibrium region. Henry's law sorption is related to dissolution of gases into dense equilibrium structure of the rubbery polymers. The Langmuir sorption site in a glassy polymer corresponds to holes or "microvoids" which arise from the non-equilibrium nature of glassy polymers. The dual-mode sorption model is expressed by:

$$C = C_D + C_H = k_D p + \frac{C'_H b p}{1 + b p} \quad (2-18)$$

where C is the total gas concentration in a glassy polymer, C_D is the gas concentration based on Henry's law sorption, C_H is the gas concentration based on Langmuir sorption, k_D is the Henry's law coefficient, b and C'_H are the Langmuir hole affinity parameter and the capacity parameter, respectively. The k_D parameter represents the penetrant dissolved in the polymer matrix at equilibrium and b characterizes the sorption affinity for a particular gas-polymer system. C'_H is often used to measure the amount of the non-equilibrium excess free volume in the glassy state. The Langmuir sorption capacity has been related to the unrelaxed non-equilibrium volume in the glassy polymer as given by:

$$C'_H = \left[\frac{V_g - V_l}{V_g} \right] \rho^* \quad (2-19)$$

where, as before, V_g and V_l are the polymer specific volumes in the glassy and hypothetical rubbery polymers, and ρ^* is the molar density of the condensed penetrant. Figure 2-4 shows schematic representation of a dual-mode sorption analysis with Henry's law and Langmuir sorption.

The solubility of a gas molecule in glassy polymers can be expressed by the dual-mode sorption parameters:

$$S \equiv \frac{C}{p} = S_D + S_H = k_D + \frac{C'_H p}{1 + bp} \quad (2-20)$$

where S is the solubility of penetrant, S_D and S_H are solubility values based on Henry's law and Langmuir-type sorption, respectively. In general, gas solubility in glassy polymers is higher than that in rubbery polymers. As previously mentioned, glassy polymers have non-equilibrium excess free volume; therefore, higher gas solubility can be attributed directly to the existence of this additional free volume into which sorption can occur.¹⁰

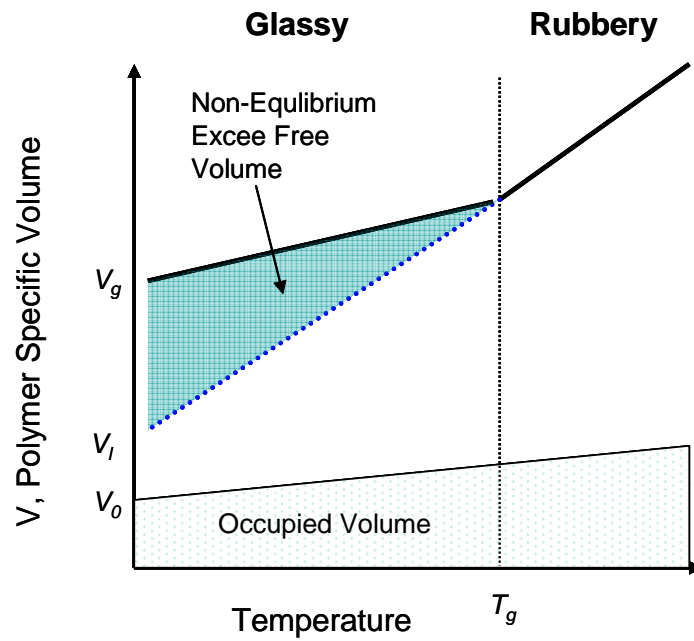


Figure 2-3. Schematic representation of the relationship between the polymer specific volume and temperature

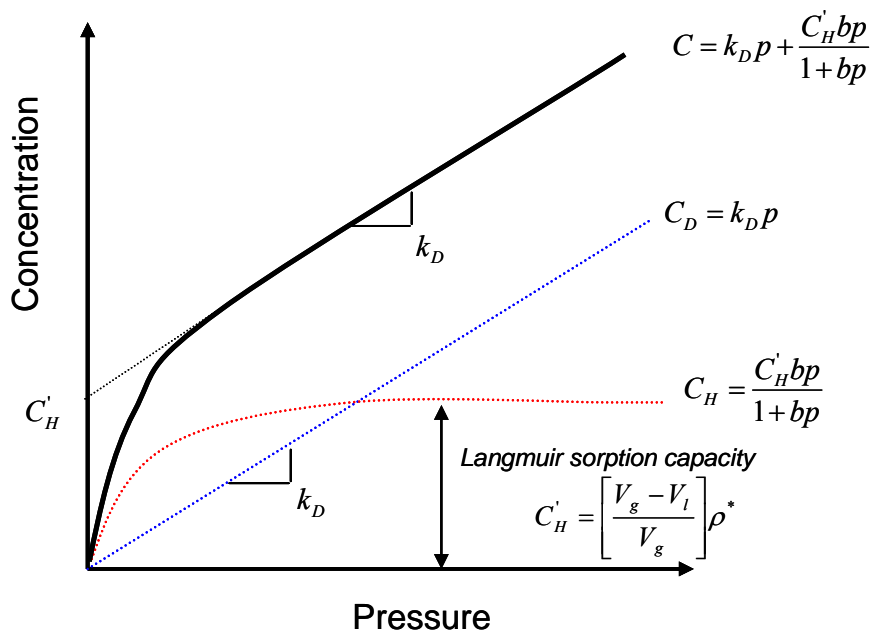


Figure 2-4. Schematic representation of a dual-mode sorption analysis

2.5.3. Transient Sorption and Diffusivity

Stand-alone inorganic molecular sieves, such as carbon molecular sieves, meant for incorporation in MMMs are likely to be difficult or impossible to characterize with steady-state permeation methods because they are too brittle to be formed into thin membrane films.¹³ Similarly, rigid polymers with attractive transport properties often lack sufficient molecular weight and flexibility required to form durable and dense films. Therefore, a method for characterizing gas transport properties in these brittle media is needed to evaluate their potential for incorporation in a highly selective MMMs.¹³ Transient (gravimetric) sorption method using a microbalance or quartz spring is an alternative to steady-state permeation measurement enabling direct determination of a diffusion and solubility coefficient.

In this method, the sample geometry dose not matter. The sample sits in a closed and fixed volume holder. The volume is evacuated for a certain period time to remove already absorbed gas molecules in the sample. The sample chamber is pressurized to a certain pressure (concentration) and monitored until equilibrium is reached. From the sorption experiments (Figure 2-5a) and data-fitting of the the mass uptake curves (Figure 2-5b), the Fick's second law for the sorption of a penetrant in film can be used to calculate a kinetic diffusivity coefficient:¹⁴

$$\frac{M_t}{M_\infty} = 1 - \frac{8}{\pi^2} \sum_{n=0}^{\infty} \frac{1}{(2n+1)^2} \exp\left[-\frac{D(2n+1)^2 \pi^2 t}{l^2}\right] \quad (2-21)$$

where M_t and M_∞ represent the amount of gas absorbed by the membrane film at time t and the equilibrium sorption at infinite time, respectively. D is the kinetic (transport) diffusion coefficient, t is the time required to attain M_t and l is the thickness of the

sample. When the mass uptake is less than 60 % ($M_t/M_\infty < 0.60$) and fractional uptake is a linear function of $t^{1/2}$, above eqn.(2-21) can be reduced to¹⁴

$$\frac{d(M_t / M_\infty)}{dt^{1/2}} = \left(\frac{16D}{l^2 \pi} \right)^{1/2} \quad (2-22)$$

Diffusion coefficients can be determined by plotting M_t / M_∞ versus $t^{1/2}$ where the slope equals $(16D/l^2\pi)^{1/2}$.

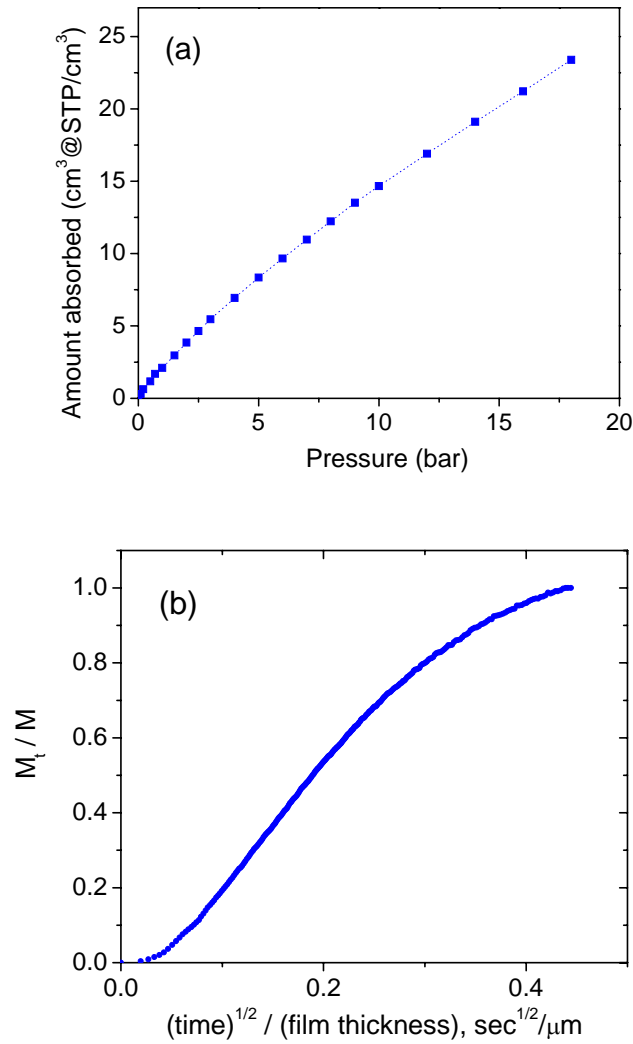


Figure 2-5. (a) CO₂ Sorption isotherm on mesoporous silica at 308 K, and (b) CO₂ mass uptake curve of mesoporous silica at 398 K and 0.1 bar.

2.6. History of Gas Separation Membranes

The first scientific observation related to gas separation membrane was made by J. K. Mitchell, as early as 1831. He observed that natural rubber balloons in gas atmospheres with different compositions expanded with different velocities, depending on the nature of the gas: hydrogen filled expanded faster than air.^{15,16}

In 1855, Fick studied gas transport through nitrocellulose membrane and formulated 'Fick's first law' which is a quantitative description of material transport through boundary layers.¹⁷ However, it is considered that the foundation for gas separation was laid by Thomas Graham in 1829, who performed the first recorded experiment on the transport of gases and vapours in polymeric membranes. He repeated Mitchell's experiments with natural rubber films and made the first quantitative measurements of the gas permeation rate. He established a series of relative permeation rates across the film for a number of gases and noted that there was no relation between these values and known diffusion coefficients in gases. In 1866, he published concepts for gas permeation in terms of a 'solution-diffusion mechanism'.¹⁸

In 1907, Benchold prepared the first series of nitrocellulose membranes with graded pore-size structure. He was also the first to define the relationship between bubble point temperature, surface tension, and pore radius.¹⁹ Subsequently, the important concept of pore-size distribution was developed by Karplus, who combined bubble point temperature and permeability measurements.²⁰ He improved the technique for preparing nitrocellulose membranes and as a result, microporous membranes became commercially available in the 1930s.⁴ During the next 20 years, other polymers like cellulose acetate were tried in microfiltration membranes. Such membranes found their first significant

applications in the filtration of drinking water in the late 1940s. A framework was subsequently developed for the treatment and understanding of diffusion across various kinds of membranes with porous, non-porous, glassy and rubbery characteristics. By 1960, the elements of modern membrane science had developed and sufficient knowledge was available on the relationships between structure and function in gas separation membranes. However, membrane processes for gas separations were still primarily limited to laboratory scale. At this time the only commercially competitive industrial membrane was an asymmetric membrane made of cellulose acetate developed by Loeb and Sourirajan.²¹ This membrane was used for water desalination via reverse osmosis (RO). This asymmetric membrane was an industrial breakthrough as it showed much higher permeability than symmetric membranes with a comparable thickness. This asymmetric membrane consisted of a very thin dense top layer with thickness $< 0.5 \mu\text{m}$ supported by a porous sublayer with thickness $50 - 200 \mu\text{m}$.²¹ The work by Henis and Tripodi made industrial gas separation economically feasible.²² They fabricated a leak-free composite membrane with a very thin polymer layer on top of an asymmetric membrane.

The separation of gas mixtures of industrial interest involving membranes became economically competitive in the late 1970s for the separation of hydrogen from the ammonia product stream using the Permea Prism membrane.²³ This was the first large scale industrial application of gas separation membranes. Cynara and the Separex company developed cellulose acetate membranes for the separation of carbon dioxide. In addition, the membranes for nitrogen separation from air were released by Generon. This

nitrogen selective membrane, based on poly(4-methyl-1-pentene), displayed an oxygen/nitrogen selectivity around 4, and produced nitrogen with roughly 95 % purity.²⁴

The progress in membrane science and technology was accelerated during the 1980s by the development and refinement of synthetic polymeric membranes. Membrane gas separation emerged as a commercial process on a large scale during the 1980s. During this period, significant progress was made in virtually every aspect of membranology, including improvements in membrane formation processes, chemical and physical structures, configurations and applications.⁴

In the 1990's, Generon, Praxair, and Medal had released new polymeric membrane with oxygen/nitrogen selectivities of 6 – 8. These membranes could produce more than 99 % nitrogen purity and offered a cost-competitive alternative to delivered liquid nitrogen for many small users. This application has grown to account for one-third of new nitrogen production, and currently, there are 5000 – 10,000 nitrogen systems operating world wide.²⁴ As of 2002, gas separation membrane equipment has grown into a \$150 million/year market. The majority of the gas separations involve the separation of non condensable gases, such as N₂ from air, CO₂ from CH₄, and H₂ from N₂, Ar or CH₄. Currently, many efforts are still underway to open up the market of condensable gases separations such as butane from methane, propylene from propane, and n-butane from isobutene.²⁵

2.7. Mixed Matrix Membrane

Polymeric membranes designed for gas separations have been known to have a trade-off between permeability and selectivity as shown in upper bound curves developed by

Robeson.²⁶ Attempts at merely altering the chemical structure of the polymer offered diminishing returns in improved performance.^{6,27} However, recent theoretical work by Freeman concluded that there is an asymptotic limit to the separation capabilities of polymeric membranes.²⁸ Recent work aimed at developing membranes capable of operating above the upper bound has focused on mixed matrix membranes (MMMs).²⁹⁻³² These membranes combine polymer with an inorganic filler, usually a zeolite or a molecular sieve. Although inorganic molecular sieves lie well above the Robeson's upper bound or near the commercially attractive region as shown in Figure 2-6 (taken from the work by Koros et al.³¹), these materials are expensive and difficult to process and handle as membranes.

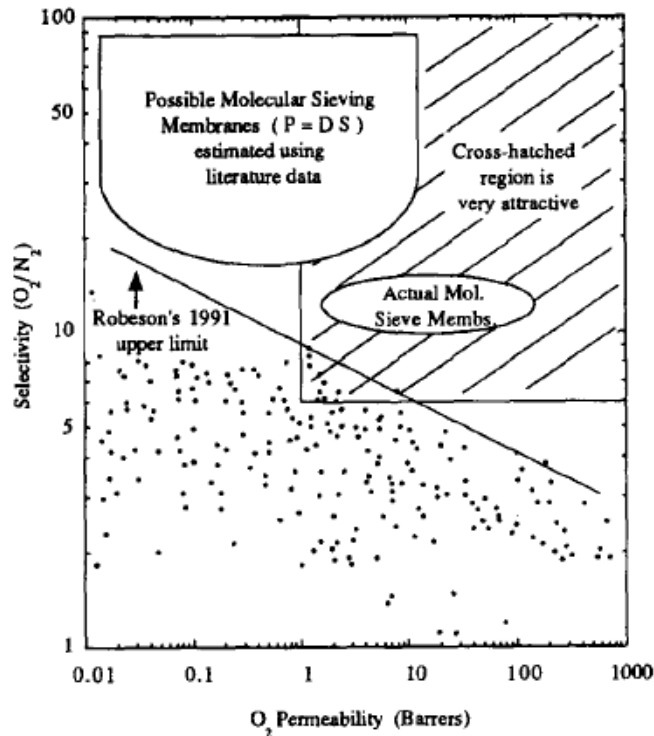


Figure 2-6. Trade-off curve of O_2/N_2 selectivity and O_2 permeability.

According to the Maxwell model predicting MMM performance, the effective steady state composite permeability is given by the following expression:³¹

$$P_{eff} = P_c \left[\frac{P_D + 2P_C - 2\phi_D(P_C - P_D)}{P_D + 2P_C + \phi_D(P_C - P_D)} \right] \quad (2-25)$$

where P_{eff} is the effective composite permeability, ϕ is the volume fraction, P is the single component permeability and the subscripts D and C refer to the dispersed and continuous phases, respectively. With this equation, Koros et al. predicted the permeability for a zeolites 4A-polysulfone MMM shown in Figure 2-7.³¹ The addition of zeolite 4A ranging from 10 to 90 vol. % decreases the predicted O_2 permeability of MMM only slightly while leading to large increase in O_2/N_2 permselectivity. A similar analysis can also be made with carbon molecular sieves. The predictions using the above equation suggest significant improvements in both permselectivity and permeability.

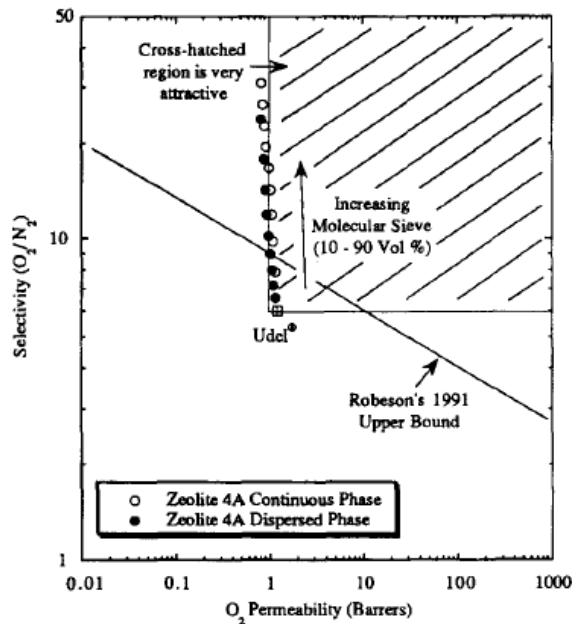


Figure 2-7. Predicted zeolite 4A-polysulfone MMM performance .

Early attempts at fabricating MMMs used rubbery polymers and zeolites.^{30,33,34} These membranes proved to be successful at pervaporation applications such as separating ethanol from water. Later work would involve using glassy polymers and zeolites to prepare MMMs suitable for gas separation applications.^{29,32,35-37} While some of the glassy MMMs did offer improvements in selectivity, they often were accompanied by losses in permeability. However, it should be noted that research on glassy MMMs is still in its early stages as the first publication on this topic appeared in the late eighties.³⁵

2.8. Carbon Nanotube

Carbon nanotubes (CNTs) have attracted an enormous amount of attention since their first discovery by Ijima in 1991.³⁸ The pore walls of CNTs are mainly composed of graphite sheets. The rolled structure of the graphite sheets has gathered much attention from both theoretical and practical aspects in physics and chemistry. There are infinitely many ways to roll a sheet into a cylinder, resulting in different diameters and microscopic structures of the tubes. These are defined by the chiral angle, the angle of the hexagon helix around the tube axis. Some properties of CNTs can be explained within a macroscopic model of an homogeneous cylinder, whereas others depend crucially on the microscopic structure of the tubes.³⁹

2.8.1. Structure of CNTs

A tube made of single graphite layer rolled up into a hollow cylinder is called a single-walled carbon nanotube (SWNT) and a tube comprising of several, concentrically arranged cylinders is referred to as a multiwall nanotube (MWNT). SWNTs are usually produced by laser ablation, high-pressure CO conversion (HiPCO), or the arc-discharge

technique and have a Gaussian distribution of diameter d with mean diameters $d_0 \approx 1.0 - 1.5$ nm.⁴⁰⁻⁴⁵ SWNT form hexagonal-packed bundles during the growth process. The wall-to-wall distance between two tubes is the same range as interlayer distance in graphite (0.34 nm). MWNTs have similar lengths to that of SWNTs, but much larger diameters. Their inner and outer diameter are around 5 and 100 nm, respectively, corresponding to around 30 coaxial tubes.³⁹ Confinement effects in MWNTs are expected to be less dominant than in SWNTs, because of the large circumference. MWNTs have similar properties to graphite.

Because the microscopic structure of CNTs is closely related to grapheme, the CNTs are usually labeled in terms of the grapheme lattice vectors as shown in Figure 2-8. The unit cell can be spanned by the two vectors (\mathbf{a}_1 and \mathbf{a}_2) and contains two carbon atoms at $\frac{1}{3}(\mathbf{a}_1 + \mathbf{a}_2)$ and $\frac{2}{3}(\mathbf{a}_1 + \mathbf{a}_2)$. The length of unit vector ($a_0 = |\mathbf{a}_1| = |\mathbf{a}_2|$) is 2.461 Å and two unit vector form an angle of 60°. In CNTs, the grapheme sheet is rolled up in such a way that a grapheme lattice vector ($\mathbf{c} = n_1\mathbf{a}_1 + n_2\mathbf{a}_2$) becomes the circumference of the nanotube. This circumferential vector, \mathbf{c} , which is usually denoted by the pair of integers (n_1, n_2) is called the chiral vector and uniquely defines a particular nanotubes. Even diameter and direction of the chiral vector of CNTs are similar, many properties of nanotubes such as electronic band structure or the spatial symmetry group vary dramatically with the chiral vector. For instance, the (10,10) CNT contains 40 carbon atoms in the unit cell and has metallic properties, while (10, 9) CNT with 1084 carbon atoms in the unit cell is a semiconducting tube.³⁹

In Figure 2-8, the chiral vector ($\mathbf{c} = 8\mathbf{a}_1 + 4\mathbf{a}_2$) of an (8,4) tube is shown. The circles indicate the four points on the chiral vector that are lattice vectors of grapheme. When the

sheet is rolled up, the first and the last circle are overlapped. The direction of the chiral vector is measured by the chiral angle (θ):

$$\cos \theta = \frac{a_1 \cdot c}{|a_1| \cdot |c|} = \frac{n_1 + n_2 / 2}{\sqrt{n_1^2 + n_1 n_2 + n_2^2}} \quad (2-23)$$

Tubes of the type $(n, 0)$ with $\theta = 0^\circ$ are referred to zig-zag tubes due to their zig-zag pattern along the circumference while (n, n) tubes are called armchair tubes as shown in Figure 2-8. Both of the zig-zag and armchair CNTs are achiral tubes, in contrast to the general chiral tubes.³⁹

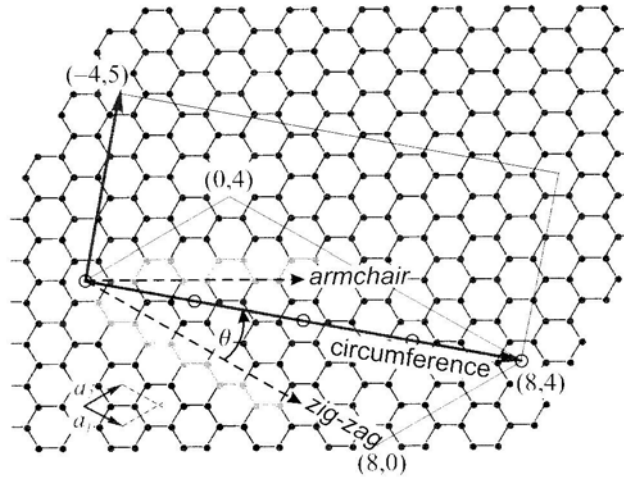


Figure 2-8. The grapheme lattice vectors of CNT

2.8.2. Diffusion in CNTs

Ackerman et al performed atomistic simulations of diffusion of pure Ar and Ne through SWNT's.⁴⁶ For comparison, they also predicted the diffusion of these gases through the zeolite silicalite, a commonly used zeolite for industrial applications with pores of about the same size as the nanotubes (0.81 and 1.36 nm). Their results predicted that the self diffusivity of Ar in SWNT's was orders of magnitude larger than in silicalite.

At low pressures the self diffusivity in the CNTs was predicted to be on the order of 10^{-1} cm^2/sec , which was much higher than the 10^{-4} cm^2/sec of silicalite. However, as the pressure was increased to 80 bar, the self diffusivity of Ar in the SWNT's dropped to 10^{-3} cm^2/sec , while that of Ar in zeolite was relatively unchanged. This was attributed to the very smooth surface of the interior of the CNT's. At low pressures the adsorbed Ar molecules are well separated from each other, but as the pressure increase this is no longer is true. Therefore, the diffusivity begins to become affected by atom-atom collisions. This same trend was predicted for Ne.

Recent theoretical work by Sholl et al. has reported atomic simulations results for both self- and transport diffusivities of light gases such as H_2 and CH_4 in carbon nanotubes and in zeolites.⁴⁷ They reported transport rates in CNTs to be orders of magnitude faster than in zeolites and the exceptionally high transport rates in nanotubes are shown to be a result of the inherent smoothness of the nanotubes. In their most recent work, they predicted that SWNT membranes would be strongly selective for CH_4 over H_2 and would exhibit very large fluxes because of the significant adsorption selectivity of CH_4 over H_2 .⁴⁸ They suggested that carbon nanotubes, if used as membranes, have flux/selectivity properties that far exceed those of any other known inorganic materials.

2.9. Ordered Mesoporous Silica

The discovery of the mesoporous M41S family of silica materials by Mobil researchers have expanded the range of uniform pore sizes from the microporous into the mesopore range (<2 nm) and generated considerable interest in open structured inorganic materials. The initial work of Mobil researchers reported only three subgroups: MCM-41

(P6mm two-dimensional hexagonal phase), MCM-48 (Ia3d cubic phase) and MCM-50 (lamellar phase).^{49,50} Since then, other numerous, surfactant-templated mesophase materials including worm-like disordered network channels have been reported: HMS, KIT, MSU, SBA series, etc.⁵¹ The procedures used for the preparation of mesoporous silica materials are similar to those in the synthesis of zeolites, except for the use of an organic surfactant template. The original mesoporous M41S molecular sieves is synthesized by reacting a silica source (e.g. tetraethylorthosilicate (TEOS), fumed silica, sodium silicate), an alkyltrimethylammonium halide surfactant (e.g. cetyltrimethylammonium bromide (CTAB)), a base (e.g. sodium hydroxide or tetramethylammonium hydroxide (TMAOH)), and water. The as-synthesized product contains occluded organic surfactant, which is removed by calcination at ~ 500 °C in air to yield an ordered mesoporous material.⁵¹

Surfactant chemistry is the key to the formation of mesoporous silica. The silicate species in solution play an important role in the organization of the surfactant molecules, and the electrostatic interaction between the inorganic and surfactant ions determines the morphology of the mesophases. Several mechanistic model have been developed to explain formation of mesoporous silica, however, to date the mechanistic details of mesoporous silica synthesis have not yet been fully agreed upon.⁵²

Interest in the mesoporous silica molecular sieves has been concentrated mostly on MCM-41, and MCM-48 on which very little information is available. These ordered mesoporous silica materials with tailor-made pore sizes and shapes have been attracting much attention as catalysts, membranes, catalyst supports and adsorbent because of their high surface area, tunable pore sizes and surface chemistry via functionalization.

2.10. References

- [1] A. Basu, J. Akhtar, M. H. Rahman and M. R. Islam, A review of separation of gases using membrane systems, *Petroleum Sci. Tech.* 22 (2004) 1343.
- [2] M. Mulder, *Basic principle of membrane technology*, Kluwer Academic Publishers, (1997)
- [3] K. Ghosal and B. D. Freeman, Gas separation using polymer membranes: an overview, *Polym. Adv. Tech.*, 5 (1994) 673.
- [4] P. Pandey and R. S. Chauhan, Membranes for gas separation, *Progr. Polym. Sci.*, 26 (2001) 853.
- [5] M. Knudsen, *The Kinetic Theory of gases*, Methuen, London (1934).
- [6] W. J. Koros and G. K. Fleming, Membrane-based gas separation, *J. Membr. Sci.*, 83 (1993) 1.
- [7] A.L.Hines and R.N.Maddox, *Mass Transfer*, Prentice Hall, Upper Saddle River, NJ, (1985).
- [8] J. D. Perry, K. Nagai and W. J. Koros, Polymer membranes for hydrogen separations, *MRS Bulletin*, 31 (2006) 745.
- [9] W. J. Koros, Gas separation membranes: needs for combined materials science and processing approaches, *Macromol. Symp.*, 188 (2002) 13
- [10] S. Kanehashi and K. Nagai, Analysis of dual-mode model parameters for gas sorption in glassy polymers, *J. Membr. Sci.*, 253 (2005) 117.
- [11] R. E. Kesting and A. K. Fritzsche, *Polymeric Gas Separation Membranes*, John Wiley and Sons, Inc., (1993).
- [12] H. Hachisuka, Y. Tsujita, A. Takizawa and T. Kinoshita, CO₂ sorption properties and enthalpy relaxation in alternating copoly(vinylidene cyanide-vinyl acetate)s, *Polymer*, 29 (1988) 2050.
- [13] C. M. Zimmerman, A. Singh and W. J. Koros, Diffusion in gas separation membrane materials: A comparison and analysis of experimental characterization techniques, *J. Polym. Sci. B: Polym. Phys.*, 36 (1998) 1747.
- [14] J. Crank, *The Mathematics of Diffusion*, Oxford Press; London (1990).
- [15] R. E. Kesting, *Synthetic Polymeric Membranes*, Wiley, New York (1985).
- [16] D. R. Paul and Y. P. Yamapol'skii, *Polymeric Gas Separation Membranes*, CRC Press, Inc.(1994).
- [17] A. Fick., Ueber Diffusion, *Annalen der Physik und Chemie* 94 (1855) 59.
- [18] T. Graham, *Phil. Mag. J.Sci.* , 32 (1866) 401.
- [19] H. Benchohd, *Biochem Zeitung* 6(1907) 379.
- [20] H. Karplus, *Kolloid Z.*, 63 (1933) 277.
- [21] S. Loeb and S. Sourirajan., Sea water demineralization by means of an osmotic membrane, *Advances in Chemistry Series (Adv. Chem. Ser.)* 38 (1963) 117.
- [22] J. M. S. Henis and M. K. Tripodi, Composite hollow fiber membranes for gas separation: the resistance model approach, *J. Membr. Sci.*, 8 (1981) 233.
- [23] K. Scott, *Handbook of Industrial Membranes*, Elsevier Science Publishers (1998).
- [24] R. W. Baker, Future directions of membrane gas separation technology, *Ind. Eng. Chem. Res.*, 41 (2002) 1393.
- [25] T. W. Pechar, Fabrication and characterization of polyimide-based mixed matrix membranes for gas separations, Ph.D. Dissertation, Virginia Tech, Blacksburg, (2004)

- [26] L. M. Robeson, Correlation of separation factor versus permeability for polymeric membranes, *J. Membr. Sci.*, 62 (1991) 165.
- [27] S. A. Stern, Polymers for gas separations: The next decade, *J. Membr. Sci.*, 94 (1994) 1.
- [28] B. D. Freeman, Basis of permeability/selectivity tradeoff relations in polymeric gas separation membranes, *Macromolecules*, 32 (1999) 375.
- [29] J.-M. Duval, A. J. B. Kemperman, B. Folkers, M. H. V. Mulder, G. Desgrandchamps and C. A. Smolders, Preparation of zeolite filled glassy polymer membranes, *J. Appl. Polym. Sci.*, 54 (1994) 409.
- [30] J. P. Boom, G. M. Pünt, H. Zwijnenberg, R. d. Boer, D. Bargeman, C. A. Smolders and H. Strathmann, Transport through zeolite filled polymeric membranes, *J. Membr. Sci.*, 138 (1998) 237.
- [31] C. M. Zimmerman, A. Singh and W. J. Koros, Tailoring mixed matrix composite membranes for gas separations, *J. Membr. Sci.*, 137 (1997) 145.
- [32] R. Mahajan and W. J. Koros, Factors Controlling Successful Formation of Mixed-Matrix Gas Separation Materials, *Ind. Eng. Chem. Res.*, 39 (2000) 2692.
- [33] M. Goldman, D. Fraenkel and G. Levin, A zeolite/polymer membrane for separation of ethanol-water azeotrope, *J. Appl. Polym. Sci.*, 37 (1989) 1791.
- [34] J.-M. Duval, B. Folkers, M. H. V. Mulder, G. Desgrandchamps and C. A. Smolders, Adsorbent filled membranes for gas separation. Part 1. Improvement of the gas separation properties of polymeric membranes by incorporation of microporous adsorbents, *J. Membr. Sci.*, 80 (1993) 189.
- [35] S. Kulprathipanja, R. W. Neuzil and N. N. Li, Separation of fluids by means of mixed matrix membranes, United States Patent 4,740,219 (1988).
- [36] R. Mahajan and W. J. Koros, Mixed matrix membrane materials with glassy polymers. Part 1, *Polym. Eng. Sci.*, 42 (2002) 1420.
- [37] R. Mahajan and W. J. Koros, Mixed matrix membrane materials with glassy polymers. Part 2, *Polym. Eng. Sci.*, 42 (2002) 1432.
- [38] S. Iijima, Helical microtubules of graphitic carbon, *Nature*, 354 (1991) 56.
- [39] S. Reich, C. Thomsen and J. Maultzsch, *Carbon Nanotubes; Basic Concepts and Physical Properties*, Wiley-VCH, Weinheim, Germany (2003).
- [40] C. Journet and P. Bernier, Production of carbon nanotubes, *Appl. Phys. A: Mater. Sci. Process.* 67 (1998) 1.
- [41] A. Fonseca, K. Hernadi, P. Piedigrosso, J.-F. Colomer, K. Mukhopadhyay, R. Doome, S. Lazarescu, L. P. Biro, P. Lambin, P. A. Thiry, D. Bernaerts and J. B. Nagy, Synthesis of single- and multi-wall carbon nanotubes over supported catalysts, *Appl. Phys. A: Mater. Sci. Process.* 67 (1998) 11.
- [42] I. W. Chiang, B. E. Brinson, A. Y. Huang, P. A. Willis, M. J. Bronikowski, J. L. Margrave, R. E. Smalley and R. H. Hauge, Purification and Characterization of Single-Wall Carbon Nanotubes (SWNTs) Obtained from the Gas-Phase Decomposition of CO (HiPco Process), *J. Phys. Chem. B*, 105 (2001) 8297.
- [43] A. G. Rinzler, J. Liu, H. Dai, P. Nikolaev, C. B. Huffman, F. J. Rodríguez-Macías, P. J. Boul, A. H. Lu, D. Heymann, D. T. Colbert, R. S. Lee, J. E. Fischer, A. M. Rao, P. C. Eklund and R. E. Smalley, Large-scale purification of single-wall carbon nanotubes: process, product, and characterization, *Appl. Phys. A: Mater. Sci. Proc.* 67 (1998) 29.

- [44] M. J. Bronikowski, P. A. Willis, D. T. Colbert, K. A. Smith and R. E. Smalley, Gas-phase production of carbon single-walled nanotubes from carbon monoxide via the HiPco process: A parametric study, *J. Vac. Sci. Tech. A: Vacuum, Surfaces, and Films* 19 (2001) 1800.
- [45] C. Journet, W. K. Maser, P. Bernier, A. Loiseau, M. L. D. L. Chapelle, S. Lefrant, P. Deniard, R. Lee and J. E. Fischer, Large-scale production of single-walled carbon nanotubes by the electric-arc technique, *Nature*, 388 (1998) 756.
- [46] D. M. Ackerman, A. I. Skoulidas, D. S. Sholl and J. K. Johnson, Diffusivities of Ar and Ne in carbon nanotubes, *Mol. Simul.*, 29 (2003) 677.
- [47] A. I. Skoulidas, D. M. Ackerman, J. K. Johnson and D. S. Sholl, Rapid transport of gases in carbon nanotubes, *Phys. Rev. Lett.*, 89 (2002) 185901.
- [48] H. Chen and D. S. Sholl, Predictions of selectivity and flux for CH₄/H₂ separations using single walled carbon nanotubes as membranes, *J. Membr. Sci.*, 269 (2006) 152.
- [49] J. S. Beck, J. C. Vartuli, W. J. Roth, M. E. Leonowicz, C. T. Kresge, K. D. Schmitt, C. T. W. Chu, D. H. Olson, E. W. Sheppard, S. B. McCullen, J. B. Higgins and J. L. Schlenker, A new family of mesoporous molecular sieves prepared with liquid crystal templates, *J. Am. Chem. Soc.*, 114 (1992) 10834.
- [50] C. T. Kresge, M. E. Leonowicz, W. J. Roth, J. C. Vartuli and J. S. Beck, Ordered mesoporous molecular sieves synthesized by a liquid-crystal template mechanism, *Nature*, 359 (1992) 710.
- [51] V. V. Guliyants, M. A. Carreon and Y. S. Lin, Ordered mesoporous and macroporous inorganic films and membranes, *J. Membr. Sci.*, 235 (2004) 53.
- [52] K. J. Edler and S. J. Roser, Growth and characterization of mesoporous silica films, *Inter. Rev. Phys. Chem.* 20 (2001) 387.

Chapter 3. Poly(imide siloxane) and Carbon Nanotube Mixed Matrix Membranes for Gas Separation

3.1. Introduction

Polymeric membranes designed for gas separations have been known to have a trade-off between permeability and selectivity as shown in upper bound curves developed by Robeson.¹ Attempts at merely altering the chemical structure of the polymer offer diminishing returns in improved performance. Recent theoretical work by Freeman concluded that there is an asymptotic limit to the separation capabilities of polymeric membranes.² Thus, unless new systems are developed to improve membrane performance, membranes will continue to be limited to few niche applications.³

Recent work aimed at developing membranes capable of operating above the upper bound has focused on mixed matrix membranes (MMMs). These membranes combine polymer with an inorganic filler, usually a zeolite or a molecular sieve. Early attempts at fabricating MMMs used rubbery polymers and zeolites.⁴⁻⁷ These membranes proved to be successful at pervaporation applications such as separating ethanol from water. Later work would involve using glassy polymers and zeolites to prepare MMMs suitable for gas separation applications.^{5,8-10} While some of the glassy MMMs did offer improvements in selectivity, they often were accompanied by losses in permeability. However, it should be noted that research on glassy MMMs is still in its early stages as the first publication on this topic appeared in late eighties.¹⁰

Potential fillers, which have not received any attention for use in MMMs for gas separations are carbon nanotubes (CNTs). In depth reviews of this type of material are available elsewhere.¹¹ Briefly stated, carbon nanotubes are graphite sheets rolled into circular bundles. They can be synthesized to have diameters of several angstroms or tens

of nanometers, and their lengths can be up to several micrometers. Additionally, these tubes can be synthesized as singular tubes called single walled nanotubes (SWNTs) or as a series of shells of different diameters spaced around a common axis called multiwalled nanotubes. In both cases the ends of the CNTs can be open or closed. Some of the attractive characteristics of CNTs are their outstanding mechanical properties, their high strength-to-weight ratio, and their excellent thermal stability.¹¹

Simulations predicting the diffusivity properties of simple gases in CNTs show that these materials may be a suitable filler in a polymer matrix to make MMMs. Ackerman et al performed atomistic simulations of diffusion of pure Ar and Ne through SWNT's.¹² For comparison, they also predicted the diffusion of these gases through the zeolite silicalite, a commonly used zeolite for industrial applications with pores of about the same size as the nanotubes (0.81 and 1.36 nm). Their results predicted that the self diffusivity of Ar in SWNT's was orders of magnitude larger than in silicalite. At low pressures the self diffusivity in the CNTs was predicted to be on the order of 10^{-1} cm²/sec, which was much higher than the 10^{-4} cm²/sec of silicalite. However, as the pressure was increased to 80 bar, the self diffusivity of Ar in the SWNT's dropped to 10^{-3} cm²/sec, while that of Ar in zeolite remained relatively unchanged. This was attributed to the very smooth surface of the interior of the CNT's. At low pressures the adsorbed Ar molecules are well separated from each other, but as the pressure increases this is no longer true. Therefore, the diffusivity begins to become affected by atom-atom collisions. This same trend was predicted for Ne.

Recent theoretical work by Sholl et al. has reported atomic simulations results for both self- and transport diffusivities of light gases such as H₂ and CH₄ in carbon

nanotubes and in zeolites.¹³ They reported transport rates in CNTs to be orders of magnitude faster than in zeolites and the exceptionally high transport rates in nanotubes are shown to be a result of the inherent smoothness of the nanotubes. They suggested that carbon nanotubes, if used as membranes, have flux/selectivity properties that far exceed those of any other known inorganic materials.

The main intent of this study is to verify this hypothesis by developing and characterizing novel nanocomposite membranes based on carbon nanotubes dispersed inside a polymer matrix. We synthesized a poly(imide siloxane) to be used with carbon nanotubes to make MMMs. The siloxane component has good wetting properties on a graphite surface and the imide segments impart good mechanical properties to the overall membrane film. The structure, the absence of defects, and the properties of CNT MMMs were characterized by NMR, FTIR, SEM, and gas permeation measurements.

3.2. Experimental and Characterization Method

3.2.1. 6FDA-6FpDA-PDMS copolymer

In order to synthesize the copolymer with a targeted PDMS weight % of 40, 6FDA-6FpDA-PDMS was synthesized using a step growth reaction. The reaction scheme to synthesize 6FDA-6FpDA-PDMS is shown in Figure 3-1. The details of the synthesis method are described elsewhere.¹⁴

3.2.2. Preparation of carbon nanotubes

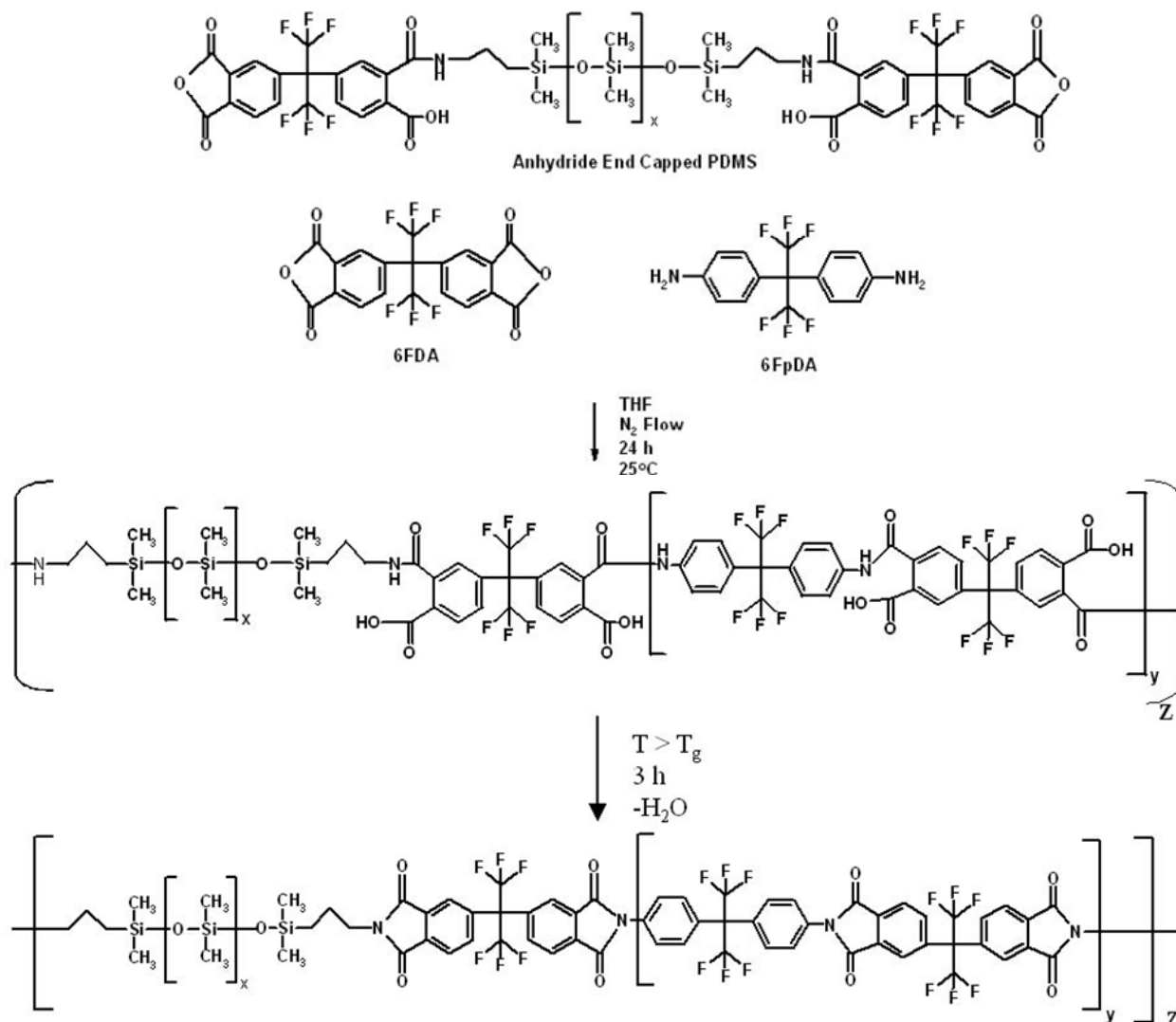


Figure 3-1. Synthesis of 6FDA-6FpDA-PDMS

Both closed-ended and open-ended single walled carbon nanotubes were purchased from Carbon Solutions, Inc. The average diameter of individual nanotubes was 1.4 ± 0.2 nm. The raw carbon nanotube materials were treated with acid to purify CNTs from impurities by the following procedure.¹⁵ Ten mg of raw CNTs were sonicated in 5 mL of concentrated nitric acid (70 vol.%) with an ultrasonic bath (60 Hz) for 5 minutes. The suspension was refluxed at 120 °C for 4 hr and then cooled. The mixture was centrifuged at 5000 rpm for 30 min, and the resulting yellow-brown solution was decanted. The wet

powder was washed with deionized water, centrifuged (5000 rpm for 30 min), and decanted. This cycle was repeated several times. Finally, the wet powder was filtered with 0.1 μm pore size of membrane filter and dried under vacuum. In order to cut CNTs into smaller length, the purified open-ended CNTs were transferred to 100 mL of 3:1 mixture of concentrated H_2SO_4 (98 vol%): HNO_3 (70% vol%) solution. The mixture was sonicated in a water bath for 4 hr at 40 $^\circ\text{C}$ and then diluted with deionized water. The diluted solution was centrifuged (5000 rpm for 30 min), and brown solution was decanted. This cycle was repeated several times, same as in the case of the purification procedure and then filtered with with 0.1 μm pore sized membrane filter and dried.¹⁶

3.2.3. Fabrication 6FDA-6FpDA-PDMS Copolymer Membranes

1.25 grams of the copolymer were dissolved in 20 mL of THF and stirred for two days. The volume of solution was evaporated to 10 mL over this time, leading to a viscous solution. The solution was cast into a 6.35 cm diameter Teflon coated pan. The pan was covered with a glass plate to slow down the evaporation of the solvent allowing for a film to form a uniform thickness without curling. The solutions were given 2 days to dry at room temperature. Once dry, the films were placed under vacuum and the temperature was raised to 100 $^\circ\text{C}$ for 12 hours. After this period the films were allowed to cool to room temperature under vacuum over a 6 hour period. A 6.35 cm diameter circular sample was cut from the film and used for permeation tests.

3.2.4. Fabrication of Poly(imide siloxane)-Carbon Nanotube Mixed Matrix Membranes

The fabrication procedure for the mixed matrix membranes was identical to the pure polymer membrane preparation, regardless of the type of nanotubes employed.

Approximately 1.3 grams of the pure polymer were dissolved in 20 mL of THF and mixed for 24 hours. After this time a predetermined mass of CNTs to make a desired loading of CNT (2 or 10 wt%) was added to the polymer solution. The mixture was allowed to mix for 24 hours at room temperature. Following this time period, the mixture was sonicated for 15 minutes, after which it was allowed to mix for 15 minutes. This process was repeated several times. During this time the volume of the mixture reduced to roughly 10 mL and became viscous. The mixture was cast into a 6.35 cm diameter Teflon coated pan and was immediately covered with a glass plate to ensure a slow down the evaporation of the solvent. A slow evaporation of the solvent would reduce solvent concentrations within the film, and lead to more uniformly thick film without curling.

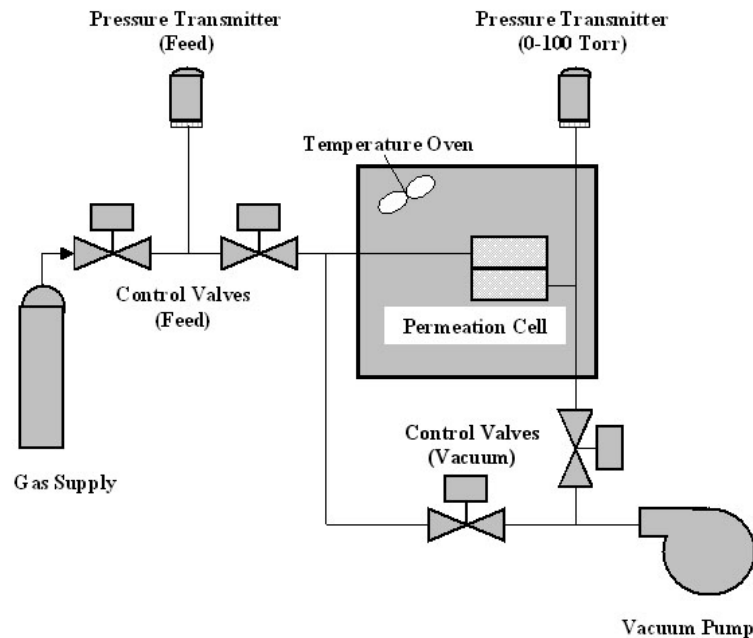


Figure 3-2. Schematic of the system used to perform permeation experiments.

The mixture was allowed to dry over a 2 day period at room temperature.

After drying the film was placed under vacuum and the temperature was raised to 100 °C for 12 hours. Following this procedures, the film was allowed to cool to room temperature under vacuum over a 6 hour period. A 6.35 cm diameter circular sample was cut from the film and used for permeation tests.

3.2.5. Gas Permeation Measurement

Permeabilities of polymeric membranes and composite membranes were measured using a constant volume varying pressure apparatus. Permeability was measured directly, and the Time Lag Method¹⁷ was applied to the recorded data to determine the diffusivity coefficient. The solubility coefficient was taken as the ratio of the permeability to diffusivity coefficient.¹⁷ A schematic of the permeation system is shown in Figure 3-2.

The gases for these measurements this research were He, CO₂, O₂, N₂, and CH₄. Each gas possessed a purity of 99.99% and was used as received from Air Products. The feed pressure and temperature were kept constant at 4 atm and 35 °C, respectively, for all experiments. Each gas was run through a membrane six times and the average results and the standard deviations were recorded. Permeabilities are reported in units of Barrer (1 Barrer = $1 \times 10^{-10} \text{ cm}^3 \cdot (\text{STP}) \cdot \text{cm} / (\text{cm}^2 \cdot \text{sec} \cdot \text{cmHg})$).

3.3. Results and Discussion

The molecular weights for the copolymers were determined via gel permeation chromatography. The results were $M_n = 62,330 \pm 4000 \text{ g/mol}$ with a M_w of $131,300 \pm 30,120 \text{ g/mol}$. ¹H-NMR was employed to more accurately determine the M_n of the PDMS monomer and the determined M_n was 885.5g/mol. The weight percent of the PDMS

segment was 41 % in the copolymer as determined by $^1\text{H-NMR}$. FTIR spectroscopy (not shown here) verified the successful imidization for the copolymer. The calculation method and data are described in detail elsewhere.¹⁴

Figure 3-3 shows the field emission scanning electron microscopy (FESEM) images of the CNT samples on a copper support. As shown in part (a), carbon nanotubes are closely entangled and impurities of metal clusters originated from the catalyst stick on the surface of the ropes. These metal impurities on the tips of the ropes can block gas stream when these unpurified samples are used in the MMMs fabrication. Samples in part (b) are seem to be well purified since most impurities appear to have been removed. However, these purified samples can be highly tangled with one another and are also quite long. In

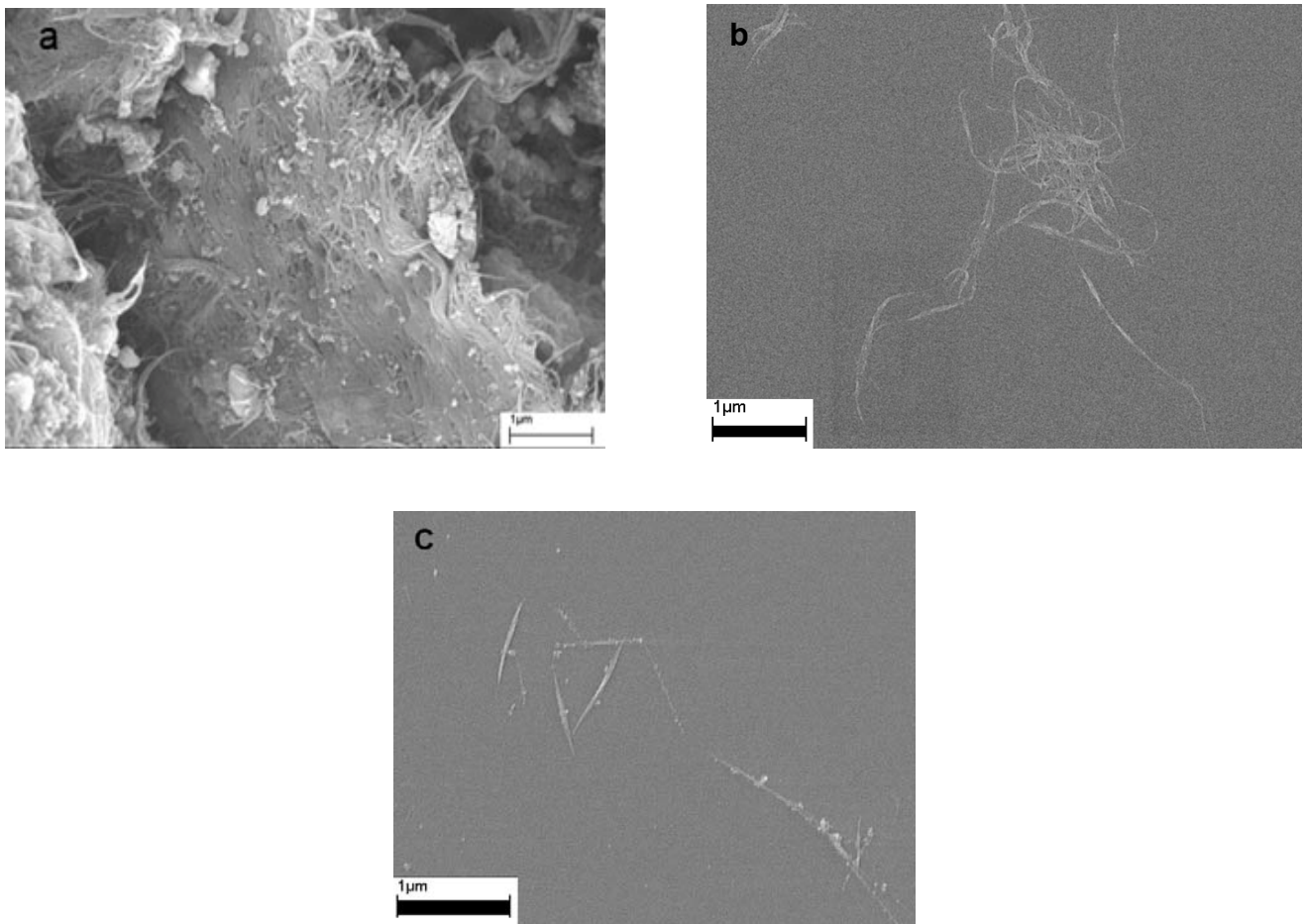


Figure 3-3. FESEM images of CNTs (a) before (b) after purification, and (c) cut CNTs

order to use nanotubes in MMM application, these nearly endless and highly tangled carbon ropes should be cut into short lengths of open tubes. After acid treatment to cut ropes, part (c) clearly shows that the length of each rope is now less than 1 μm . The mean length of SWNTs was measured to be 700 ± 200 nm from several FESEM images. These cut samples can be suspended and manipulated as individual macromolecules without entanglement in MMM fabrication.

The MMM films were analyzed using FESEM. Figure 3-4 shows the cross sectional area images of MMM samples. Cross sectional images were taken of each membrane to

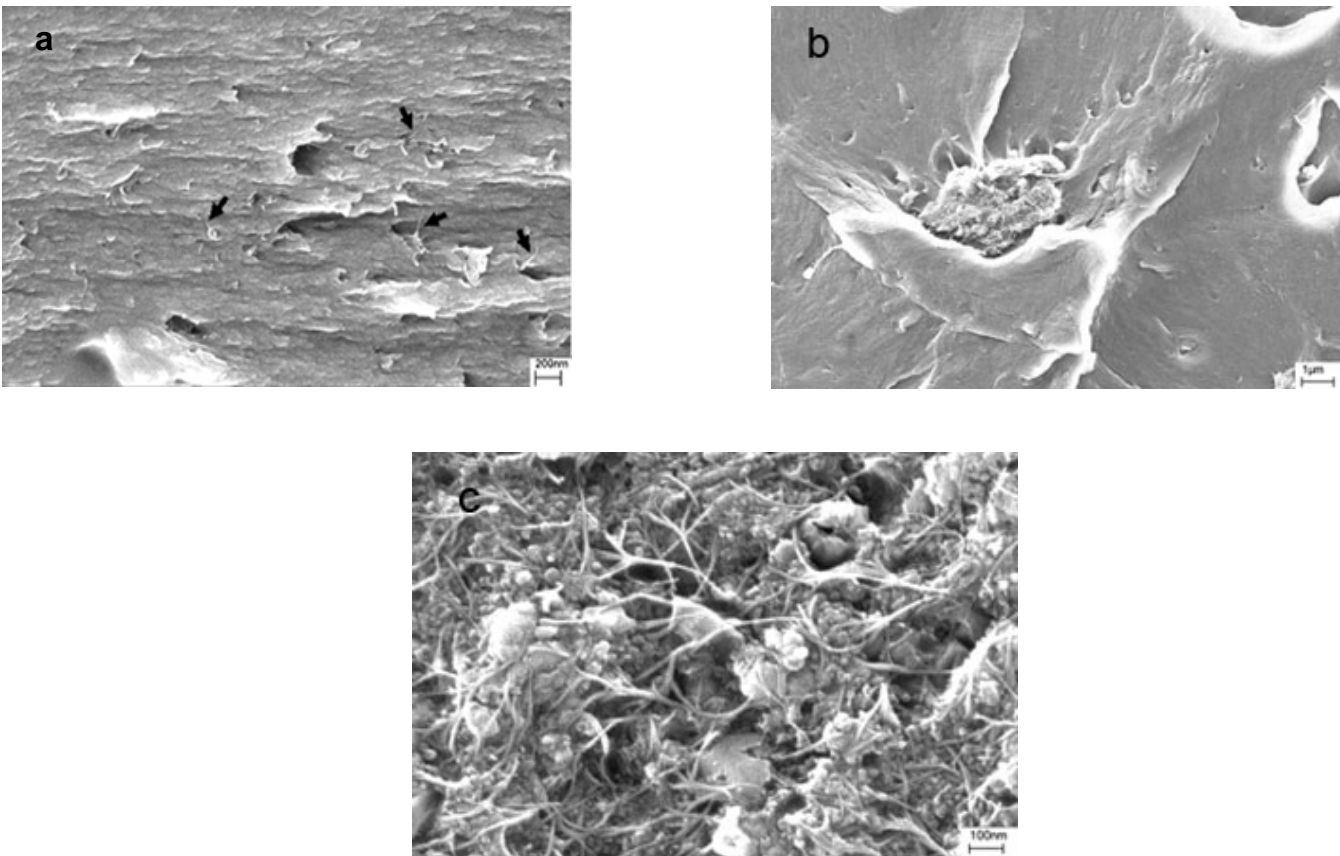


Figure 3-4. FESEM cross-sectional images of MMMs (a) 2 wt% CNTs (arrows indicated CNTs in copolymer matrix) , (b) and (c) 10 wt% CNTs.

determine the extent of nanotubes dispersion within the polymer matrix. Figure 4-(a) shows well dispersed CNTs in polymer matrix at 2 wt% of CNT loading. However, at higher CNT loading, 10 wt%, the tubes agglomerated and formed domains in the polymer as shown in part (b) and (c).

In order to verify the compatibility of CNTs with copolymer and check for the presence of unselective void in CNT MMM membranes, permeability measurements for He and N₂ were gathered for the pure 40 wt % PDMS poly(imide siloxane), and a 1 wt % closed-ended CNT poly(imide siloxane) MMM. Due to its small kinetic diameter He serves as an excellent probing gas for identifying the presence of voids. The kinetic diameter of the gases used in this study have been listed Table 3-1.¹⁸ The presence of unselective voids at the interface between the polymer and nanotubes should offer sites of high permeability for He. The permeability results for the pure poly(imide siloxane) and the 1 wt % close-ended CNT MMM are show in Table 3-2.

Table 3-1. Kinetic diameter in various gases

Molecule	Kinetic Diameter (nm)
He	0.26
H ₂	0.289
CO ₂	0.33
O ₂	0.346
N ₂	0.364
CH ₄	0.38

Table 3-2. Gas permeabilities of the pure PDMS poly(imide siloxane) and close-ended CNT MMMs

Wt % CNT	Gas permeability (Barrer)	
	He	N ₂
0	85.85 ± 0.55	18.48 ± 1.56
1	63.80 ± 0.70	19.51 ± 0.24

Table 3-3. Diffusivity and solubility (N₂) of the pure PDMS poly(imide siloxane) and close-ended CNT MMM

Wt % CNT	Diffusivity, D (cm ² s ⁻¹)	Solubility, S (cm ³ @ STP cm ⁻³ polymer atm)
0	175.92 ± 10.48	0.08 ± 0.01
1	127.04 ± 22.24	0.12 ± 0.03

Permeability of He drops with the addition on CNTs. This large drop in permeability of He suggests that the copolymer adhered well to the CNTs and that the prepared CNT MMMs are defect free. The average permeability of nitrogen increased roughly 6%, but the standard deviations of the measurement overlap each other. Therefore, statistically there was no change in nitrogen's permeability. Table 3-3 shows the diffusion and solubility coefficients for nitrogen in the same MMM sample. Helium diffusion coefficients are not reported for any of the membranes in this paper. This is because the diffusion of He and H₂ is fast and the time lag method introduces too much error.¹⁷

From table 3-3, it is evident that nitrogen experiences a large drop in the diffusion coefficient. This would be consistent if the closed-ended CNTs behaved as an impermeable filler. While the average permeability of the MMM exceeds that of the pure copolymer, implying that solubility must have increased to overcome the losses in diffusivity, the standard deviations of the permeability measurements overlap each other.

Based on these results, it is believed that the addition of closed-ended CNTs to the copolymer adds an impermeable filler, lowering the permeability of He, and hindering the diffusion of nitrogen. Furthermore, the CNT MMMs have no evidence of unselective voids.

The permeability results for the pure poly(imide siloxane) and CNT MMM based on open-ended and cut carbon nanotubes are shown in Table 3-4. The pure poly(imide siloxane) used to make these samples is from a different batch than the one reported in Table 3-2. Hence, the gas permeability values for the pure polymers are slightly different. For the O₂, N₂ and CH₄, the permeability values increased in proportion to the amount of CNTs in the polymer matrix. Addition of 10 wt% CNTs to poly(imide siloxane) resulted in a 48% increase in the permeability of N₂ (11.99 to 17.83 Barrers). Similarly, the permeability of CH₄ and O₂ increased by 30% (28.19 to 36.71 Barrers) and 24% (32.24 to 39.81 Barrers), respectively. For the small gas molecules such as He, H₂ and CO₂, permeability increased after the addition of 2 wt% CNTs. However, there was no difference in permeability between 2 and 10 wt% of CNTs loading in copolymer matrix. From FESEM data, CNTs are well dispersed in polymer matrix and all gas molecules pass through the CNTs tunnel which provide high diffusivity. However, the permeability of He and H₂ in the polymer matrix is already very high due to their small size. In the presence of low CNTs loadings, the He and H₂ permeation increases. However, at higher CNTs loadings, the increase is offset by increased tortuosity around the entangled CNTs domains. Hence, the net effect is no change in permeability.

Table 3-4. Gas permeabilities (Barrer) of various gases in the pure PDMS poly(imide siloxane) and CNT MMMs

Membrane	Carbon nanotube wt %	He	H ₂	CO ₂	O ₂	N ₂	CH ₄
PDMS41	0	59.54±0.53	70.57±0.15	166.02±1.76	32.24±0.30	11.99±0.03	28.19±0.03
CNT/PDMS41	2	66.95±0.63 (12.45%) ^a	79.62±0.38 (12.82%)	190.67±0.59 (14.85%)	36.57±0.89 (13.43%)	14.42±0.19 (20.27%)	34.16±0.19 (21.18%)
CNT/PDMS41	10	67.92±0.14 (14.08%)	79.15±0.70 (12.16%)	191.30±0.55 (14.85%)	39.81±0.37 (23.48%)	17.83±0.31 (48.71%)	36.71±0.31 (30.22%)

^a () increment from pure copolymer

Table 3-5. Diffusivity (10⁻⁸, cm²/sec) of various gases in the pure PDMS poly(imide siloxane) and CNT MMMs

Membrane	Carbon nanotube wt %	He	H ₂	CO ₂	O ₂	N ₂	CH ₄
PDMS41	0	-	-	78.04±0.92	147.74±7.83	83.29±2.83	64.37±0.33
CNT/PDMS41	2	-	-	88.21±1.21 (13.03%)	164.30±8.54 (11.21%)	107.36±5.42 (28.90%)	76.16±1.67 (18.32%)
CNT/PDMS41	10	-	-	88.60±1.02 (13.53%)	204.47±19.17 (38.39%)	149.37±2.81 (79.34%)	90.52±2.54 (40.63%)

^a () increment from pure copolymer

The diffusivity coefficients for the tested gases are shown in Table 3-5. He and H₂ diffusion coefficients were not calculated because the limitation of the time-lag method as previously stated. After incorporation of 2 wt% CNTs to the polymer, diffusivity coefficients for CO₂, O₂, N₂ and CH₄ increased by 13%, 11%, 29%, and 18%, respectively. The diffusivity of N₂ has increased dramatically by 79% at 10 wt% CNTs loading. Similarly, the permeability of CH₄ and O₂ increased by 41% and 38%,

respectively. Similar to the observed increase in permeability, the monotonic increase in diffusivity could be a consequence of the presence of high diffusivity tunnels in the CNTs within the poly(imide siloxane) matrix.

Table 3-6. Solubility ($\text{cm}^3 @ \text{STP cm}^{-3} \text{polymer atm}$) of various gases in the pure PDMS poly(imide siloxane) and CNT MMMs

Membrane	Carbon nanotube wt %	He	H ₂	CO ₂	O ₂	N ₂	CH ₄
PDMS41	0	-	-	1.62±0.01	0.17±0.01	0.11±0.00	0.33±0.00
CNT/PDMS41	2	-	-	1.64±0.02	0.17±0.01	0.10±0.00	0.34±0.01
CNT/PDMS41	10	-	-	1.64±0.02	0.15±0.01	0.09±0.00	0.34±0.01

Table 3-6 shows the solubility coefficients for CO₂, O₂, N₂ and CH₄. Despite increases in permeability and diffusivity, solubility decreased slightly or remained unchanged. These results agree well with simulation estimations of the diffusivity properties of simple gases by Sholl et al.^{12,13} The authors reported that transport rates of light gases in CNTs are orders of magnitude faster than in any microporous material. This exceptionally high transport rates in nanotubes are shown to be result of the inherent smoothness of the CNTs. From this series of experiments, then, it may be concluded that addition of open-ended CNTs to a polymer matrix can improve its permeability properties by increasing diffusivity.

3.4. Conclusion

A poly(imide siloxane) was synthesized using an aromatic dianhydride, an aromatic diamine and amine-terminated PDMS for the siloxane block. The weight percent of PDMS was determined to be 41 using $^1\text{H-NMR}$. The prepared copolymer was mixed with carbon nanotubes for the purpose of fabricating mixed matrix membranes suitable for gas separations. SEM images of CNTs showed that the nanotubes were well purified and cut into few hundred nanometer scale. The SEM for the cross sectional area images of MMM films indicated that CNTs were well dispersed in polymer matrix at 2 wt% of CNT loading, while at 10 wt% of CNTs loading, the tubes agglomerated and formed domains in the copolymer matrix. Permeability of He dropped with the addition of close-ended CNTs. This large drop in He permeability suggests that the copolymer adhered well to the CNTs and that the prepared CNT MMMs were defect free. The permeability of O_2 , N_2 and CH_4 increased in proportion to the amount of open-ended CNTs in the polymer matrix. The permeability of He, H_2 and CO_2 increased after the addition of 2 wt% CNTs. However, there was no difference in permeability between 2 and 10 wt% of CNTs loading in copolymer matrix. The increase in the diffusion coefficients for O_2 , N_2 and CH_4 in MMMs based on open-ended CNTs indicate the presence of high diffusivity CNT tunnels within the poly(imide siloxane) matrix. Therefore, it may be concluded that CNTs offer an attractive additive for universally enhancing the gas permeability of polymers.

3.5. References

- [1] L. M. Robeson, Correlation of separation factor versus permeability for polymeric membranes, *J. Membr. Sci.*, 62 (1991) 165.
- [2] B. D. Freeman, Basis of permeability/selectivity tradeoff relations in polymeric gas separation membranes, *Macromolecules*, 32 (1999) 375.
- [3] K. Scott, *Handbook of Industrial Membranes*, Elsevier Science Publishers (1998).
- [4] M. Goldman, D. Fraenkel and G. Levin, A zeolite/polymer membrane for separation of ethanol-water azeotrope, *J. Appl. Polym. Sci.*, 37 (1989) 1791.
- [5] R. Mahajan and W. J. Koros, Factors controlling successful formation of mixed-matrix Gas Separation Materials, *Ind. Eng. Chem. Res.*, 39 (2000) 2692.
- [6] J.-M. Duval, B. Folkers, M. H. V. Mulder, G. Desgrandchamps and C. A. Smolders, Adsorbent filled membranes for gas separation. Part 1. Improvement of the gas separation properties of polymeric membranes by incorporation of microporous adsorbents, *J. Membr. Sci.*, 80 (1993) 189.
- [7] S. B. Tantekin-Ersolmaz, Ç. Atalay-Oral, M. Tatlier, A. Erdem-enatalar, B. Schoeman and J. Sterte, Effect of zeolite particle size on the performance of polymer-zeolite mixed matrix membranes, *J. Membr. Sci.*, 175 (2000) 285.
- [8] R. Mahajan and W. J. Koros, Mixed matrix membrane materials with glassy polymers. Part 1, *Polym. Eng. Sci.*, 42 (2002) 1420.
- [9] R. Mahajan and W. J. Koros, Mixed matrix membrane materials with glassy polymers. Part 2, *Polym. Eng. Sci.*, 42 (2002) 1432.
- [10] S. Kulprathipanja, R. W. Neuzil and N. N. Li, Separation of fluids by means of mixed matrix membranes United States Patent 4,740,219 (1988)
- [11] V. N. Popov, Carbon nanotubes: properties and application, *Mater. Sci. Eng. Rep.*, 43 (2004) 61.
- [12] D. M. Ackerman, A. I. Skoulidas, D. S. Sholl and J. K. Johnson, Diffusivities of Ar and Ne in carbon nanotubes, *Mol. Simul.*, 29 (2003) 677.
- [13] A. I. Skoulidas, D. M. Ackerman, J. K. Johnson and D. S. Sholl, Rapid transport of gases in carbon nanotubes, *Phys. Rev. Lett.*, 89 (2002) 185901.
- [14] T. W. Pechar, Fabrication and Characterization of Polyimide-based Mixed Matrix Membranes for Gas Separations, Ph.D. Dissertation, Virginia Tech, Blacksburg (2004).
- [15] E. Dujardin, T. W. Ebbesen, A. Krishnan and M. M. J. Treacy, Purification of single-shell nanotubes, *Adv. Mater.*, 10 (1998) 611.
- [16] J. Liu, A. G. Rinzler, H. Dai, J. H. Hafner, R. K. Bradley, P. J. Boul, A. Lu, T. Iverson, K. Shelimov, C. B. Huffman, F. Rodriguez-Macias, Y. Shon, T. R. Lee, D. T. Colbert and R. E. Smalley, Fullerene pipes, *Science*, 280 (1998) 1253.
- [17] J. Crank, *The Mathematics of Diffusion*, Oxford Press; London (1990).
- [18] D. Breck, *Zeolite Molecular Sieves*, John Wiley & Sons; New York (1974).

Chapter 4. Polysulfone and Functionalized Carbon Nanotube Mixed Matrix Membranes for Gas Separation: Theory and Experiment

4.1.Introduction

Novel membrane technologies can potentially offer economic, environmental, and high performance benefits to virtually any process reliant on gas separations. Currently, gas separation membranes are fabricated from polymeric materials that are typically processed as hollow fibers. However, despite the ability to produce robust, large-area membranes at relatively low cost, a wider implementation of polymer membranes is hindered by their intrinsic permeability and selectivity limitations. These limitations were first identified by Robeson as an upper bound trade-off between permeability and selectivity and later more fully characterized by Freeman.^{1,2} To improve polymeric membrane performance, a considerable research effort has focused on the addition of inorganic materials such as zeolites or carbon molecular sieves to polymers.³⁻¹⁰ These so called mixed matrix membranes (MMM) combine useful molecular sieving properties of inorganic molecular sieves with the desirable mechanical and processing properties of polymers.³⁻⁷ However, the effective incorporation of zeolites in mixed matrix membranes is hindered by poor interfacial compatibility of the zeolite with the polymer, leading to unselective voids in the membrane.^{5,8-11} Attempts to enhance the compatibility between the inorganic and polymeric components by introducing mutually interactive functional groups on the polymer and the molecular sieve have lead to partial blockage of the sieve pores, thus hindering separation performance.^{12,13} Thus, there is a need for alternative molecular sieves whose surface can be modified to increase polymer compatibility without blocking or affecting the pore structure.

Recently, computer simulations have been used to investigate the adsorption,¹⁴⁻²⁰ selectivity,²¹⁻²⁴ and transport properties²⁵⁻⁴² of light gases in single-walled carbon nanotubes (SWNTs). Sholl et al. were the first to predict that transport diffusivities (and hence fluxes) of gases in single walled carbon nanotubes (SWNTs) are orders of magnitude faster than in zeolites having comparable pore sizes.^{25,26} Given the high selectivities theoretically possible due to the precise diameters of the nanotubes, SWNT membranes are a fundamentally new nanoporous material having the potential for transcending Robeson's upper bound. They demonstrated that the exceptionally high transport rates are a result of the inherent smoothness of the nanotubes. Recent computer simulation work by Chen and Sholl have shown that SWNT membranes should be strongly selective for CH₄ over H₂ and if used as membranes should have flux/selectivity properties that far exceed those of any other known membrane materials.⁴³

These theoretical predictions of exceptionally high diffusivities for fluids in carbon nanotubes have recently been experimentally verified by Holt et al., who have constructed nanotube-Si₃N₄ composite membranes using chemical vapor deposition.⁴⁴ They used aligned double walled carbon nanotubes having a diameter of about 1.6 nm. Holt et al. confirmed the theoretical predictions that gas flow through narrow carbon nanotubes is at least one order of magnitude faster than would be expected for flow through a traditional nanoporous material.⁴⁴ They also found that liquid water flow through their nanotube membranes was more than three orders of magnitude faster than expected from hydrodynamic flow and that gas and liquid permeabilities were orders of magnitude higher than those of commercial polycarbonate polymer membranes with larger pores. Moreover, their nanotube membranes exhibited extraordinarily high size

exclusion selectivity.⁴⁴ In a related work, Hinds and coworkers⁴⁵⁻⁴⁹ constructed polymer-nanotube composite membranes using multiwall carbon nanotubes having much larger diameters (6-7 nm) than those used by Holt. They have verified that transport of liquids (alkanes, water) is orders of magnitude faster than can be accounted for by conventional hydrodynamic flow.⁴⁷

However, these initial experiments have not led to the development of a practical membrane material because the methods they used to construct the membranes are not easily scaled up to large-scale production. The main purpose of this study is to construct highly permeable and selective membranes containing carbon nanotubes inside a polymer matrix that could easily be scaled-up to large-area membranes. These novel nanocomposite membranes consist of well-dispersed SWNTs inside a commercial polysulfone (PSF) matrix. The SWNTs were functionalized with long chain alkyl amines to facilitate the dispersion and were added to the matrix in different amounts. The structure, the absence of defects, and the properties of the SWNT/PSF MMMs were characterized by field emission scanning microscopes (FESEM), dynamic mechanical testing, sorption studies, and gas permeation measurements.

We present atomistic simulation studies of gas sorption in SWNT bundles in order to compare with experimental sorption measurements presented here. Comparison of experiments and simulations help characterize the SWNT samples used in the experiments and provide an estimate for the fraction of nanotubes that are opened and accessible to sorption of gases.

4.2. Experimental and Characterization Method

4.2.1. Functionalization of Carbon Nanotubes

Electric arc-discharged and HiPco SWNTs were purchased from Carbon Solutions, Inc. (Riverside, CA) and Carbon Nanotechnologies, Inc. (Huston, TX), respectively. Raw carbon nanotube materials produced by electric arc method were treated by multistage purification (a combination of wet-oxidation and acid treatments) to purify SWNTs from impurities. The purified samples were cut into small lengths with 3:1 mixture of concentrated H_2SO_4 (98 vol%): HNO_3 (70% vol%) solution. The details of the purification and cutting method are described elsewhere.⁵⁰⁻⁵³ HiPco SWNTs were purified by a two-step purification procedure. The first step was to debundle the nanotube ropes using a dimethylformamide (DMF)/ethylene diamine (EDA) treatment. The second step involved a combination of HCl treatment and wet-oxidation to remove metals and amorphous carbon, thus opening the pores.^{54,55} Nitrogen sorption isotherms at 77 K were carried out to characterize the pore structure. Table 1 summarizes the pore properties of the raw and purified SWNTs. The surface areas were calculated using the Brunauer-Emmett-Teller (BET) method⁵⁶, and the micropore volumes, total pore volume (including the meso-pore volume), and pore diameters were calculated by the t-plot,⁵⁷ Barret-Joyner-Halenda (BJH)⁵⁸ method, and Horvath-Kawazoe (H-K) model for cylindrical pores,⁵⁹ respectively. After purification of the SWNTs, the surface area, micropore volume, and total pore volume increased without changing the pore size distribution.

To produce soluble SWNTs, we formed an octadecylammonium (ODA) and SWNT-Carboxylate zwitterions by the following procedure.^{60,61} Shortened SWNTs were heated with ODA at 393 K for 96 hours. After cooling to room temperature, the black-colored

ODA and SWNTs mixture was washed with tetrahydrofuran (THF) and filtered through a membrane filter (0.2 μm). Because unreacted ODA was expected to block the entrance to the channels of SWNTs, ODA was further removed by Soxhlet extraction in ethanol at 393 K for 10 days.

Table 4-1. Pore properties of SWNTs

	Surface area, $\text{m}^2/\text{g}^{\text{i}}$	Micropore volume, $\text{cm}^3/\text{g}^{\text{ii}}$	Total pore volume, $\text{cm}^3/\text{g}^{\text{iii}}$	Pore diameter, nm^{iv}
Raw electric arc SWNTs	174	0.006	0.23	1.2 ± 0.2
Raw HiPco SWNTs	281	0.003	0.77	1.5 ± 0.3
Purified electric arc SWNTs	464	0.051	0.63	1.2 ± 0.2
Purified HiPco SWNTs	1032	0.165	0.83	1.5 ± 0.3

i: BET surface area
ii:t-plot
iii: BJH pore volume
iv:H-K method

4.2.2. Fabrication of PSF Membrane

Before fabrication of membranes, PSF (UDEL P-3500, Solvay) was degassed at 413 K for 3 hours under vacuum to remove adsorbed water. Then, 0.6 g of the PSF was dissolved in 3 mL of chloroform and stirred for one day leading to a viscous solution. The membranes were cast onto a glass substrate using a Doctor Blade from Paul N. Gardner Company. The glass substrate was covered with a glass cover to slow the evaporation of solvent, allowing for a film with a uniform thickness without curling. The

solutions were given 1 day to dry at room temperature. Once dry, the films were placed under vacuum and the temperature was raised to its glass transition temperature, 458 K for 1 hour and then cooled down to room temperature. A 6.35 cm diameter circular sample was cut from the film and used for permeation tests.

4.2.3. Fabrication of Functionalized Carbon Nanotube-Polysulfone MMMs

For economic reason, we used the electric arc-discharged SWNTs in the fabrication of nano-composite membranes. The fabrication procedure for the mixed matrix membranes was identical to the pure polymer membrane preparation with the additional step of incorporating SWNTs. For a 10 wt % of functionalized SWNTs/PSF MMMs, approximately 0.45 g of the pure PSF was dissolved in 3 mL of chloroform and mixed for 24 hours. A predetermined mass of the purified SWNTs (0.05 g) was dissolved in 4.5 g of chloroform. This SWNT solution was added to the polymer solution and the mixture was allowed to mix for 6 hours at room temperature. Following this time period, the mixture was sonicated for 10 minutes and allowed to mix for 10 minutes. This process was repeated several times. The membranes were cast onto a glass substrate using a Doctor Blade. The evaporation and heat treatments for the mixed matrix membranes were identical to that of the pure polymer membrane.

4.2.4. Characterization

A BioRad FTS-40A FTIR spectrometer was used to obtain the IR spectra of the functionalized SWNTs. FESEM (LEO 1550) was used to study the morphology of the membranes. Dynamic mechanical thermal analysis (DMTA) measurements were carried

out on a Rheometrics DMTA IV. All experiments were performed with a 1 Hz frequency, 0.1% strain, and 2 K/min heating rate.

Sorption studies were conducted on an IGA-002 gravimetric system (Hidden Isochema, UK). For each measurement, the samples were degassed at 403 K for 10 hours at $P \leq 10^{-6}$ mbar. All tubings and chambers were also degassed by applying vacuum ($P \leq 10^{-6}$ mbar). The degassed samples were then cooled down to the specified temperature (308 K) with a ramping rate of 1 K /min. The gases used in this research were Air Products He, CO₂, O₂, N₂, and CH₄ with a reported purity of 99.99% and purified again by passing through a molecular sieve trap attached to the gravimetric system. The adsorption isotherms were measured by a small stepwise pressure (or concentration) change, i.e. 100 mbar ($P \leq 1.3$ bar) and 250 mbar ($P > 1.3$ bar). The gravimetric sorption studies in this research were conducted at a temperature of 308 ± 0.1 K and pressure range of 0.01 – 18 bar.

Kinetic diffusion coefficients were calculated from the mass uptake curves (M_t/M_∞) by fitting them Fick's second law for the sorption of a penetrant in film as described by Crank.⁶²

$$\frac{M_t}{M_\infty} = 1 - \frac{8}{\pi^2} \sum_{n=0}^{\infty} \frac{1}{(2n+1)^2} \exp\left[-\frac{D(2n+1)^2 \pi^2 t}{l^2}\right] \quad (1)$$

where M_t and M_∞ represent the amount of gas absorbed by the membrane film at time t and the equilibrium sorption after infinite time, respectively. D is the kinetic (transport) diffusion coefficient, t is the time required to attain M_t and l is the thickness of the sample.

Permeabilities of the polymeric and composite membranes were measured using a constant volume varying pressure apparatus. Permeability was measured directly, and the Time Lag Method was applied to the recorded data to determine the diffusion coefficients.⁶² The solubility coefficients were taken as the ratio of the permeability to diffusivity. The feed pressure and temperature were kept constant at 4 atm and 308 K, respectively, for all experiments. Each gas was run through a membrane six times and the average results and the standard deviations were recorded. Permeabilities are reported in units of Barrer ($1 \text{ Barrer} = 1 \times 10^{-10} \text{ cm}^3 \cdot (\text{STP}) \cdot \text{cm} / (\text{cm}^2 \cdot \text{sec} \cdot \text{cmHg})$).

4.3. Molecular Simulations

The grand canonical Monte Carlo simulation technique⁶³ was used to model the gas adsorption process in SWNT bundles. The atomically detailed modeling employed gas potentials taken from the literature. The H₂ potential used in this work has the Lennard-Jones (LJ) form and was developed by Buch.⁶⁴ The well depth and diameter parameters are $\epsilon=34.2 \text{ K}$ and $\sigma=0.296 \text{ nm}$, respectively. The LJ parameters used for methane are $\epsilon=161.35 \text{ K}$ and $\sigma=0.372 \text{ nm}$.⁶⁵ The O₂ potential was a two-site LJ model, with an O-O bond length of 0.1208 nm , $\epsilon=52 \text{ K}$, and $\sigma=0.299 \text{ nm}$.⁶⁶ The CO₂ model used in this work is the EPM2 potential developed by Harris and Yung.⁶⁷ The solid-fluid potentials invoked graphene LJ potential parameters from Steele,⁶⁸ $\epsilon=28.0 \text{ K}$ and $\sigma=0.34 \text{ nm}$, along with the Lorentz-Berthelot combining rules. Potentials were truncated at $> 15 \text{ \AA}$, the simulation cell was greater than 30 \AA with imposed periodic boundary conditions. The number of molecules adsorbed in a system was calculated as a function of the chemical potential

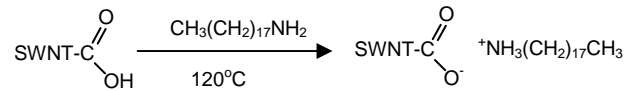
(bulk pressure) of the gas. Total (absolute) adsorption, N_{tot} , was computed in the simulations and excess amount adsorbed, N_{ex} , was calculated from

$$N_{\text{ex}} = N_{\text{tot}} - V_{\text{free}} \rho_{\text{bulk}} \quad (2)$$

where V_{free} is the volume not occupied by the nanotubes and ρ_{bulk} is the number density of the gas in the bulk. The excess adsorption isotherms calculated from simulations can be directly compared with experimentally measured isotherms. Simulation cells contained from 100s to 1000s of adsorbed gas molecules, depending on the pressure.

4.4. Results and Discussion

Soluble SWNTs were produced by forming ODA and SWNT-carboxylate zwitterions by the following acid-base reaction:^{60,61}



In the FTIR spectrum of carboxylated SWNTs with a mixture of acids, shown in Figure 4-1a, the peak at $\sim 1714 \text{ cm}^{-1}$ is attributed to the C=O stretch of the carboxylic (COOH) group.^{61,69} After modification of SWNTs with ODA, the FTIR spectrum of the functionalized SWNTs (Figure 1-(b)) shows the disappearance of the band at 1714 cm^{-1} and the appearance of a corresponding band with lower frequency, 1639 cm^{-1} , assigned to the carboxylate group.⁶¹ In addition, new bands at 1547 cm^{-1} appear, corresponding to the N-H in-plane vibration.^{60,69} Similar results for amine-functionalized SWNTs have been previously published in the literature.^{60,61,69,70} These prepared functionalized SWNTs were soluble in chloroform and no precipitation occurred upon prolonged standing.

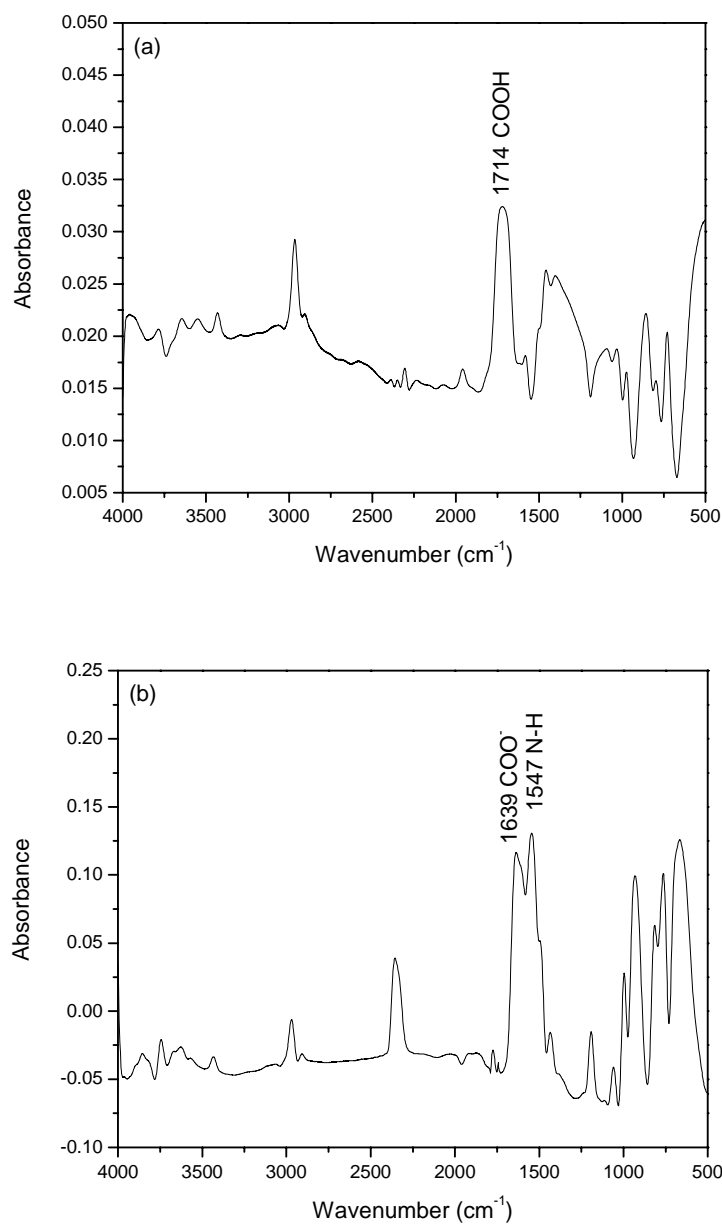


Figure 4-1. FT-IR spectrum of SWNTs samples. (a) carboxylated, and (b) ODA-functionalized.

In order to further investigate the dispersion of the functionalized SWNTs in MMMs, careful FESEM inspections were carried out. The FESEM images of 10 ~ 15 wt % of unmodified and functionalized SWNT/PSF MMMs are shown in Figures 4-2 - 4. In Figure 4-2, the cross sectional FESEM images of the PSF MMMs with the untreated

SWNTs show a nonuniform dispersion, agglomeration and cluster forming of nanotubes in the polymer matrix. At 10 wt % of functionalized SWNT loading, shown in Figure 4-3a, the SWNTs are well distributed throughout the PSF matrix. In addition, Figure 4-3b does not show any agglomerated nanotubes throughout matrix. However, at 15 wt % of SWNTs not all functionalized SWNTs are well distributed throughout the matrix and some carbon nanotubes form rather dense nanotube regions. These regions are evident in Figure 4-4a and b. Despite that, there are still other SWNTs which are well-dispersed in the polymer matrix even at this high concentration as is shown in the higher magnification FESEM image in Figures 4-4c.

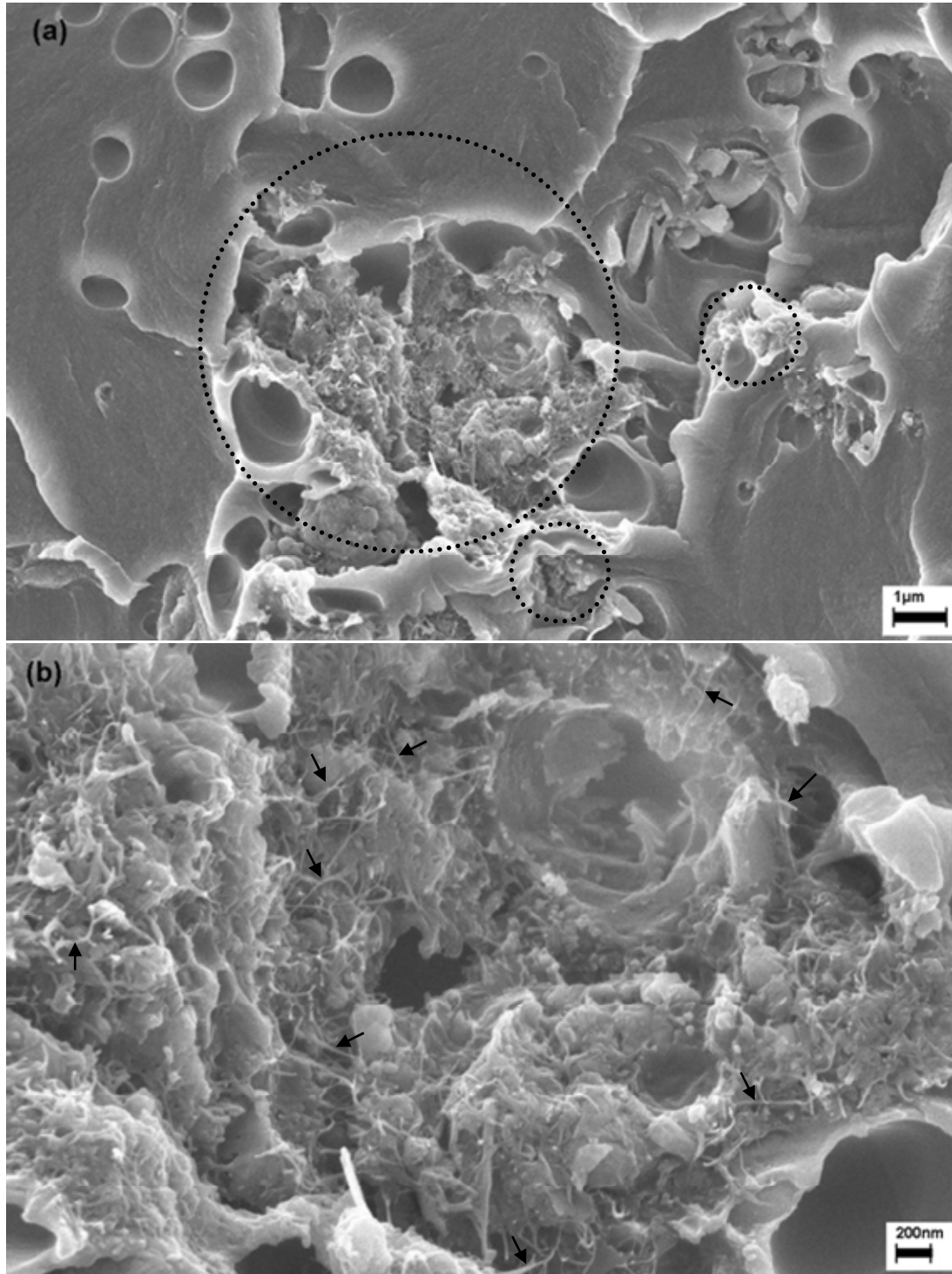


Figure 4-2. Cross-sectional FESEM images of 10 wt % unmodified SWNT/PSF MMMs at (a) lower magnification. Dotted circle indicates cluster forming of nanotubes. (b) higher magnification. Arrow indicates SWNTs in polymer matrix. For clarity, not all visible nanotubes were marked.

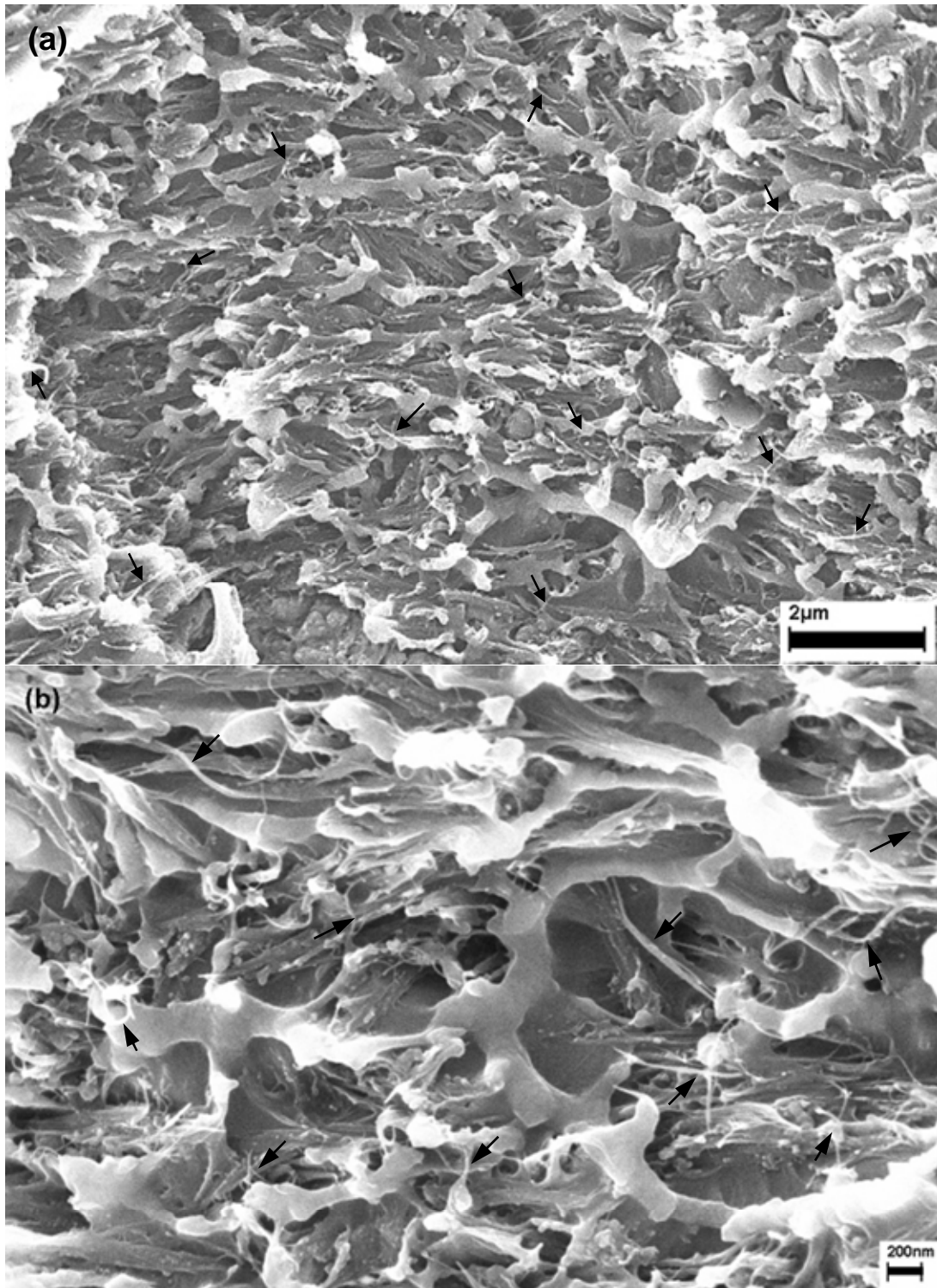


Figure 4-3. Cross-sectional FESEM images of 10 wt % functionalized SWNT/PSF MMMs at (a) lower and (b) higher magnification. Arrow indicates SWNTs in polymer matrix. For clarity, not all visible nanotubes were marked.

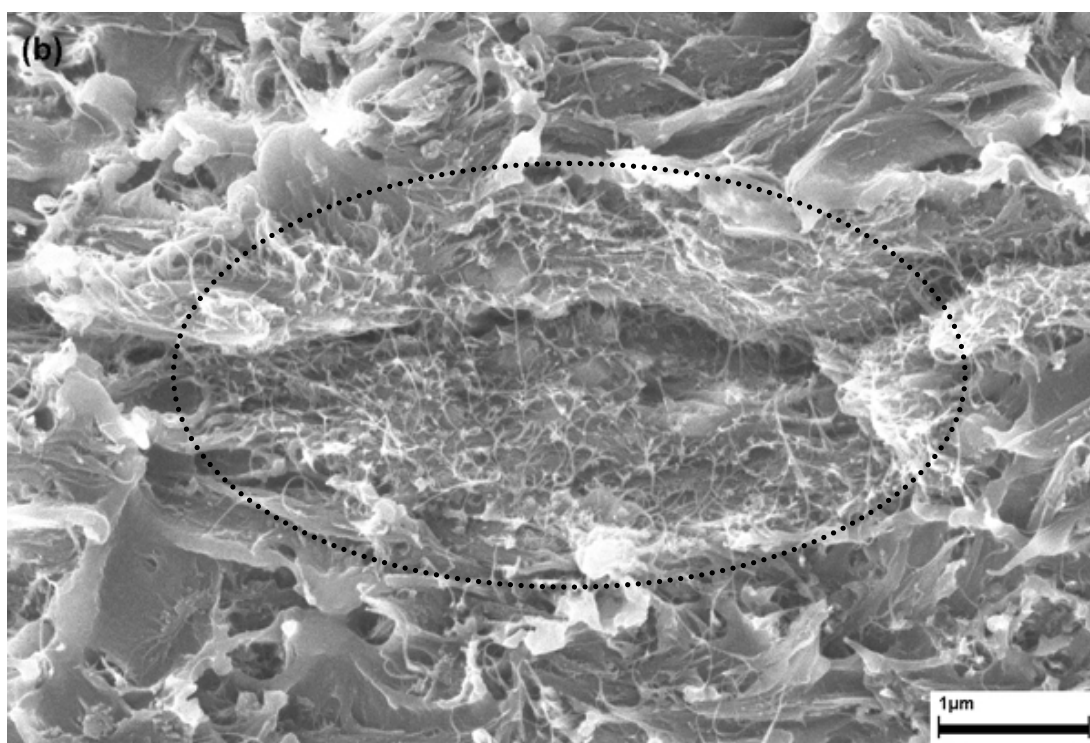
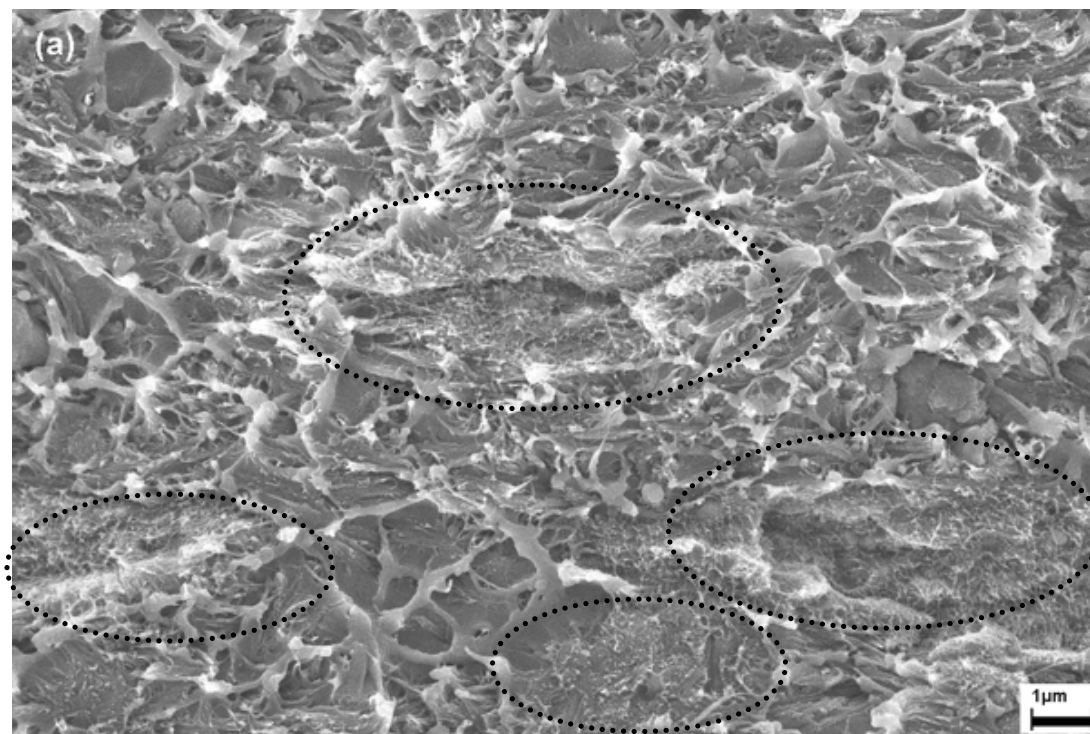


Figure 4-4. FESEM images of 15 wt % functionalized SWNT/PSF MMMs. (a) cross sectional view (lower magnification), (b) dense SWNTs region, and (c) less dense region (higher magnification). Dotted circle and arrow indicates dense SWNTs region and well dispersed SWNTs in polymer matrix, respectively. For clarity, not all visible nanotubes were marked.

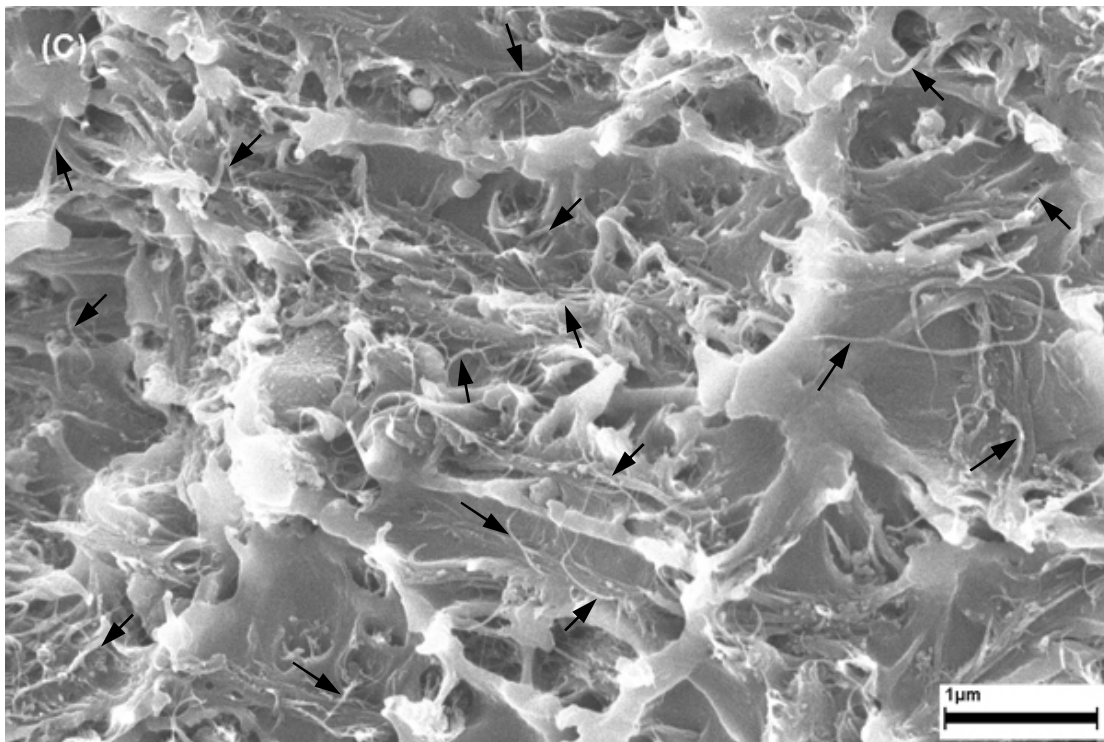
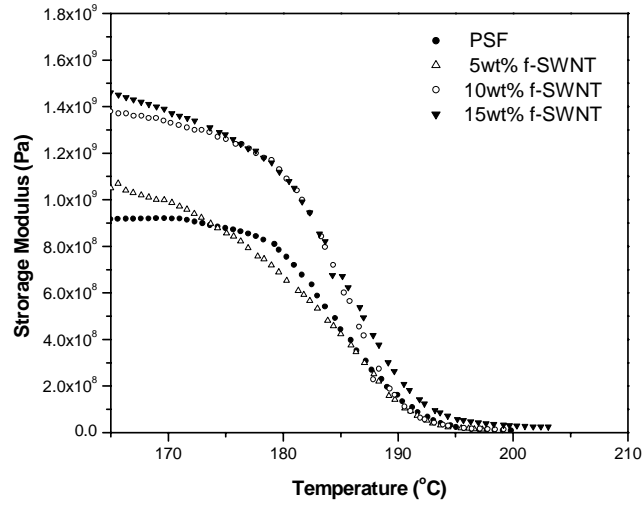
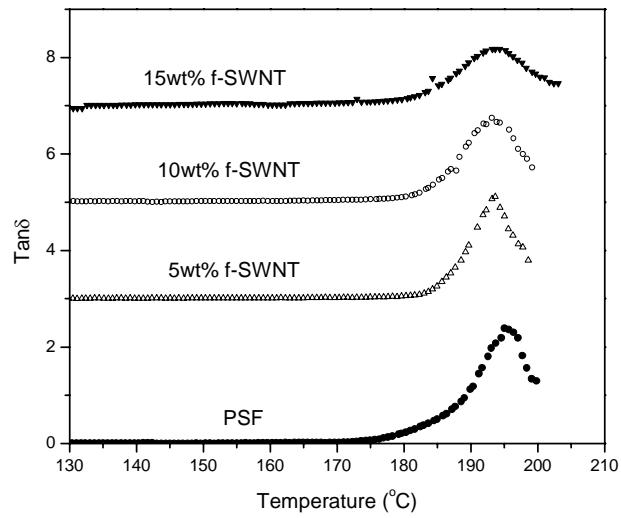


Figure 4-4. FESEM images of 15 wt % functionalized SWNT/PSF MMMs. (a) cross sectional view (lower magnification), (b) dense SWNTs region, and (c) less dense region (higher magnification). Dotted circle and arrow indicates dense SWNTs region and well dispersed SWNTs in polymer matrix, respectively. For clarity, not all visible nanotubes were marked (continued).

DMTA results of PSF and functionalized SWNT/PSF MMMs are shown in Figure 4-5. The storage modulus of PSF increased with increasing carbon nanotube content and the addition of 15 wt% nanotubes caused the storage modulus to increase by approximately 70% as shown in Figure 4-5a. Figure 4-5b shows the behavior of $\tan \delta$ with the addition of the functionalized SWNT. In addition to a small shift to lower T_g , the $\tan \delta$ peak is significantly broadened as the SWNT content increases. Similar effects have been observed in various polymer/carbon nanotube systems by other research groups.⁷¹⁻⁷⁴ The broadening in T_g has been attributed to local heterogeneity in nanocomposites with well-dispersed nanotubes.⁷⁵ Hence, it is possible that the favorable molecular interactions between the SWNTs and the polymer molecules create an interfacial zone of polymer segments with distributions in mobility.⁷¹⁻⁷⁴



(a)



(b)

Figure 4-5. DMTA results for pure polysulfone and functionalized SWNT/PSF MMMs. (a) storage modulus and (b) tan δ .

Adsorption isotherms for various gases at 308 K in SWNTs, measured experimentally and predicted from simulations, are plotted in Figure 4-6. The simulations were performed using a heterogeneous bundle of nanotubes that included large interstitial sites due to imperfect packing of the nanotubes. The bundle contained 45 nanotubes of various diameters. The mean diameter of the tubes in the bundle is about 13.6 Å, which is the diameter of a (10,10) SWNT. Experimental data in Figures 4-6a and 6b demonstrates the differences in sorption capacities between carbon nanotubes produced by the electric arc method and those fabricated via the HiPco process. The latter seems to have sorption capacities in reasonable agreement with those predicted theoretically shown in Figure 4-6c. The trends of the simulated isotherms are in good qualitative agreement with both sets of experiments, showing the same progression of gases increasing in sorption, H₂ showing the lowest uptake, followed by O₂, CH₄, and finally CO₂ having highest sorption. The lower absolute sorption amounts in SWNTs produced by the electric arc method 4-6a in comparison to isotherms on the HiPco nanotubes can be attributed to two factors. The purified electric arc nanotubes are partially closed or blocked by impurities to internal adsorption, which would be consistent with the lower surface area and micropore volume seen in the electric arc nanotubes when compared to the purified HiPco nanotubes. Another possibility is that the carboxylic acid groups created by the acid cutting procedure block the entrance to the interior of the nanotubes. It is known that heating in vacuum is required to remove the functional groups and open the nanotubes to adsorption, in at least some cases.^{51,52}

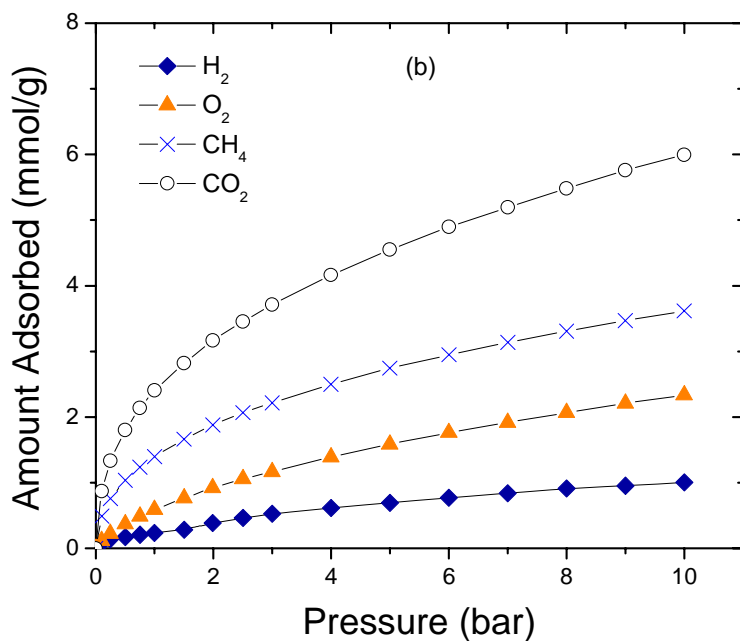
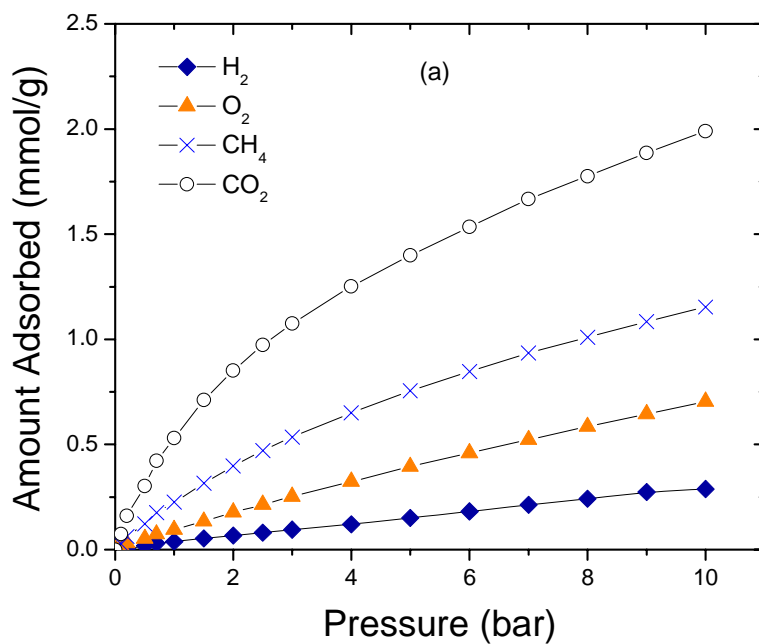


Figure 4-6. Adsorption isotherms for various gases from experiments, (a) and (b), and from simulations, (c). (a) Electric arc-discharged SWNTs purified by the wet-oxidation method, (b) HiPco SWNTs purified by the two-stage purification step, and (c) Atomistic simulations. The density used for the SWNTs in experiments was 1.3 g/cm³ and the sample was assumed to be 100% pure SWNTs by weight.

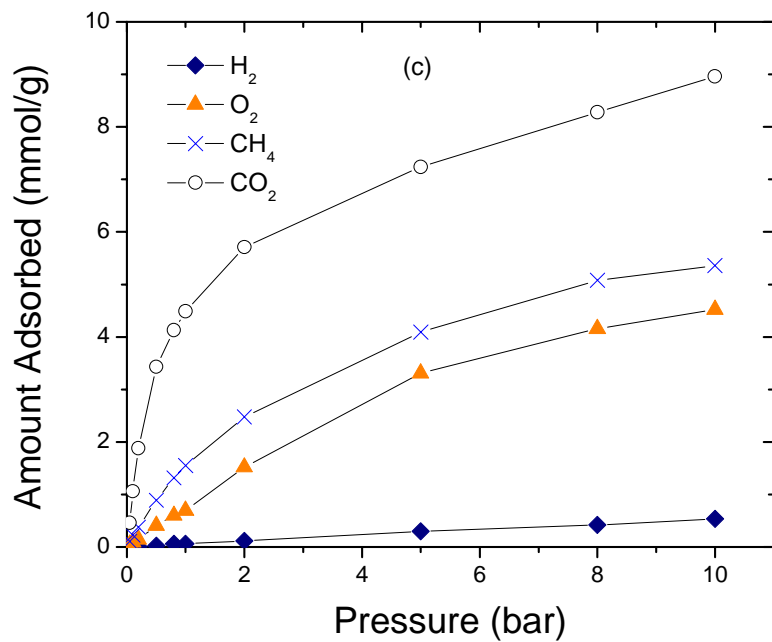


Figure 4-6. Adsorption isotherms for various gases from experiments, (a) and (b), and from simulations, (c). (a) Electric arc-discharged SWNTs purified by the wet-oxidation method, (b) HiPco SWNTs purified by the two-stage purification step, and (c) Atomistic simulations. The density used for the SWNTs in experiments was 1.3 g/cm³ and the sample was assumed to be 100% pure SWNTs by weight (continued).

We have simulated the adsorption of CO₂ at 308 K on closed-ended carbon nanotubes and have plotted our results in Figure 4-7 along with the experimental data for the purified electric arc nanotubes. We used the same heterogeneous nanotube bundle as in Figure 4-6c in our calculations, but not allowing adsorption inside the nanotubes. Thus, adsorption takes place only on the outside of the bundle and in large interstitial defects sites.⁷⁶ The simulated adsorption isotherm shows somewhat higher uptake than the experimental isotherm, indicating that in the real system some interstitial and exterior

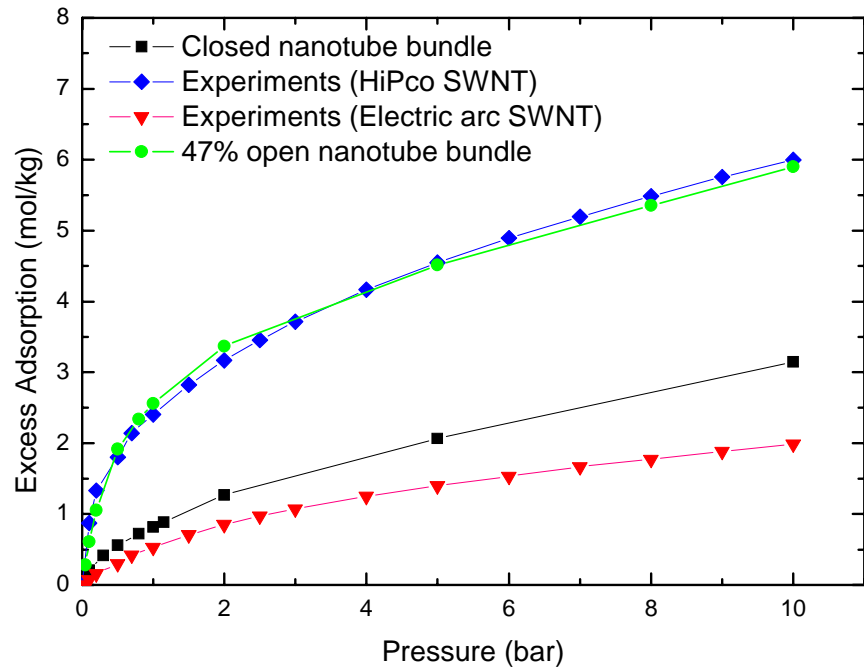


Figure 4-7. Comparison of closed and open nanotubes for adsorption of CO₂ at 308 K. The electric arc experimental data (triangles) are in reasonable agreement with simulations for adsorption onto a bundle of closed nanotubes (squares). The adsorption isotherm for the HiPco nanotubes (diamonds) is in excellent agreement with simulations for a bundle with 47% of the nanotubes opened (circles).

sites may be blocked, perhaps by impurities, amorphous carbon, or residual functional groups. The adsorption isotherm for CO₂ on the HiPco sample is also plotted in Figure 7-7, along with a fit of the simulation data for adsorption onto partially opened nanotubes. The simulation data were fitted adjusting the fraction of nanotubes in the bundle that were opened through a linear least squares method. The best fit was obtained by setting the fraction of open nanotubes to 47%. Our method is similar to that used by Agnihotri et al. to characterize adsorption of gases on HiPco nanotube bundles.¹⁷

Figure 4-8 represents N₂, O₂, and CH₄ sorption isotherms in PSF and PSF containing 2.5, 5, and 15 wt% functionalized SWNTs at 308 K. The dashed line in Figure 8 represents the predicted gas uptake for PSF containing 15 wt% functionalized SWNTs based on the pure materials (PSF and SWNTs) and the additive solubility model.⁷⁷ As shown in Figure 4-8, the amount of gas absorbed in mixed matrix films for each gas depends on the SWNTs content. However, the relative increase in gas absorption is small at 15 wt% of SWNT loading in comparison to the increases seen at 2.5 and 5 wt% of nanotube loading. In addition, the measured values for N₂ and O₂ at 15 wt% nanotube loading are lower than the values predicted by additive model. From DMTA data, it has been implied that the interaction between the SWNT and the polymer molecules can create an interfacial zone with reoriented polymer chains with different mobility. These results suggest that while the presence of SWNT increases the relative sorption of gases in the membrane, at higher SWNT contents, this increase may be countered by constrained polymer chain packing at the SWNT/polymer interface.

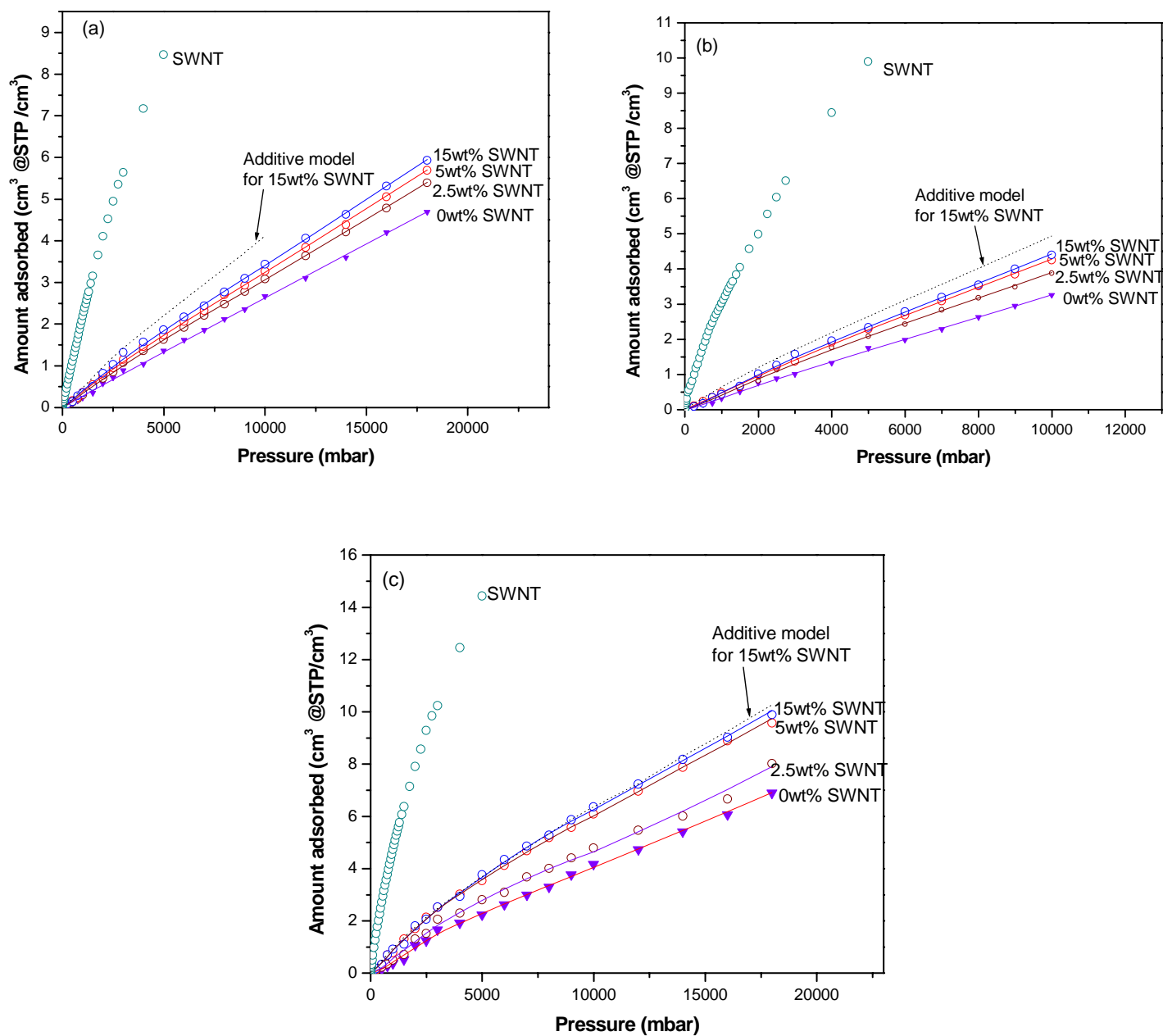


Figure 4-8. Adsorption isotherms on 0 wt%, 2.5 wt%, 5 wt%, 10 wt% functionalized SWNT/PSF MMMs, and SWNT. (a) N₂ (b) O₂, and (c) CH₄.

The permeability results for the functionalized SWNT and PSF MMMs are shown in Table 4-2. Because of different polymer processing and film preparation history, the permeability values for pure PSF membranes are somewhat lower than those previously reported by other research groups.⁷⁸ The addition of 5 wt% of SWNT loading to PSF resulted in ~30 % increases in permeability of He and CO₂, while permeability of O₂, N₂ and CH₄ increased ~40% and 60%, respectively. However, there were slight increases in permeability as SWNT loading in polymer matrix increased from 5 wt% to 10 wt%. The permeability for gas molecules such as He, CO₂, O₂, and N₂ decreased as SWNT loading in polymer matrix increased from 10 wt% to 15 wt%. For the CH₄, the permeability did not change at 15 wt% of SWNT loading. From FESEM data, SWNTs are well dispersed in polymer matrix at 5 and 10 wt% loading, whereas not all functionalized nanotubes are well distributed through matrix at 15 wt% of SWNT loading. At lower loadings, nanotubes are well dispersed in the polymer matrix and all gas molecules pass through the SWNT tunnels which provide high permeability. However, at higher SWNT loading, it is possible that the tortuosity around the agglomerated SWNT domains limits further permeability increases.

Table 4-2. Gas permeabilities (Barrer) of various gases in the pure polysulfone and functionalized SWNT MMMs

Membrane	He	CO ₂	O ₂	N ₂	CH ₄
PSF	7.88±0.01	3.90±0.05	0.84±0.00	0.17±0.01	0.17±0.01
5 wt % SWNT /PSF	10.20±0.00 (29.44%) ^a	5.12±0.04 (31.28%)	1.16±0.00 (38.10%)	0.23±0.00 (35.29%)	0.27±0.00 (58.82%)
10 wt % SWNT /PSF	10.27±0.02 (30.33%)	5.19±0.00 (33.08%)	1.23±0.00 (46.43%)	0.23±0.04 (35.29%)	0.28±0.00 (64.71%)
15 wt % SWNT /PSF	8.88±0.56 (12.69%)	4.52±0.02 (15.90%)	1.11±0.01 (32.14%)	0.22±0.00 (29.41%)	0.28±0.00 (64.71%)

^a () increment from pure polymer

$$1 \text{ Barrer} = 1 \times 10^{-10} \cdot \frac{\text{cm}^3(\text{STP}) \cdot \text{cm}}{\text{cm}^2 \cdot \text{sec} \cdot \text{cmHg}}$$

Table 4-3. Diffusivity (10⁻⁸, cm²/sec) of various gases in the pure polysulfone and SWNT MMMs

	CO ₂	O ₂	N ₂	CH ₄
PSF	1.17±0.01	3.03±0.05	1.24±0.00	0.30±0.01
5wt% SWNT	2.10±0.01 (79.49%)	5.45±0.42 (79.87%)	1.70±0.08 (37.10%)	0.54±0.00 (80.00%)
10wt% SWNT	2.12±0.02 (95.00%)	6.48±0.51 (113.86%)	1.83±0.03 (47.58%)	0.55±0.01 (83.33%)
15wt% SWNT	1.97±0.01 (68.38%)	5.54±0.11 (82.84%)	1.94±0.06 (56.45%)	0.55±0.00 (83.33%)

The differences in permeabilities of each MMMs can be better understood by analyzing the contributions of diffusivity and solubility coefficients to the overall permeabilities. The diffusion coefficients calculated by time-lag method are shown in Table 4-3. Helium diffusion coefficients are not reported for any of the membranes here. This is because the diffusion of He is fast and the time lag method introduces too much error.⁶² After incorporation of 5 wt% functionalized SWNTs to the polymer, diffusion

coefficients for CO₂, O₂, and CH₄ increased by around 80%, and by 37% for N₂. At 10 wt% SWNTs loading in the polymer matrix, the diffusivities of all gases increased further, for example up to 114% for O₂. However, at 15wt% SWNTs the diffusivities for some gases were lower than those observed at 10wt% SWNT. The reasons for this are not presently clear. For comparison, kinetic diffusion coefficients were also calculated from sorption data. Figure 4-9 presents CO₂ kinetic sorption fractional uptake curves in PSF containing 0 wt%, 5 wt% and 15 wt% SWNTs. The CO₂ sorption uptake curves reached their equilibrium rapidly at 5 wt% SWNTs loading. However, at 15 wt% SWNTs loading in PSF, the slope of the CO₂ sorption curve is identical to that of the 5 wt% SWNT loading sample. Figure 4-10 shows CO₂ diffusion coefficients in PSF and SWNT/PSF composite films determined from the kinetic sorption studies. Also included in this figure are the diffusion coefficients calculated from time-lag method for comparison. Although the absolute values of the diffusion coefficients obtained by the time-lag and kinetic sorption methods are different,⁷⁹ qualitatively the changes are consistent. Typically, kinetic diffusion coefficients measured by gravimetric sorption method are lower than those obtained by the time-lag method. This discrepancy results because kinetic (transient) uptake experiments involve additional diffusion into the dead-end pores, while transport through dead-end pores does not play a role in steady-state permeation (time-lag) experiments.⁸⁰

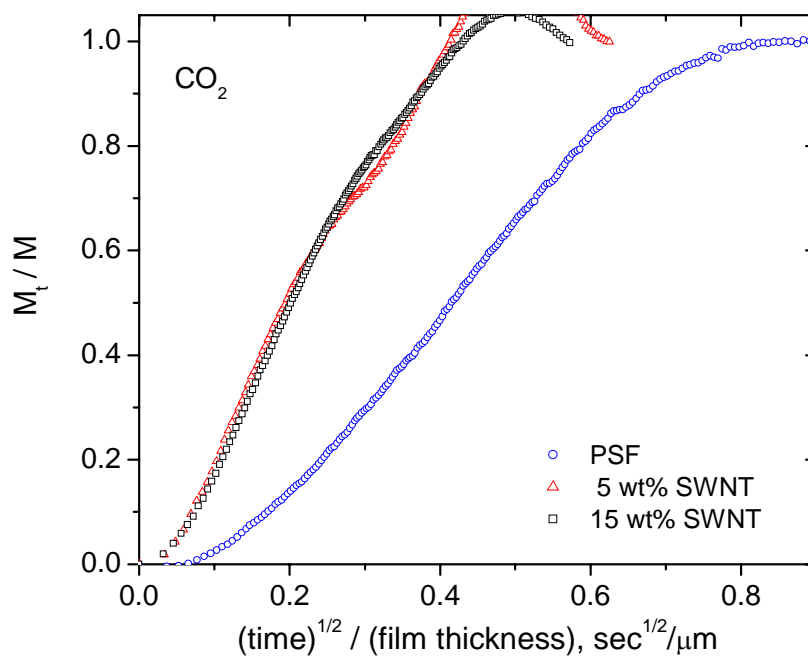


Figure4-9. CO₂ kinetic uptake curves curves in SWNT/PSF MMMs at 308 K and 0.1 bar.

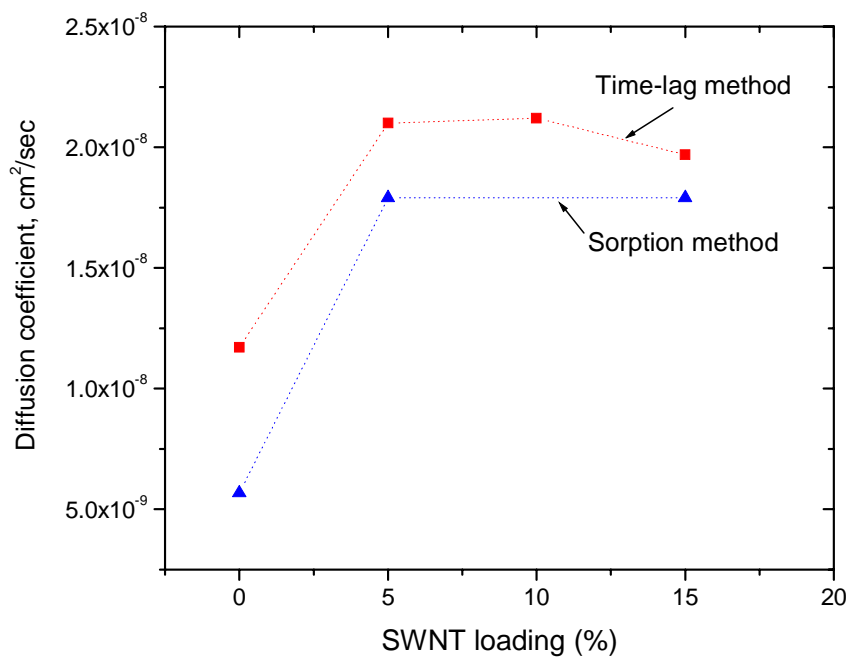


Figure 4-10. CO₂ diffusion coefficients in SWNT/PSF MMMs at 308 K.

The solubility coefficients calculated from time-lag method as well as sorption measurements for CO₂, O₂, N₂, and CH₄ are shown in Figure 4-11. Despite increases in permeability and diffusivity, the solubility derived from time lag method and the kinetic gravimetric method remained relatively unchanged. These results are consistent with the separate gravimetric sorption measurements shown in Figures 4-8(a-c), which indicate very little change in sorption capacity at 4 atm with the addition of SWNTs. However, larger sorption differences between the pure polysulfone and the mixed matrix membranes can be inferred as the pressure is increased over 10 bar. As seen in Figures 4-8(a-c), the sorption capacity of the mixed matrix membranes having 15 wt% SWNTs approaches the sorption predicted by a simple series model.

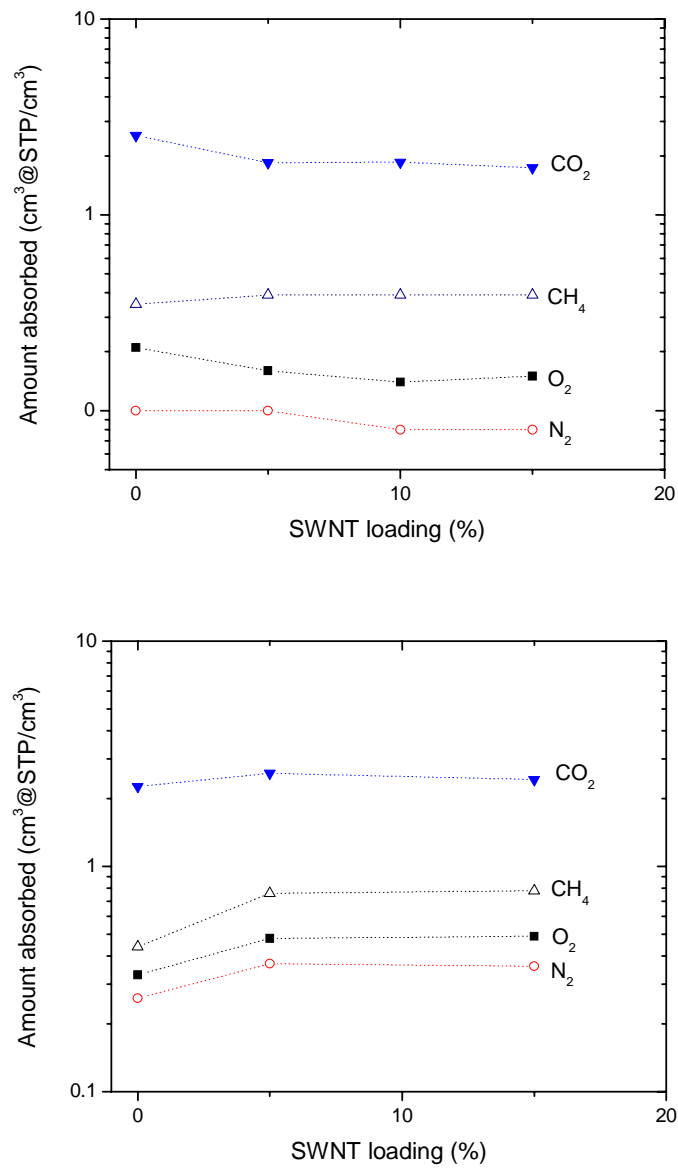


Figure 4-11. Solubility coefficients of SWNT/PSF MMMs at 308 K and 4 bar from (a) time-lag, and (b) gravimetric sorption method.

Table 4-4. Selectivity for polysulfone and functionalized SWNT MMMs

Membrane	He/CH ₄	CO ₂ /CH ₄	O ₂ / N ₂	CH ₄ / N ₂
PSF	47.50	23.55	5.07	1.00
5 wt % SWNT /PSF	37.51	18.82	5.04	1.17
10 wt % SWNT /PSF	36.43	18.41	5.35	1.21
15 wt % SWNT /PSF	31.66	16.09	5.10	1.27

Table 4-4 shows ideal separation factors for the functionalized SWNTs and PSF MMMs. The separation factors for He/CH₄ and CO₂/CH₄ decreased in proportion to the amount of SWNTs in the polymer matrix. The observed decrease in He/CH₄ selectivity agrees well with the selectivity and flux for CH₄/H₂ separations in SWNTs membrane calculated by atomistic simulations by Sholl et al.⁴³ This simulation study argues that SWNT membranes should be strongly selective for CH₄ over H₂ and should exhibit very large fluxes because of the significant adsorption selectivity for CH₄ over H₂ and extremely fast diffusion of gas molecules adsorbed inside SWNTs. From experimental and calculated absorption data for SWNT, nanotubes do show higher absorption capacity for CH₄ over H₂, O₂, and N₂. Again this was seen in Table 4-2, which showed an increase in CH₄ permeability to be ~60%, while He permeability increased by 30% at 5 wt% of SWNT loading. Hence, ideal separation factors for He/CH₄ and CO₂/CH₄ decreased with the addition of SWNT due to preferential sorption of CH₄ in the SWNT. Similarly, the CH₄/N₂ separation factor increased as the amount of SWNT increased because of higher adsorption capacity for CH₄ over N₂. Despite increases in permeability of O₂ and N₂, the

O₂/N₂ separation factor remained virtually unchanged because SWNT are not selective for either O₂ or N₂. In addition, constant O₂/N₂ separation factor in MMMs suggests that the prepared membranes do not have any unselective voids at the SWNTs/PSF interface.

4.5. Conclusions

Nanocomposite membranes were prepared using SWNTs functionalized with ODA and a polysulfone as the polymer matrix. The modified nanotubes dispersed well in the polymer matrix as well as in chloroform. The FESEM for the cross sectional area images of MMM films indicated that SWNTs were well dispersed in the polymer matrix at a loading of 5 wt% SWNTs, while at 15 wt% the tubes formed two domains in the copolymer matrix: a well dispersed SWNTs region and a dense SWNTs region. DMTA and gas adsorption results suggested the presence of an interfacial zone between the SWNTs and the polymer matrix, possibly consisting of constrained polymer segments. However, the permeability performance of the prepared MMMs mainly depended on the addition of carbon nanotubes rather than the effect of interfacial zone because the O₂/N₂ separation factor was constant for all membranes. Overall increases in permeance and diffusivity for all tested gases suggested that carbon nanotubes can provide high diffusivity tunnels in the SWNTs within the PSF matrix. In addition, the observed decreases in He/CH₄ selectivity agree well with H₂/CH₄ selectivities in SWNTs predicted by atomistic simulations.

This is the first report of the gas-transport properties of nanocomposite membranes using the functionalized SWNT and a commercial polymer. It is clear that addition of SWNTs to a polymer matrix can improve certain selectivities as well as permeabilities of

small molecules. However, the true potential of these membranes will be realized when carbon nanotubes, having tube diameters less than 10 Å are incorporated into the polymer matrix. Then the combination of size-selectivity and high permeability should propel the performance of these nano-composite membranes above Robeson's upper bound.¹

4.6. References

- [1] L. M. Robeson, Correlation of separation factor versus permeability for polymeric membranes, *J. Membr. Sci.*, 62 (1991) 165.
- [2] B. D. Freeman, Basis of Permeability/selectivity tradeoff relations in polymeric gas separation membranes, *Macromolecules*, 32 (1999) 375
- [3] W. J. Koros and R. Mahajan, Pushing the limits on possibilities for large scale gas separation: which strategies? , *J. Membr. Sci.*, 175 (2000) 181.
- [4] R. Mahajan and W. J. Koros, Factors Controlling Successful Formation of Mixed-Matrix Gas Separation Materials, *Ind. Eng. Chem. Res.*, 39 (2000) 2692.
- [5] W. J. Koros and R. Mahajan, Mixed matrix membrane materials with glassy polymers. Part 1, *Polym. Eng. Sci.*, 42 (2002) 1420
- [6] W. J. Koros and R. Mahajan, Mixed matrix membrane materials with glassy polymers. Part 2, *Polym. Eng. Sci.*, 42 (2002) 1432
- [7] S. Kulprathipanja, R. W. Neuzil and N. N. Li, Separation of fluids by means of mixed matrix membranes, U.S. Patent 4,740,219 (1988)
- [8] J.-M. Duval, A. J. B. Kemperman, B. Folkers, M. H. V. Mulder, G. Desgrandchamps and C. A. Smolders, Preparation of zeolite filled glassy polymer membranes, *J. Appl. Polym. Sci.*, 54 (1994) 409.
- [9] J.-M. Duval, B. Folkers, M. H. V. Mulder, G. Desgrandchamps and C. A. Smolders, Adsorbent filled membranes for gas separation. Part 1. Improvement of the gas separation properties of polymeric membranes by incorporation of microporous adsorbents, *J. Membr. Sci.*, 80 (1993) 189.
- [10] M. G. Sürer, N. Baç and L. Yilmaz, Gas permeation characteristics of polymer-zeolite mixed matrix membranes, *J. Membr. Sci.*, 91 (1994) 77.
- [11] Fundamental and practical aspects of mixed matrix gas separation membranes, *Polymer Membranes for Gas and Vapor Separation*, in B. Freeman and I. Pinnau (Ed.), ACS Symposium Series, 1999, pp. 277-286.
- [12] T. W. Pechar, S. Kim, B. Vaughan, E. Marand, V. Baranauskas, J. Riffle, H. K. Jeong and M. Tsapatsis, Preparation and characterization of a poly(imide siloxane) and zeolite L mixed matrix membrane, *J. Membr. Sci.*, 277 (2006) 210.
- [13] T. W. Pechar, S. Kim, B. Vaughan, E. Marand, M. Tsapatsis, H. K. Jeong and C. J. Cornelius, Fabrication and characterization of polyimide-zeolite L mixed matrix membranes for gas separations, *J. Membr. Sci.*, 277 (2006) 195.
- [14] Q. Wang and J. K. Johnson, Molecular simulation of hydrogen adsorption in single-walled carbon nanotubes and idealized carbon slit pores, *J. Chem. Phys.*, 110 (1999) 577.
- [15] V. V. Simonyan, P. Diep and J. K. Johnson, Molecular simulation of hydrogen adsorption in charged single-walled carbon nanotubes, *J. Chem. Phys.*, 111 (1999) 9778.
- [16] M. M. Calbi, F. Toigo and M. W. Cole, Dilation-Induced Phases of Gases Absorbed within a Bundle of Carbon Nanotubes, *Phys. Rev. Lett.*, 86 (2001) 5062–5065.
- [17] S. Agnihotri, J. P. B. Mota, M. Rostam-Abadi and M. J. Rood, Structural characterization of single-walled carbon nanotube bundles by experiment and molecular simulation, *Langmuir*, 21 (2005) 896.

- [18] P. Kondratyuk, Y. Wang, J. K. Johnson and J. T. Yates, Observation of a one-dimensional adsorption site on carbon nanotubes: Adsorption of alkanes of different molecular lengths, *J. Phys. Chem. B*, 109 (2005) 20999.
- [19] S. Rols, M. R. Johnson, P. Zeppenfeld, M. Bienfait, O. E. Vilches and J. Schneble, Argon adsorption in open-ended single-wall carbon nanotubes, *Phys. Rev. B*, 71 (2005) 155411.
- [20] A. Striolo, K. E. Gubbins, A. A. Chialvo and P. T. Cummings, Simulated water adsorption isotherms in carbon nanopores, *Molecular Phys.*, 102 (2004) 243.
- [21] S. R. Challa, D. S. Sholl and J. K. Johnson, Adsorption and separation of hydrogen isotopes in carbon nanotubes: multicomponent grand canonical Monte Carlo simulations, *J. Chem. Phys.*, 116 (2002) 814.
- [22] G. Arora, N. J. Wagner and S. I. Sandler, Adsorption and diffusion of molecular nitrogen in single wall carbon nanotubes, *Langmuir*, 20 (2004) 6268.
- [23] J. W. Jiang, Pore size or geometry: Which determines the shape and inverse-shape selective adsorption of alkane isomers?, *J. Phys. Chem. B*, 110 (2006) 8670.
- [24] J. W. Jiang and S. I. Sandler, Monte Carlo simulation for the adsorption and separation of linear and branched alkanes in IRMOF-1, *Langmuir*, 22 (2006) 5702.
- [25] D. M. Ackerman, A. I. Skoulidas, D. S. Sholl and J. K. Johnson, Diffusivities of Ar and Ne in carbon nanotubes, *Mol. Simul.*, 29 (2003) 677.
- [26] A. I. Skoulidas, D. M. Ackerman, J. K. Johnson and D. S. Sholl, Rapid transport of gases in carbon nanotubes, *Phys. Rev. Lett.*, 89 (2002) 185901.
- [27] D. A. Newsome and D. S. Sholl, Influences of interfacial resistances on gas transport through carbon nanotube membranes, *Nano Lett.*, 6 (2006) 2150.
- [28] K. T. Adjemian, R. Dominey, L. Krishnan, H. Ota, P. Majsztrik, T. Zhang, J. Mann, B. Kirby, L. Gatto, M. Velo-Simpson, J. Leahy, S. Srinivasan, J. B. Benziger and A. B. Bocarsly, Function and Characterization of Metal Oxide-Nafion Composite Membranes for Elevated-Temperature H₂O₂ PEM Fuel Cells, *Chem. Mater.*, 18 (2006) 2238.
- [29] S. Jakobtorweihen, C. P. Lowe, F. J. Keil and B. Smit, A novel algorithm to model the influence of host lattice flexibility in molecular dynamics simulations: Loading dependence of self-diffusion in carbon nanotubes, *J. Chem. Phys.*, 124 (2006) 154706/1.
- [30] K. H. Lee and S. B. Sinnott, Comparison of CH₄ and O₂ transport through opened carbon nanotubes: Predictions from molecular dynamics simulations, *Inter. J. Multi. Comp. Eng.*, 3 (2005) 379.
- [31] S. Jakobtorweihen, M. G. Verbeek, C. P. Lowe, F. J. Keil and B. Smit, Understanding the loading dependence of self-diffusion in carbon nanotubes, *Phys. Rev. Lett.*, 95 (2005) 044501.
- [32] K. H. Lee and S. B. Sinnott, Equilibrium and nonequilibrium transport of oxygen in carbon nanotubes, *Nano Lett.*, 5 (2005) 793.
- [33] K. H. Lee and S. B. Sinnott, Computational studies of non-equilibrium molecular transport through carbon nanotubes, *J. Phys. Chem. B*, 108 (2004) 9861.
- [34] J. J. Ge, H. Hou, Q. Li, M. J. Graham, A. Greiner, D. H. Reneker, F. W. Harris and S. Z. D. Cheng, Assembly of well-aligned multiwalled carbon nanotubes in confined polyacrylonitrile environments: electrospun composite nanofiber sheets, *J. Am. Chem. Soc.*, 126 (2004) 15754.

- [35] D. P. Cao and J. Z. Wu, Self-diffusion of methane in single-walled carbon nanotubes at sub- and supercritical conditions, *Langmuir*, 20 (2004) 3759.
- [36] V. P. Sokhan, D. Nicholson and N. Quirke, Transport properties of nitrogen in single walled carbon nanotubes, *J. Chem. Phys.*, 120 (2004) 3855.
- [37] Z. G. Mao and S. B. Sinnott, Predictions of a spiral diffusion path for nonspherical organic molecules in carbon nanotubes, *Phys. Rev. Lett.*, 89 (2002) 278301.
- [38] T. Duren, F. J. Keil and N. A. Seaton, Molecular simulation of adsorption and transport diffusion of model fluids in carbon nanotubes, *Mol. Phys.*, 100 (2002) 3741.
- [39] T. Duren, F. J. Keil and N. A. Seaton, Composition dependent transport diffusion coefficients of CH₄/CF₄ mixtures in carbon nanotubes by non-equilibrium molecular dynamics simulations, *Chem. Eng. Sci.*, 57 (2002) 1343.
- [40] Z. G. Mao and S. B. Sinnott, Separation of organic molecular mixtures in carbon nanotubes and bundles: Molecular dynamics simulations, *J. Phys. Chem. B*, 105 (2001) 6916.
- [41] Z. G. Mao and S. B. Sinnott, A computational study of molecular diffusion and dynamic flow through carbon nanotubes, *J. Phys. Chem. B*, 104 (2000) 4618.
- [42] Z. G. Mao, A. Garg and S. B. Sinnott, Molecular dynamics simulations of the filling and decorating of carbon nanotubes, *Nanotechnology*, 10 (1999) 273.
- [43] H. Chen and D. S. Sholl, Predictions of selectivity and flux for CH₄/H₂ separations using single walled carbon nanotubes as membranes, *J. Membr. Sci.*, 269 (2006) 152.
- [44] J. K. Holt, H. G. Park, Y. Wang, M. Stadermann, A. B. Artyukhin, C. P. Grigoropoulos, A. Noy and O. Bakajin, Fast mass transport through sub-2-nanometer carbon nanotubes, *Science*, 312 (2006) 1034.
- [45] B. J. Hinds, N. Chopra, T. Rantell, R. Andrews, V. Gavalas and L. G. Bachas, Aligned multiwalled carbon nanotube membranes, *Science*, 303 (2003) 62.
- [46] M. Majumder, N. Chopra and B. J. Hinds, Effect of tip functionalization on transport through vertically oriented carbon nanotube membranes, *J. Am. Chem. Soc.*, 127 (2005) 9062.
- [47] M. Majumder, N. Chopra, R. Andrews and B. J. Hinds, Nanoscale hydrodynamics: Enhanced flow in carbon nanotubes, *Nature*, 438 (2005) 44.
- [48] N. C. P. Nednoor, V. Gavalas, L. G. Bachas, and B. J. Hinds, Reversible biochemical switching of ionic transport through aligned carbon nanotube membranes, *Chem. Mater.*, 17 (2005) 3595.
- [49] C. Matranga, B. Bockrath, N. Chopra, B. J. Hinds and R. Andrews, Raman spectroscopic investigation of gas interactions with an aligned multiwalled carbon nanotube membrane, *Langmuir*, 22 (2006) 1235.
- [50] I. W. Chiang, B. E. Brinson, A. Y. Huang, P. A. Willis, M. J. Bronikowski, J. L. Margrave, R. E. Smalley and R. H. Hauge, Purification and characterization of single-wall carbon nanotubes (SWNTs) obtained from the gas-phase decomposition of CO (HiPco Process), *J. Phys. Chem. B*, 105 (2001) 8297.
- [51] A. Kuznetsova, D. B. Mawhinney, V. Naumenko, J. T. Yates. Jr., J. Liu and R. E. Smalley, Enhancement of adsorption inside of single-walled nanotubes: opening the entry ports, *Chem. Phys. Lett.*, 321 (2000) 292.
- [52] A. Kuznetsova, J. Liu, J. T. Yates. Jr., J. Liu and R. E. Smalley, Physical adsorption of xenon in open single walled carbon nanotubes: Observation of a quasi-one-dimensional confined Xe phase, *J. Chem. Phys.*, 112 (2000) 9590.

- [53] J. Liu, A. G. Rinzler, H. Dai, J. H. Hafner, R. K. Bradley, P. J. Boul, A. Lu, T. Iverson, K. Shelimov, C. B. Huffman, F. Rodriguez-Macias, Y. Shon, T. R. Lee, D. T. Colbert and R. E. Smalley, Fullerene Pipes, *Science*, 280 (1998) 1253.
- [54] M. Cinke, J. Li, B. Chen, A. Cassell, L. Delzeit, J. Han and M. Meyyappan, Pore structure of raw and purified HiPco single-walled carbon nanotubes, *Chem. Phys. Lett.*, 365 (2002) 69.
- [55] M. Cinke, J. Li, J. Charles W. Bauschlicher, A. Ricca and M. Meyyappan, CO₂ adsorption in single-walled carbon nanotubes, *Chem. Phys. Lett.*, 376 (2003) 761.
- [56] S. Brunauer, P. H. Emmett and E. Teller, Adsorption of gases in multimolecular layers, *J. Am. Chem. Soc.*, 60 (1938) 309.
- [57] B. C. Lippens and J. H. d. Boer, Studies on pore systems in catalysts: V. The t method, *J. Catalysis*, 4 (1965) 319.
- [58] E. P. Barrett, L. G. Joyner and P. P. Halenda, The Determination of pore volume and area distributions in porous substances. I. Computations from nitrogen isotherms, *J. Am. Chem. Soc.*, 73 (1951) 373.
- [59] A. Saito and H. C. Foley, Curvature and parametric sensitivity in models for adsorption in micropores, *AIChE J.*, 37 (1991) 429.
- [60] M. A. Hamon, J. Chen, H. Hu, Y. Chen, M. E. Itkis, A. M. Rao, P. C. Eklund and R. C. Haddon, Dissolution of single-walled carbon nanotubes, *Adv. Mater.*, 11 (1999) 834.
- [61] J. Chen, A. M. Rao, S. Lyuksyutov, M. E. Itkis, M. A. Hamon, H. Hu, R. W. Cohn, P. C. Eklund, D. T. Colbert, R. E. Smalley and R. C. Haddon, Dissolution of full-length single-walled carbon nanotubes, *J. Phys. Chem.B*, 105 (2001) 2525.
- [62] J. Crank, *The Mathematics of Diffusion*, Oxford Press, London, 1990.
- [63] M. P. Allen and D. J. Tildesley, *Computer Simulation of Liquids*, Clarendon Press, Oxford, 1987.
- [64] V. Buch, Path integral simulations of mixed *para*-D₂ and *ortho*-D₂ clusters: The orientational effects, *J. Chem. Phys.*, 100 (1994) 7610.
- [65] M. M. Calbi, S. M. Gatica, M. J. Bojan and M. W. Cole, Phases of neon, xenon, and methane adsorbed on nanotube bundles, *J. Chem. Phys.*, 115 (2001) 9975.
- [66] J. Jiang and S. I. Sandler, Nitrogen and oxygen mixture adsorption on carbon nanotube bundles from molecular simulation, *Langmuir*, 20 (2004) 10910.
- [67] J. G. Harris and K. H. Yung, Carbon dioxide's liquid-vapor coexistence curve and critical properties as predicted by a simple molecular model, *J. Phys. Chem.*, 99 (1995) 12021.
- [68] W. A. Steele, The physical interaction of gases with crystalline solids, I. Gas-solid energies and properties of isolated adsorbed atoms, *Surf. Sci.*, 36 (1973) 317.
- [69] T. Ramanathan, F. T. Fisher, R. S. Ruoff and L. C. Brinson, Amino-functionalized carbon nanotubes for binding to polymers and biological systems, *Chem. Mater.*, 17 (2005) 1290.
- [70] J. Chen, M. A. Hamon, H. Hu, Y. Chen, A. M. Rao, P. C. Eklund and R. C. Haddon, Solution properties of single-walled carbon nanotubes, *Science*, 282 (1998) 95.
- [71] B. P. Grady, F. Pompeo, R. L. Shambaugh and D. E. Resasco, Nucleation of polypropylene crystallization by single-walled carbon nanotubes, *J. Phys. Chem. B*, 106 (2002) 5852.

- [72] J. Yang, Y. Lin, J. Wang, M. Lai, J. Li, J. Liu, X. Tong and H. Cheng, Morphology, thermal stability, and dynamic mechanical properties of atactic polypropylene/carbon nanotube composites, *J. Appl. Polym. Sci.*, 98 (2005) 1087.
- [73] Y. T. Sung, C. K. Kum, H. S. Lee, N. S. Byon, H. G. Yoon and W. N. Kim, Dynamic mechanical and morphological properties of polycarbonate/multi-walled carbon nanotube composites, *Polymer*, 46 (2005) 5656.
- [74] T. Ramanathan, H. Liu and L. C. Brinson, Functionalized SWNT/polymer nanocomposites for dramatic property improvement, *J. Polym. Sci. B: Polym. Phys.*, 43 (2005) 2269.
- [75] T. P. Lodge and T. C. B. McLeish, Self-Concentrations and effective glass transition temperatures in polymer blends, *Macromolecules*, 33 (2000) 5278.
- [76] W. Shi and J. K. Johnson, Gas adsorption on heterogeneous single-walled carbon nanotube bundles, *Phys. Rev. Lett.*, 91 (2003) 015504.
- [77] T. C. Merkel, B. D. Freeman, R. J. Spontak, Z. He, I. Pinnau, P. Meakin, and A. J. Hill, Sorption, transport, and structural evidence for enhanced free volume in poly(4-methyl-2-pentyne)/fumed silica nanocomposite membranes, *Chem. Mater*, 15 (2003) 109.
- [78] T. M. Gür, Permselectivity of zeolite filled polysulfone gas separation membranes, *J. Membr. Sci.*, 93 (1994) 283.
- [79] T. C. Merkel, Z. He, I. Pinnau, B. D. Freeman, P. Meakin and A. J. Hill, Sorption and transport in poly(2,2-bis(trifluoromethyl)-4,5-difluoro-1,3-dioxole-co-tetrafluoroethylene) containing nanoscale fumed silica, *Macromolecules*, 36 (2003) 8406.
- [80] S. Lagorsse, F. D. Magalhães and A. Mendes, Carbon molecular sieve membranes: Sorption, kinetic and structural characterization, *J. Membr. Sci.*, 241 (2004) 275.

Chapter 5. Carbon Nanotube/Polymer Nanocomposites for Large Surface Area Membrane Applications

5.1. Introduction

Carbon nanotubes (CNT) have been identified as fundamentally new nanoporous materials that show great potential for sensors^{1,2}, composites³, catalytic supports⁴, and as membrane materials^{5,6}. Their advantage stems from the fact that their open cylindrical pores are in the nanometer range and thus allow transport of only certain size particles. In particular, CNTs, whose inner core diameter can be as low as 4 Å^{7,8} have been earmarked as possible selective nanopores in membrane materials^{9,10}. In fact, recent atomistic simulations predict that if used as membranes, CNT should have unprecedented flux and selectivity properties that far exceed those of any other known inorganic material. The transport of gases in carbon nanotubes was predicted be orders of magnitude faster than for instance in zeolites^{9,10}. These exceptionally high transport rates have been attributed to the inherent molecular smoothness of the nanotubes. Some of these theoretical predictions have been verified experimentally with much larger carbon nanotubes^{5,6}. Holt et al.⁶ have constructed nanotube-Si₃N₄ composite membranes using chemical vapor deposition. They used aligned double walled carbon nanotubes (DWNT) having a diameter of about 1.6 nm and showed that gas flow through the carbon nanotubes is one to two orders of magnitude faster than would be expected for flow through a commercial polycarbonate nanoporous membrane with 15 nm pore size. They also found that liquid water flow through their nanotube membranes was more than three orders of magnitude faster than expected from hydrodynamic flow calculations. Moreover, these nanotube membranes exhibited extraordinarily high size exclusion selectivity. In related work, Hinds and coworkers⁵ constructed polymer-nanotube composite membranes using

multiwalled carbon nanotubes (MWNT) having large diameters (6-7 nm). They have verified that transport of liquids (alkanes, water) is orders of magnitude faster than can be accounted for by conventional hydrodynamic flow.

The use of single-walled (SWNT), smaller diameter carbon nanotubes as membranes is particularly intriguing, because in addition to fast transport rates, the 4 to 12 Å poreopenings can start to be size-selective for gas mixtures. In order for SWNTs to effectively act as channels in a membrane, however, they have to be aligned vertically along the penetrant stream. This is the single most important challenge facing the employment of SWNT as membranes. In their studies, Hinds et al and Holt et al have used chemical vapor deposition to grow oriented carbon nanotubes^{5,6}. While producing well-aligned carbon nanotubes, this process is expensive, tedious and is limited to fabricating samples with small areas (e.g. sub cm²). Alternatively, CNTs have been aligned by employing filtration methods^{11,12}, although to date this approach has been successful only with MWNTs.

In this paper, we report on the transport properties of SWNT/polymer nano-composite membranes fabricated by orienting functionalized SWNT with a filtration method. We believe that the alignment of the SWNT results from a self-assembly mechanism directed by the shear forces of the flowing solvent stream in combination with repulsive forces between the carbon nanotubes and the nearby membrane filter surface. It has been reported that shear forces align SWNT in the flow direction¹³. In our samples the SWNT orient in shear flow and propagate the perpendicular alignment to the filter substrate via long range repulsive forces that exist between zwitterions attached to the carbon nanotube surface. This phenomena is similar to the orientation behaviour of rigid rodlike polyelectrolytes near charged surfaces¹⁴.

5.2. Experimental and Characterization Method

5.2.1. Purification and Functionalization of CNTs

Electric arc-discharged CNTs was purchased from Carbon Solutions, Inc. (Riverside, CA). Raw carbon nanotube materials was treated by multistage purification (a combination of wet-oxidation and acid treatments) to purify SWNTs from impurities and cut into small length with 3:1 mixture of concentrated H₂SO₄ (98 vol%):HNO₃ (70% vol%) solution. The details of the purification and cutting method are described elsewhere^{15,16}. To produce soluble CNTs, we formed an octadecylammonium (ODA) and SWNT-Carboxylate zwitterions by the following procedure.^{17,18} Shortened CNTs were heated with ODA at 393 K for 96 hours. After cooling to room temperature, the black-colored ODA and CNTs mixture was washed with tetrahydrofuran (THF) and filtered through a membrane filter (0.2 μm). Because unreacted ODA was expected to block the entrance to the channels of SWNTs, ODA was further removed by Soxhlet extraction in ethanol at 393 K for 10 days.

5.2.2. CNT/Polymer Nanocomposit Membrane Fabrication

Filtered and dried functionalized CNT and were dispersed in tetrahydrofuran (THF) solution using ultra-sonication for 30 min. The dilute CNT/THF solution (6.7×10^{-5} wt % of CNT) was then filtered through a 0.2 μm pore-size hydrophobic polytetrafluoroethylene (PTFE; Millipore) filter. Vertically-aligned CNTs remained on the filter support. This assembly was then dried at room temperature for 8 hours and subsequently coated with a thin PSF (UDEL P-3500, Solvay) or PDMS (RTV615, GE) layer using dilute < 10 wt% polymer solution. For typical spin coating method, dilute polymer solution was poured dropwise onto the filtered CNT sample and waited for 1

min to penetrate well into CNT layer followed by spin coating for 10 sec at 1500 rpm. The prepared nanocomposites were given 1 day to dry at room temperature. Once dry, the composite films were placed under vacuum and the temperature was raised to its glass transition temperature, 458 K for 1 hour and then cooled down to room temperature.

5.2.3. CNT/polymer Nanocomposite Sample Preparation for High-resolution TEM Experiments

CNT / polymer nanoporous membrane samples for high-resolution TEM experiments in cross-sectional orientation were prepared by an ultramicrotoming method. After embedding the membrane in a resin, slices having a thickness less than 50nm have been cut using a standard diamond microtome knife. The slices were placed onto a meshed copper TEM grid for support. Finally, the TEM specimen was coated with a thin amorphous carbon film prior to the TEM experiment to prevent specimen charging and to minimize beam damage. High-resolution TEM observations were made on a FEI Titan XT at 200keV. The post-column Gatan Image Filter (GIF) has been utilized for zero-loss (ZL) filtered imaging with an energy slit width of 10eV to improve image contrast and visibility of the graphene layers in CNTs by minimizing the blurring that is caused by inelastic scattering.

5.2.4. Calculation of Knudsen diffusion flow

The gas flow rate in Knudsen flow regime can be estimated from⁶

$$Q = \frac{2}{3} \sqrt{\frac{8\pi}{MRT}} \left(\frac{d}{2}\right)^3 V_m \frac{\Delta P}{L} \sigma A$$

where Q is the flow rate, M is molecular weight of penetrant, R is the universal gas constant, T is absolute temperature, d is the inner diameter of nanotube, V_m is the molar

volume, $\Delta P = 4$ atm is the pressure difference between permeate and feed side, $L = 1 \mu\text{m}$ is the thickness of the membrane, $\sigma = \sim (7.0 \pm 1.75) \times 10^{10}$ nanotubes/cm² is the area density, and $A = 13.85 \text{ cm}^2$ is the effective membrane area.

5.3. Results and Discussions

Arc discharge SWNTs were treated using a mixture of H₂SO₄/HNO₃ to cut the nanotubes into small lengths and open end tips¹⁶. The average pore diameter of the SWNT estimated from porosimetry measurements is 1.2 nm. The pore-size distribution is shown in Figure 5-1a. It has been reported that acids can be intercalated into SWNT bundles and disintegrate the tube walls into graphitic flakes and then reform them into MWNTs¹⁹. After acid treatment, the prepared CNTs samples are mostly composed of multiwalled carbon nanotubes, or transformed SWNTs created during the oxidation, shown in Figure 5-1b and bundled SWNTs shown in Figure 5-1c. The transformed SWNTs have pore diameters of less than 2 nm and are surrounded by multilayered graphitic shells and amorphous-like carbon materials (Figure 4-1b).

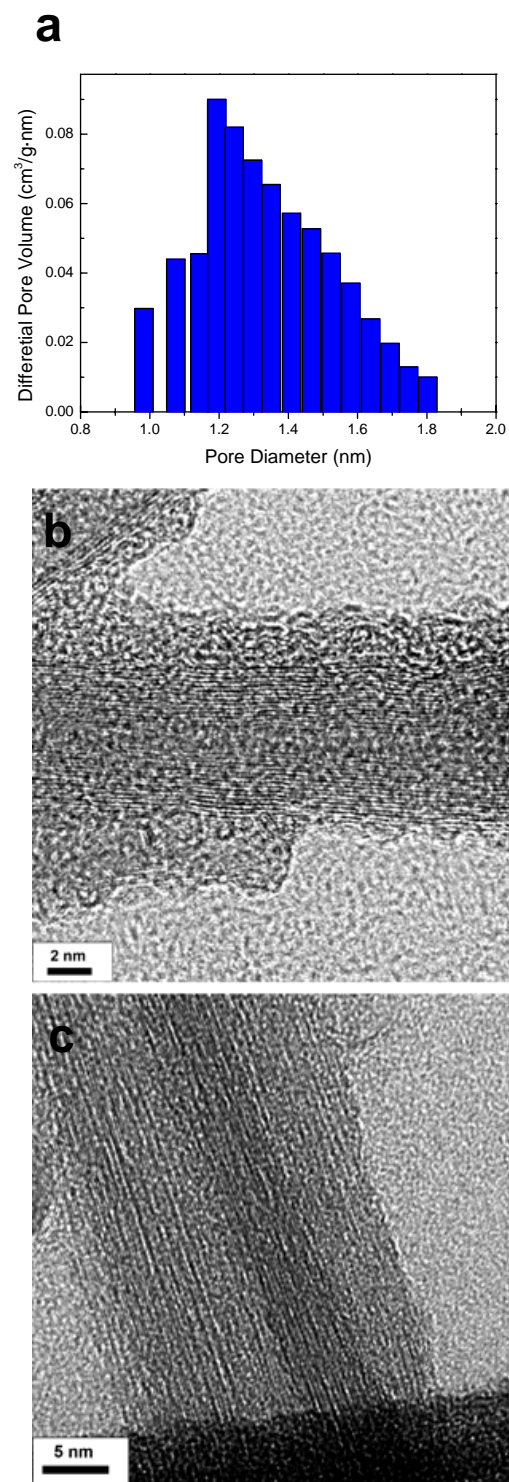


Figure 5-1. SWNT pore structure. **a**, Differential pore volume plot of SWNT at 77 K using N₂. Pore diameter of the SWNT sample was calculated by the Horvath-Kawazoe (H-K) method. The H-K method used here was derived for cylindrical pores. The distribution in micropore diameter of the SWNT ranges from 0.95 to 1.8 nm showing strong peak intensity at 1.2 nm. Therefore, the average pore diameter of the SWNT in this study is estimated to be 1.2 nm. **b**, Zero-loss filtered (energy slit width of 10eV) high resolution TEM (HRTEM) image of multiwalled CNT that is transformed from SWNTs after acid treatment. **c**, HRTEM image of several SWNT bundles.

Schematic membrane fabrication process are shown in Figure 5-2a. Figure 5-2b presents the scanning electron microcopy (SEM) images of the CNT on a PTFE membrane filter with a thin carbon nanotube layer of ca. 2 μm thickness. Most of the nanotubes are “standing up”, although some are not fully aligned vertically to the membrane filter. A cross-section of the CNT composite membrane is shown in Figure 5-2. Polysulfone (PSF) was chosen as the matrix to impart the membrane with mechanical strength and to seal the structure. The effect of excess polymer on membrane performance was investigated by coating additional PSF or polydimethylsiloxane (PDMS) layers. These structures are shown in Figure 5-2d and 2e. An SEM image of the composite film in Figure 5-2c shows that spin-coating the polymer from a dilute solution allows the polymer to penetrate well around the nanotubes. As shown in Figure 2c, there is very little excess polymer on top of the CNTs and several nanotube tips are slightly exposed above the polymer matrix. Figures 5-2d and 2e show SEM images of other samples containing additional PSF (Figure 5-2d) and PDMS layers (Figure 5-2e) on top of the original carbon nanotubes/PSF system.

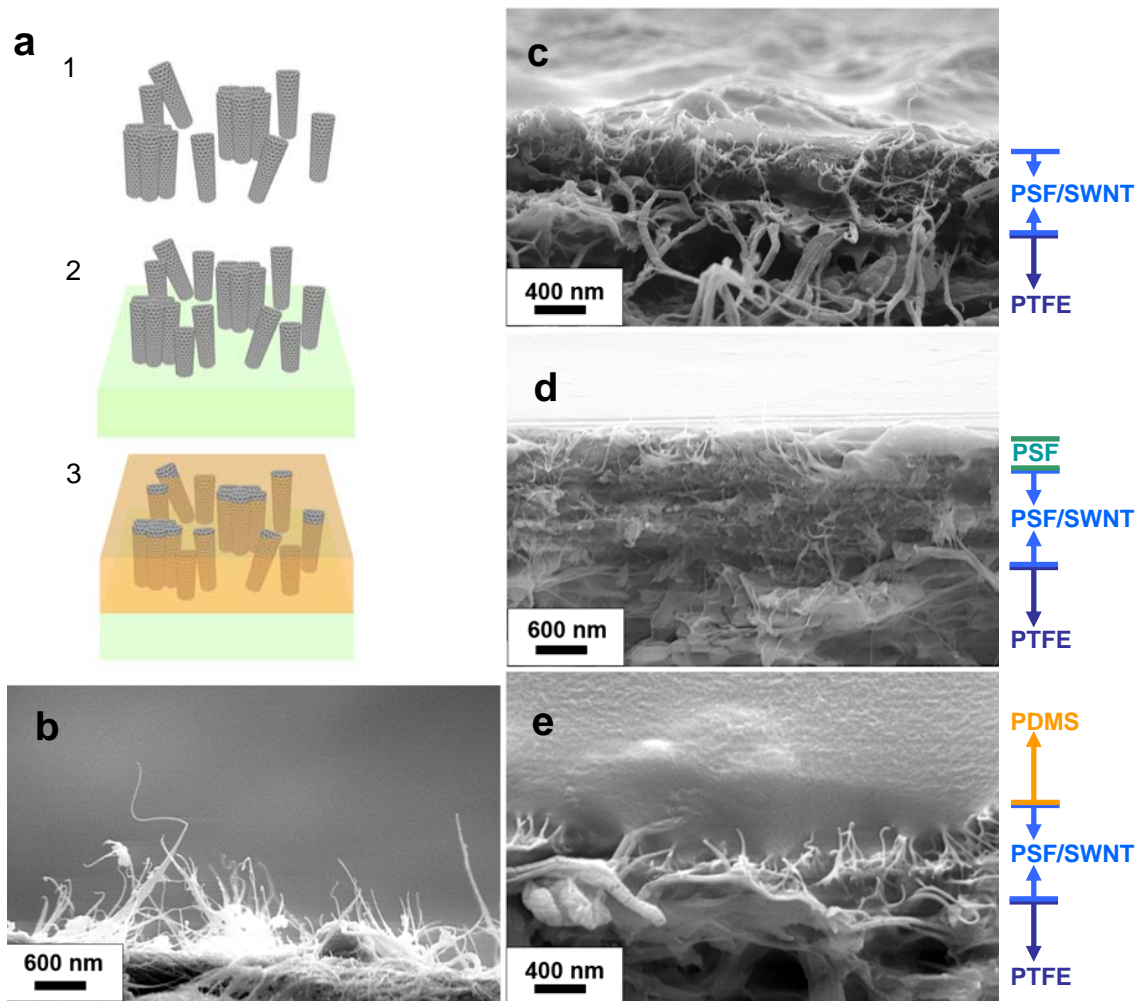


Figure 5-2. CNT nanocomposite membrane process. **a**, Schematic membrane fabrication process. Step 1: The functionalized CNTs are dispersed in THF solution. Step 2: The CNTs/THF solution is filtered through 0.2 μm pore size hydrophobic polytetrafluoroethylene (PTFE) membrane filter. Step 3: The CNTs/PTFE is spin-coated with a dilute polymer solution. Some nanotube tips are embedded in polymer matrix. **b**, Side-view SEM image of carbon nanotubes standing vertically on a membrane filter. **c**, Side-view SEM image of aligned nanotube/PSF nanocomposite membrane after spin coating. Polymer coating is so thin that some carbon nanotube tips are exposed on top the surface. **d**, Side-view SEM image of aligned nanotube/PSF/PSF composite membrane having an additional PSF layer of 300 nm. **e**, Side-view SEM image of aligned nanotube/PSF/PDMS composite membrane with a protective PDMS coating of 4 μm .

High-resolution transmission electron microscopy (HRTEM) images of the CNT cross-sections in a polymer matrix are shown in Figure 5-3a. These images have been used to estimate the area density of the carbon nanotubes, which is $\sim (7.0 \pm 1.75) \times 10^{10}$ nanotubes per cm^2 . Similar to HRTEM images of the acid-treated CNTs sample in Figures 5-1b. and 4-1c., HRTEM images of nanotubes in the polymer matrix reveal mostly two types of structures, i.e. encapsulated SWNT bundles and SWNTs with additional graphite sheets shown in Figure 5-3b. A single SWNT which has been transformed into a MWNT by encapsulation with additional graphite layers is shown in Figure 5-3c. We believe that the increase in outer diameter of the transformed SWNT also aids in the vertical orientation of the carbon nanotube during the filtration process.

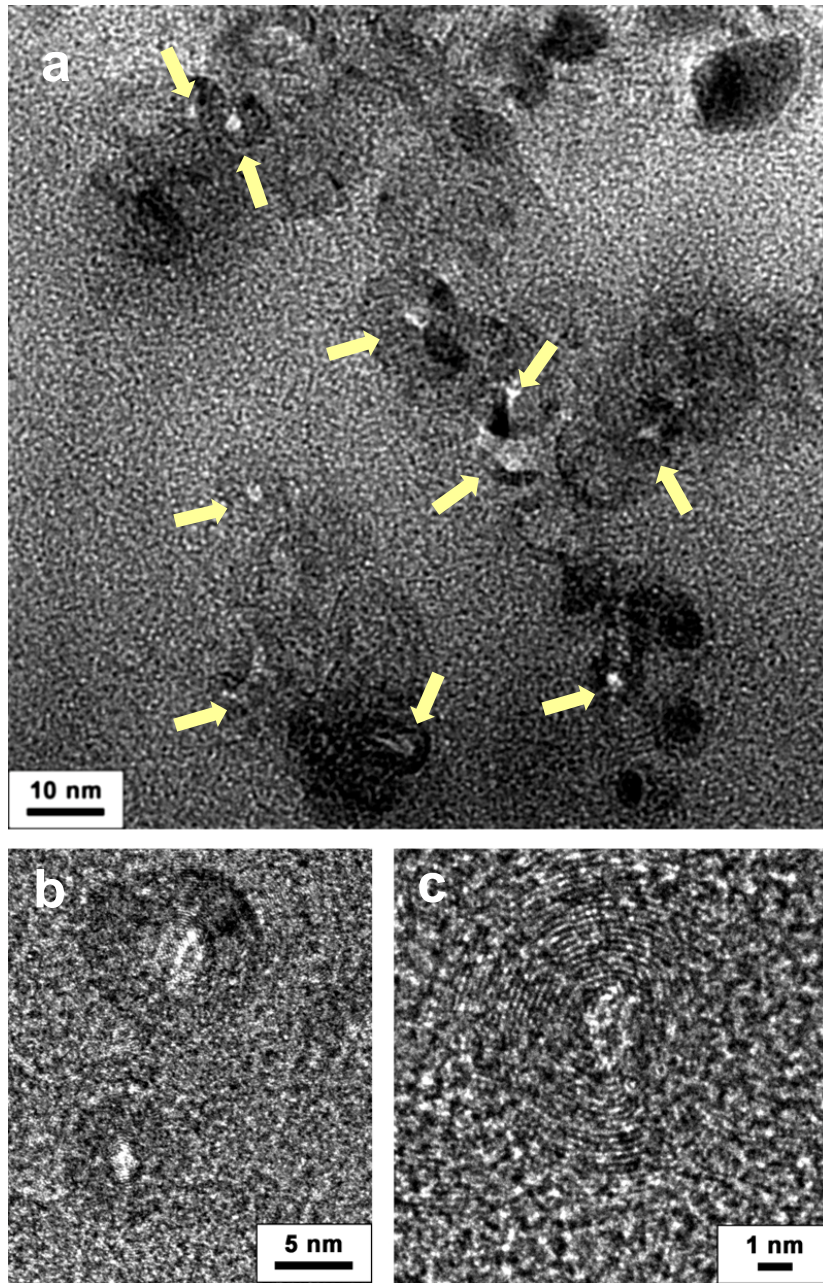


Figure 5-3. HRETM images in plan-view orientation of CNTs in a polymer matrix. The TEM specimen has been coated with a thin amorphous carbon film prior to the TEM experiment to prevent specimen charging. In **a**, bright white spots (indicated by arrows) represent open nanotube pores. (**b** and **c**) HRTEM images at higher magnification reveal the structure of these pores. In **b**, an encapsulated SWNT bundle is shown in the upper part of the image and an encapsulated individual SWNT is in the lower part of the image. This SWNT bundle has an inner diameter of 4 nm. **c**, The individual SWNT with an inner diameter of ~ 1.5 nm is clearly encapsulated by additional graphite layers. The area density of SWNTs was measured to be $\sim (7.0 \pm 1.75) \times 10^{10}/\text{cm}^2$ from several HRTEM images.

The quality of the CNT/PSF composite membranes has been tested by measuring its permeation to helium. In general, the transport of pure gases through a porous membrane can be described by one of three mechanisms: viscous flow, Knudsen diffusion, and surface flow²⁰. Knudsen diffusion occurs when the mean free path of the gas molecules (λ) is larger than the pore radius (r) of the membrane and there are more collisions with the pore walls than between gas molecules. When r/λ becomes much larger than 1 ($r \gg \lambda$), as would be the case for gas transport in pinholes and other structural defects, viscous flow dominates the gas transport mechanism. Since we don't expect that the transport of gases in CNTs is strongly dependent on adsorbate-nanotube interactions¹⁰, we can assume that the surface diffusion term is negligible. Therefore, high quality membranes can be characterized by the absence of viscous flow and more by Knudsen-type diffusion. For porous membranes which are governed by Knudsen diffusion, a plot of permeability versus average pressure should give a horizontal line because gas transport in a Knudsen regime is independent of the feed pressure. Alternatively, the permeation should increase with increasing pressure across the membrane when viscous flow takes place. As shown in Figure 5-4, the helium permeance through the CNT membranes is independent of the pressure drop across the membrane. This is evidence that there is no viscous flow through any large pinholes and that the prepared SWNT membrane is defect free.

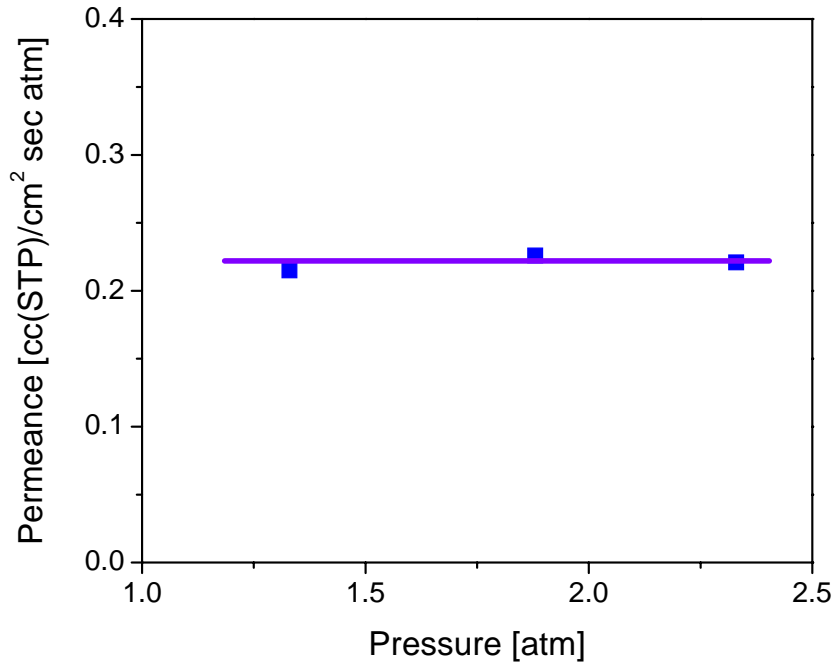


Figure 5-4. Effect of the pressure drop on the permeance of helium through CNTs/PSF membrane.

When Knudsen diffusion occurs, the permeance is inversely proportional to the square root of the molecular weight of the permeating gas molecule. Figure 5-5 shows the effective gas permeability in the three oriented CNTs/polymer nanocomposite membranes as a function of the square root of the reciprocal of the gas molecular weight, $M^{-1/2}$. The solid line represents the Knudsen flow model. While the permeabilities of all samples are proportional to $M^{-1/2}$, the absolute permeability of the CNTs/PSF membrane is significantly higher than that predicted by Knudsen diffusion. The reason for this is that the diffusion in this sample takes place primarily through the carbon nanotubes and very little through the ultra-thin polymer matrix. This gas flow enhancement above the Knudsen regime is consistent with the atomistic simulations discussed previously¹⁰. On the other hand, the permeabilities of samples having additional polymer coatings, CNTs/PSF/PDMS and CNTs/PSF/PSF, are lower than those predicted by the Knudsen

diffusion model. This decrease in permeability is proportional to the transport resistance offered by the additional polymer layers, being the greatest in the sample with the secondary polysulfone layer. Carbon dioxide exhibits some deviation from this behavior, because its permeability is inherently higher as a result of increased sorption in the presence of the octadecyl ammonium ion on the carbon nanotube surface.

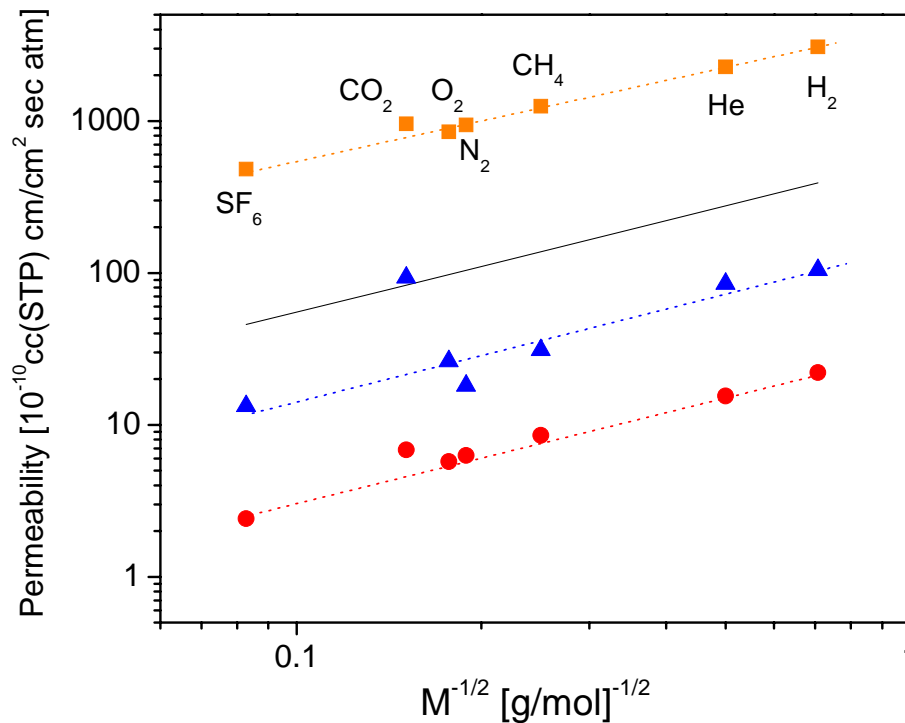


Figure 5-5. Single gas transport properties of CNT nanocomposite membrane. Gas transport properties of CNTs/PSF/PSF membrane (red circle), CNT/PSF/PDMS membrane (blue triangle), CNTs/PSF membrane (orange square), and Knudsen diffusion model (solid line). Single gas permeability as a function of the inverse square root of the molecular weight of the penetrant.

Figure 5-6 shows the single gas selectivities for various gas/helium pairs of all three CNTs membranes as a function of the gas molecular weight. With the exception of CO₂, the selectivity exhibits the inverse-square-root of the molecular mass dependence predicted by the Knudsen diffusion model. Again the higher-than Knudsen CO₂/He selectivity can be attributed to the presence of the ammonium ion.

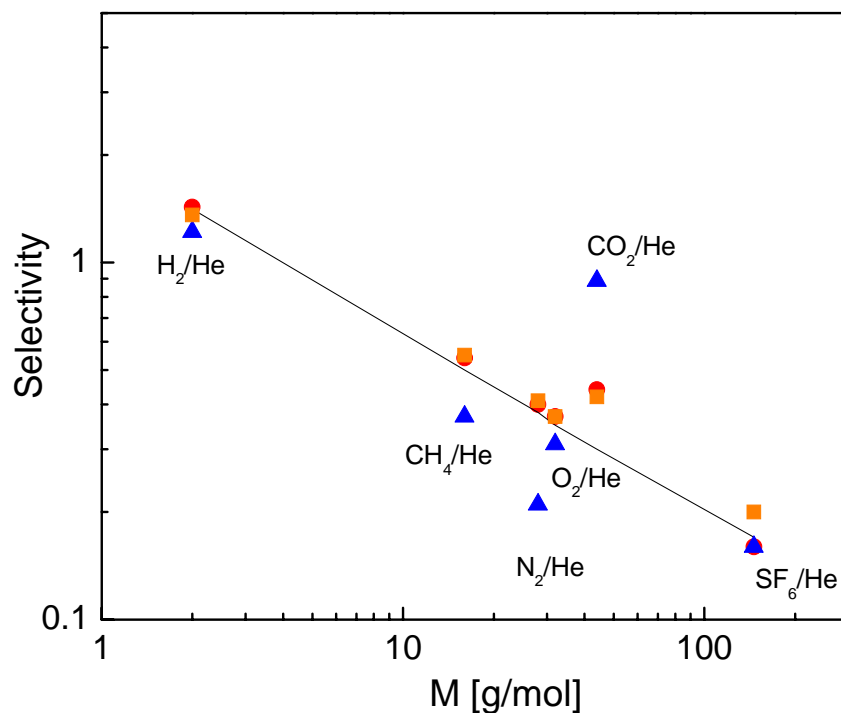


Figure 5-6. Gas transport properties of CNT nanocomposite membrane. Gas transport properties of CNTs/PSF/PSF membrane (red circle), CNT/PSF/PDMS membrane (blue triangle), CNTs/PSF membrane (orange square), and Knudsen diffusion model (solid line). Single gas selectivity with respect to helium calculated from single gas permeability data.

The same holds true for the single gas as well as mixed gas CO_2/CH_4 selectivities shown in Figure 5-7. Here the mixed gas CO_2/CH_4 selectivity is approximately three times that of the ideal selectivity predicted by the Knudsen model. In other studies, functional groups at the end of MWNT have been utilized to investigate a “gatekeeper” mechanism for controlling the flux and selectivity of chemical transport through the CNT membranes²¹. Amine functional groups have widely been used to modify sorbents and catalysts to increase CO_2 selectivity by carbamate formation in the absence of water²². The same “gatekeeper” mechanism is playing a role in the SWNT/polysulfone membranes, since most of the zwitterions are located at the carbon nanotube tips.

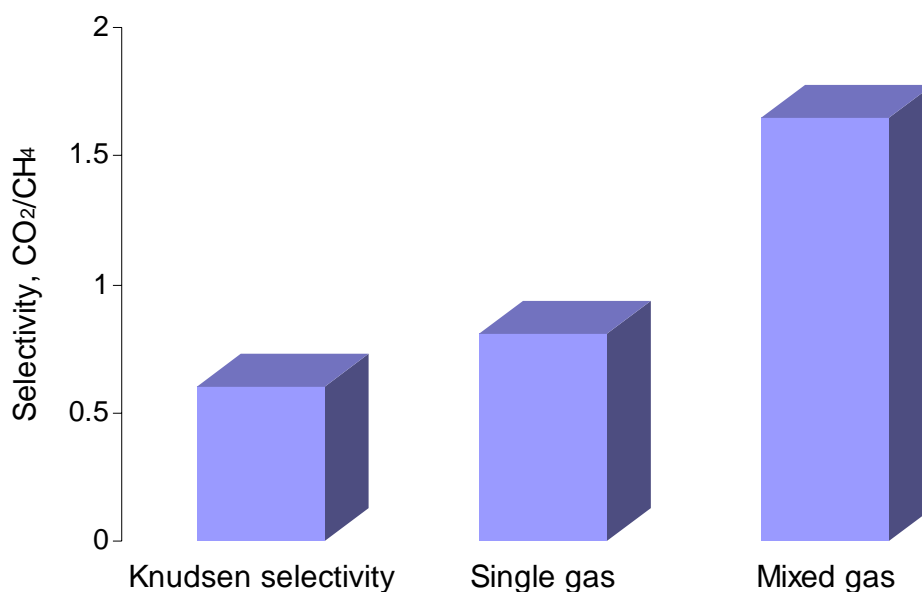


Figure 5-7. Mixed gas selectivity (CO_2/CH_4) of CNTs/PSF membrane. The composition of gas mixture was $\text{CO}_2:\text{CH}_4 = 50 : 50$. The feed pressure was 50 psi and the pressure differential across membrane was maintained by drawing a vacuum on the permeate side. Operating temperature was maintained at 308 K.

5.4. Conclusions

In summary, the filtration method presented here facilitates the orientation of carbon nanotubes on porous supports and can be easily adapted to large-scale membrane formation. The resulting nanocomposite membranes have the same fast gas transport properties as those observed in carbon nanotube membranes grown by chemical vapor deposition. The introduction of functional groups at the carbon nanotube pore can serve to enhance the selectivity of gas mixtures.

5.5. References

- [1] J. Kong, N. R. Franklin, C. Zhou, M. G. Chapline, S. Peng, Kyeongjae Cho and H. Dai, Nanotube molecular wires as chemical sensors, *Science*, 28 (2000) 622.
- [2] P. G. Collins, K. Bradley, M. Ishigami and A. Zettl, Extreme oxygen sensitivity of electronic properties of carbon nanotubes, *Science*, 287 (2000) 1801.
- [3] P. Calvert, Nanotube composites: A recipe for strength, *Nature*, 399 (1999) 210.
- [4] J. M. Planeix, N. Coustel, B. Coq, V. Brotons, P. S. Kumbhar, R. Dutartre, P. Geneste, P. Bernier and P. M. Ajayan, Application of carbon nanotubes as supports in heterogeneous catalysis, *J. Am. Chem. Soc.*, 116 (1999) 7935.
- [5] B. J. Hinds, N. Chopra, T. Rantell, R. Andrews, V. Gavalas and L. G. Bachas, Aligned multiwalled carbon nanotube membranes, *Science*, 303 (2003) 62.
- [6] J. K. Holt, H. G. Park, Y. Wang, M. Stadermann, A. B. Artyukhin, C. P. Grigoropoulos, A. Noy and O. Bakajin, Fast mass transport through sub-2-nanometer carbon nanotubes, *Science*, 312 (2006) 1034.
- [7] L.-C. Qin, X. Zhao, K. Hirahara, Y. Miyamoto, Y. Ando and S. Iijima, The smallest carbon nanotube, *Nature*, 408 (2000) 50.
- [8] N. Wang, Z. K. Tang, G. D. Li and J. S. Chen, Materials science: Single-walled 4 Å carbon nanotube arrays, *Nature*, 408 (2000) 50.
- [9] D. M. Ackerman, A. I. Skoulidas, D. S. Sholl and J. K. Johnson, Diffusivities of Ar and Ne in carbon nanotubes, *Mol. Simul.*, 29 (2003) 677.
- [10] A. I. Skoulidas, D. M. Ackerman, J. K. Johnson and D. S. Sholl, Rapid transport of gases in carbon nanotubes, *Phys. Rev. Lett.*, 89 (2002) 185901.
- [11] W. A. d. Heer, W. S. Bacsá, A. Chatelain, T. Gerfin, R. Humphrey-Baker, L. Forro and D. Ugarte, Aligned carbon nanotube films: production and optical and electronic properties, *Science*, 268 (1995) 845.
- [12] W. Li, X. Wang, Z. Chen, M. Waje and Y. Yan, Carbon nanotube film by filtration as cathode catalyst support for proton-exchange membrane fuel cell, *Langmuir*, 21 (2005) 9386.
- [13] Z. H. Fan and S. G. Advani, Characterization of orientation state of carbon nanotubes in shear flow, *Polymer*, 46 (2005) 5232.
- [14] D. A. Hoagland, Electrostatic interactions of rodlike polyelectrolytes with repulsive, charged surfaces, *Macromolecules*, 23 (1990) 2781
- [15] I. W. Chiang, B. E. Brinson, A. Y. Huang, P. A. Willis, M. J. Bronikowski, J. L. Margrave, R. E. Smalley and R. H. Hauge, Purification and characterization of single-wall carbon nanotubes (SWNTs) obtained from the gas-phase decomposition of CO (HiPco Process), *J. Phys. Chem. B*, 105 (2001) 8297.
- [16] J. Liu, A. G. Rinzler, H. Dai, J. H. Hafner, R. K. Bradley, P. J. Boul, A. Lu, T. Iverson, K. Shelimov, C. B. Huffman, F. Rodriguez-Macias, Y. Shon, T. R. Lee, D. T. Colbert and R. E. Smalley, Fullerene Pipes, *Science*, 280 (1998) 1253.
- [17] M. A. Hamon, J. Chen, H. Hu, Y. Chen, M. E. Itkis, A. M. Rao, P. C. Eklund and R. C. Haddon, Dissolution of single-walled carbon nanotubes, *Adv. Mater.*, 11 (1999) 834.
- [18] J. Chen, A. M. Rao, S. Lyuksyutov, M. E. Itkis, M. A. Hamon, H. Hu, R. W. Cohn, P. C. Eklund, D. T. Colbert, R. E. Smalley and R. C. Haddon, Dissolution of full-length single-walled carbon nanotubes, *J. Phys. Chem. B*, 105 (2001) 2525.
- [19] K. H. An, K. K. Jeon, J.-M. Moon, S. J. Eum, C. W. Yang, G.-S. Park, C. Y. Park and Y. H. Lee, Transformation of singlewalled carbon nanotubes to multiwalled carbon

nanotubes and onion-like structures by nitric acid treatment, *Synthetic Metals* 140 (2004) 1.

[20] R. J. R. Uhlhorn, K. Keizer and A. J. Burggraaf, Gas and Surface Diffusion in Modified γ -Alumina Systems, *J. Membr. Sci.*, 46 (1989) 225.

[21] M. Majumder, N. Chopra and B. J. Hinds, Effect of Tip Functionalization on transport through vertically oriented carbon nanotube membranes, *J. Am. Chem. Soc.*, 127 (2005) 9062.

[22] S. Satyapal, T. Filburn, J. Trela and J. Strange, Performance and properties of a solid amine sorbent for carbon dioxide removal in space life support applications, *Energy Fuels*, 15 (2001) 250.

Chapter 6. Polysulfone and Mesoporous Molecular Sieve MCM-48 Mixed Matrix Membranes for Gas Separation

6.1. Introduction

Polymeric membranes have been very successful in addressing industrially important gas separations, thereby providing economical alternatives to conventional separation processes. However, polymeric membranes for gas separations have been known to have a trade-off between permeability and selectivity as shown in upper bound curves developed by Robeson.¹ Many research efforts have been aimed at modifying the backbones and side-chains of polymers experimentally in order to surpass the permeability-selectivity tradeoff.^{2,3} This has been difficult to achieve and in fact also, as shown by Freeman⁴, theoretically improbable. Thus, the use of polymeric materials as membranes has technical limitations.²

In order to enhance gas separation membrane performances, recent work has focused on enhancing polymer selectivity and permeability by fabricating mixed matrix membranes (MMMs). The incorporation of various inorganic materials, such as zeolites or carbon molecular sieves, into a polymer matrix has been investigated.⁵⁻⁸ However, the application of zeolites is limited by the poor interaction with the polymer matrix and the relatively small zeolite pores. Transport limitations can also occur after modification of external surface of zeolite with silane coupling agents which can block pore access.^{9,10} Weak interactions between a glassy polymer matrix and inorganic molecular sieves may lead to the formation of nonselective voids resulting in Knudsen flow.⁶

Since the discovery of the M41S family of mesoporous molecular sieves by Kresge *et al.*,^{11,12} these materials have received widespread interest as catalysts, adsorbents and

membranes because of their high surface areas, tunable pore sizes (2-50 nm) and surface chemistry via functionalization. The surface of mesoporous silica is decorated with reactive silanol groups, which can be used for surface modification to introduce favorable interactions with polymers. Surface functionalization of mesoporous materials with several types of functional groups for application in adsorption and catalysis has been reported.¹³⁻¹⁷ Recently, the application of these molecular sieves as membranes has been investigated by some research groups. Nishiyama *et al* fabricated mesoporous MCM-48 membranes on a porous alumina support and reported that the permeation of gases through calcined MCM-48 membranes was governed by Knudsen diffusion.^{18,19} Reid *et al.* reported polysulfone (PSF) MMMs with mesoporous silica MCM-41 for gas separation.²⁰ They showed that mesoporous materials offered the favorable effect of increasing the permeability of the polysulfone MMMs without decreasing its selectivity due to its good compatibility with the polymer matrix. However, their study has focused on MCM-41 silica, which has one-dimensional pore channel structure prone to diffusion limitations and pore blockage.²¹ Therefore, MCM-48 silica is more attractive than MCM-41 for potential applications in molecular sieves in MMM areas due to its three-dimensional interconnected cubic pore structure.

The main intent of this study is to develop and characterize novel hybrid membranes based on mesoporous MCM-48 silica dispersed inside a polymer matrix. We synthesized a MCM-48 mesoporous silica by a templating method and characterized it with X-ray diffraction (XRD), pore size analysis, and field emission scanning microscopes (FESEM). The structure, the absence of defects, and the properties of MCM-48/PSF MMMs were characterized by FESEM, sorption studies and gas permeation measurements.

6.2. Experimental and Characterization Method

6.2.1. Synthesis of MCM-48 Silica.

Mesoporous MCM-48 silica was synthesized according to a previously published procedure.^{18,19} In this method, the aqueous micellar solution containing a quaternary ammonium surfactant, $C_{16}H_{33}(CH_3)_3NBr$ (CTAB, Sigma-Aldrich), NaOH, and deionized water was prepared under stirring for 1 hour. Then, the solution was added to tetraethylorthosilicate (TEOS, Alfa-Aesar Chemical). The molar composition of the mixture was 0.59 CTAB: 1.0 TEOS: 0.5 NaOH: 61 H_2O . The mixture was stirred for 90 minutes and transferred to an autoclave. The reaction was carried out at 363 K for 96 hours. The MCM-48 silica was filtered, and washed with deionized water. At this stage, the as-synthesized MCM-48 still contained organic templates. Calcined MCM-48 silica used in the fabrication of MMMs was obtained after as-synthesized MCM-48 silica was calcined in air at 723 K for 5 hours. In order to obtain a fine MCM-48 silica particle, a combination of sonication and sedimentation was performed. Following these steps, the MCM-48 silica was vacuum-dried overnight in order to be used in the fabrication of MMM.

6.2.2. Fabrication of PSF membranes.

Before fabrication of membranes, PSF (UDEL P-3500, Solvay) was degassed at 413 K for 3 h under vacuum to remove adsorbed water. Then, 0.6 g of the PSF was dissolved in 3 mL of chloroform and stirred for one day leading to a viscous solution. The membranes were cast onto a glass substrate using a doctor blade. The glass substrate was covered with a glass cover to slow the evaporation of solvent, allowing for a film with a uniform thickness without curling. The solutions were given 1 day to dry at room temperature. Once dry, the films were placed under vacuum and the temperature was raised to its glass

transition temperature, 458 K for 1 hour and then cooled down to room temperature. A 6.35 cm diameter circular sample was cut from the film and used for permeation tests.

6.2.3. Fabrication of MCM-48/PSF MMMs.

The fabrication procedure for the mixed matrix membranes was identical to the pure polymer membrane preparation with the additional step of incorporating MCM-48 silica. For a 10 wt % of MCM-48/PSF MMMs, approximately 0.68 g of the pure PSF was dissolved in 3 mL of tetrahydrofuran (THF) and mixed for 24 hours. A predetermined mass of MCM-48 (0.078 g) was dissolved in 1 mL of THF with small amount of PSF solution (~5 drops) and sonicated for 10 minutes to enable the dilute polymer solution to coat the mesoporous silica. This MCM-48 solution was added to the polymer solution and the mixture was allowed to mix for 6 hours at room temperature. Following this time period, the mixture was sonicated for 10 minutes, after which it was allowed to mix for 10 minutes. This process was repeated several times. The membranes were cast onto a glass substrate using a doctor blade. The evaporation and heat treatments for the mixed matrix membranes were identical to that of the pure polymer membrane.

6.2.4. Characterization.

The powder XRD patterns of MCM-48 mesoporous silica were recorded on a Scintag Inc., XDS 2000 spectrometer using $\text{CuK}\alpha$ radiation with a step size of 0.02 °/s. The N_2 adsorption-desorption isotherms were collected at 77 K using Micromeritics ASAP 2010. The MCM-48 silica samples were outgassed prior to these measurements at 423 K overnight under N_2 flow. The surface areas were calculated using the Brunauer-Emmett-Teller (BET) method, and the pore volumes and pore diameters were calculated by the

Barret-Joyner-Halenda (BJH) method. FESEM (LEO 1550) was used to study the morphology of the membranes. Sorption studies were conducted by the gravimetric system (IGA-002, Hiden Isochema, UK). For each measurement, the samples were degassed at 403 K for 10 hours at $P \leq 10^{-6}$ mbar. All tubings and chambers were also degassed by applying vacuum ($P \leq 10^{-6}$ mbar). The degassed samples were then cooled down to the specified temperature (308 K) with a ramping rate of 1 K /minute. The gases used in this research were He, CO₂, O₂, N₂, and CH₄ with a reported purity of 99.99% and purified again by passing through a molecular sieve trap attached to the gravimetric system. The adsorption isotherms were measured by the small stepwise pressure (or concentration) change, i.e. 100 mbar ($P \leq 1.3$ bar) and 250 mbar ($P > 1.3$ bar). The gravimetric sorption studies in this research were conducted at a temperature of 308 ± 1 K and pressure range of 0.01 – 4 bar.

Permeabilities of the polymeric and composite membranes were measured using a constant volume varying pressure apparatus. Permeability was measured directly, and the Time Lag Method²² was applied to the recorded data to determine the diffusivity coefficient. The solubility coefficient was taken as the ratio of the permeability to diffusivity coefficient.²² The gases used in this research were He, CO₂, O₂, N₂, and CH₄. Each gas possessed a purity of 99.99% and was used as received from Air Products. The feed pressure and temperature were kept constant at 4 atm and 308 K, respectively, for all experiments. Each gas was run through a membrane six times and the average results and the standard deviations were recorded. Permeabilities are reported in units of Barrer ($1 \text{ Barrer} = 1 \times 10^{-10} \text{ cm}^3 \cdot (\text{STP}) \cdot \text{cm} / (\text{cm}^2 \cdot \text{sec} \cdot \text{cmHg})$).

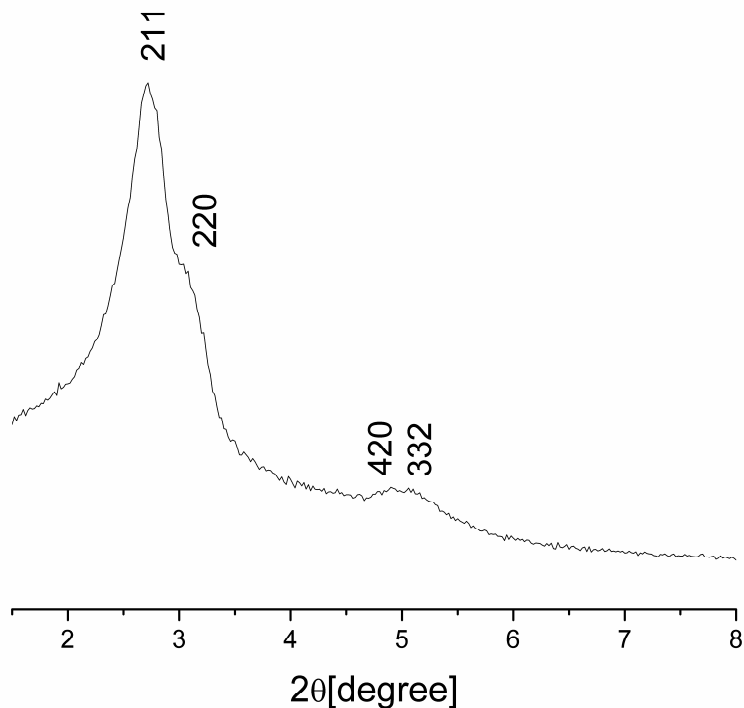


Figure 6-1. XRD pattern of MCM-48 silica

6.3. Results and Discussion

The powder X-ray diffraction patterns (XRD) of the calcined MCM-48 silica is shown in Figure 6-1. The XRD patterns displayed Bragg peaks in the $2\theta = 1.5\text{--}8^\circ$ range, which can be indexed to different hkl reflections. The XRD patterns of the as-synthesized (not shown here) and calcined mesoporous MCM-48 powders consisted of the typical reflection at 2.7° (211) and weak reflections at 3.1° (220), 4.9° (420) and 5.2° (332) which corresponded to the d -spacings of ca. 32.5, 28.7, 17.7 and 17.1 Å, respectively. These d -spacings are indicative of MCM-48 structure possessing the cubic $Ia3d$ space group.^{18,19} The N_2 adsorption-desorption isotherms at 77 K for the MCM-48 silica is shown in Figure 6-2. The N_2 adsorption isotherm of the MCM-48 is a typical reversible type IV adsorption isotherm characteristic of a mesoporous material. The MCM-48 silica

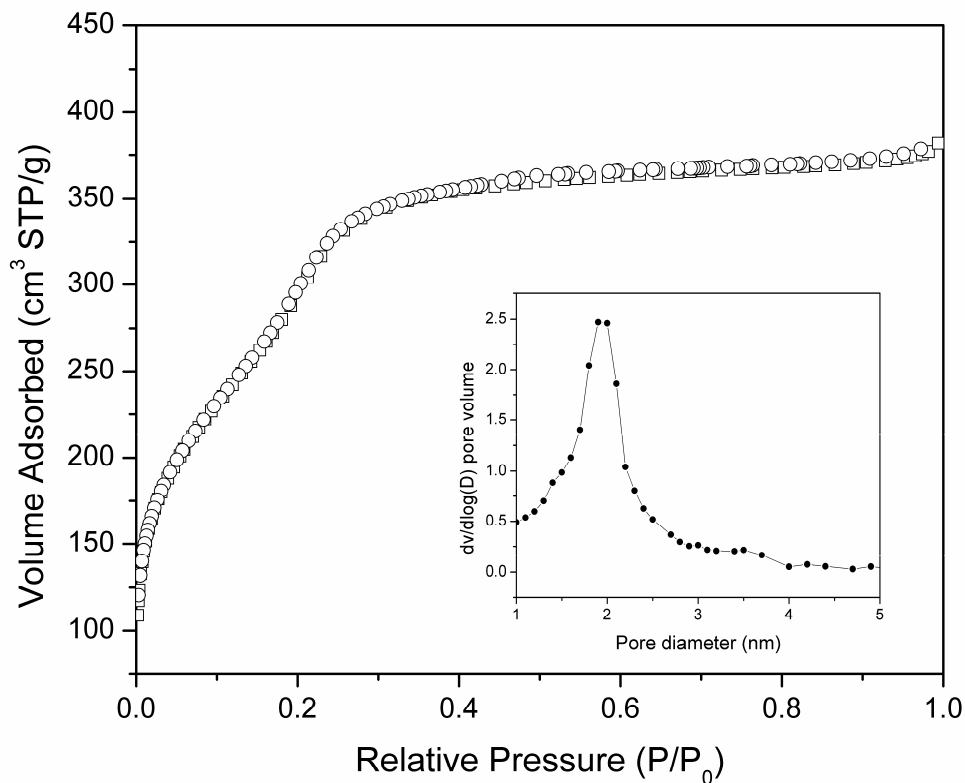


Figure 6-2. The N₂ adsorption-desorption isotherms of MCM-48 silica at 77 K

had a very high surface area of around 1007 m²/g, indicating high quality. The unimodal pore size distribution is centered at 2.0 nm by BJH method. These results are in agreement with previously published results on micellar templated mesoporous silica materials.^{11,12,18,19,21} The FESEM images of the calcined MCM-48 particles in Figure 4-3 show that a narrow distribution of particle sizes (~ 1 μm) was obtained through a combination of sonication and sedimentation.

In order to verify the compatibility of MCM-48 silica with the glassy polymer and to check for the presence of unselective voids in the MCM-48/PSF MMMs, permeability measurements for He and O₂ were conducted using the PSF MMM containing 10 wt %

as-synthesized MCM-48 silica (before calcinations) as shown in Table 6-1. The external surface of uncalcined mesoporous silica is covered with surfactant molecules electrostatically bonded to the external surface.²³ However, uncalcined mesoporous silica materials which have been extensively washed provide external silanol groups for surface selective modifications.^{17,24,25} Because the pores of the as-synthesized MCM-48 silica are none the less filled with organic surfactant, this silica is a good system for checking wetting properties with polymers and for the presence of defects. The presence of any

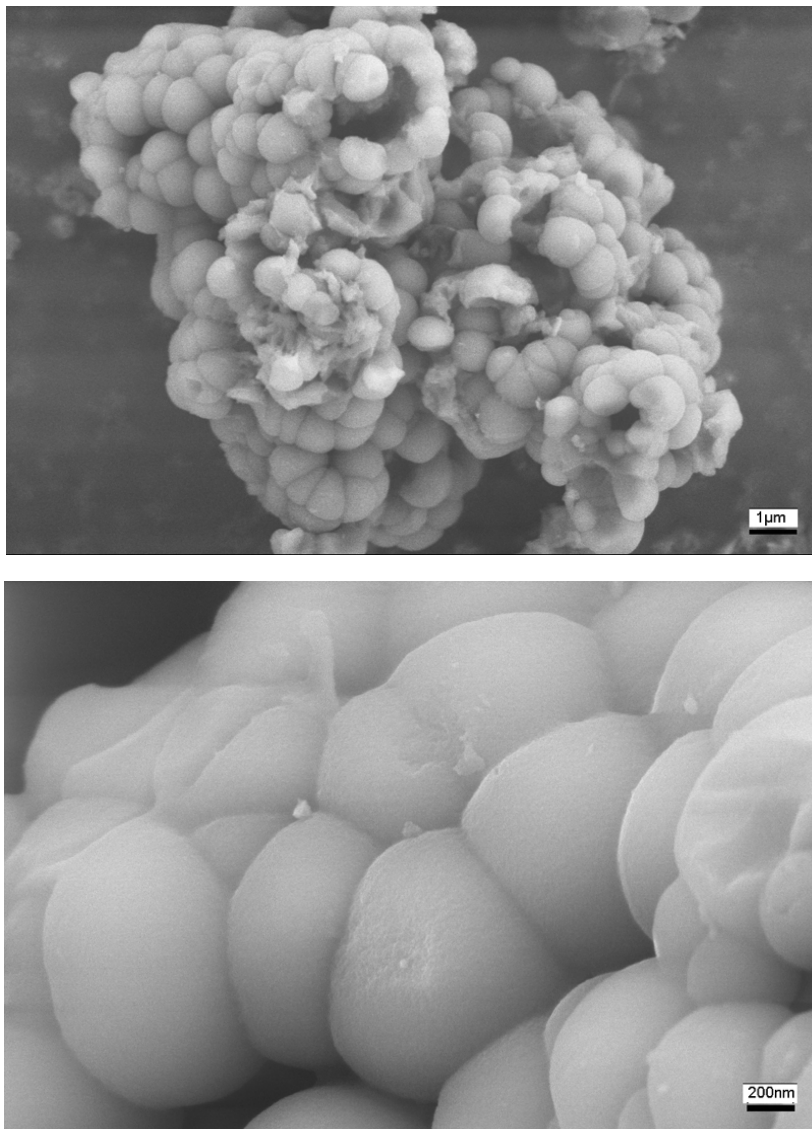


Figure 6-3. FESEM images of MCM-48 at (a) lower and (b) higher magnification

Table 6-1. Gas permeabilities of the pure polysulfone and as-synthesized MCM-48 MMMs

Wt % As-syn.MCM-48	He		O ₂	
	P	P	D	S
0	8.02 ± 0.19	0.98 ± 0.06	3.33 ± 0.17	0.22 ± 0.02
10	7.98 ± 0.12	0.95 ± 0.07	3.08 ± 0.29	0.24 ± 0.01

P = Permeability, Barrer

D = Diffusivity, 10⁻⁸, cm²/sec

S = Solubility, cm³@ STP / (cm³ polymer atm)

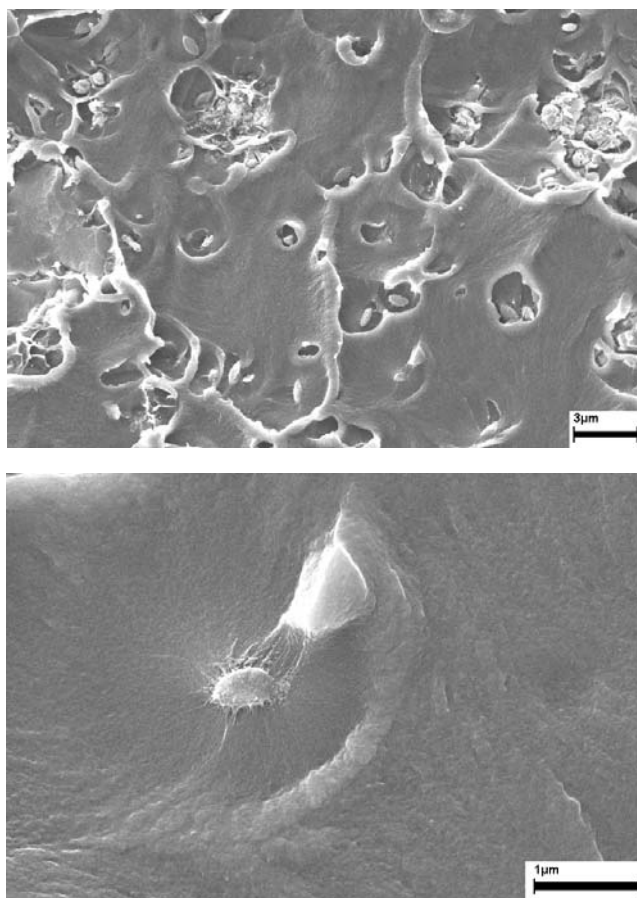


Figure 6-4. Cross-sectional FESEM images of 10 wt % as-synthesized MCM-48/PSF MMMs at (a) lower and (b) higher magnification

In order to further investigate the presence of unselective voids in MMMs, careful FESEM inspections were carried out. FESEM cross-sectional images of 10 wt % as-synthesized MCM-48/PSF MMMs are shown in Figure 6-4. Figure 6-4-(a) shows that MCM-48 silica particles appear to be well dispersed throughout the PSF matrix and few empty cavities remain representing replicas of MCM-48 silica cleaved away when FESEM sample was prepared with liquid nitrogen. The FESEM image at higher magnification, Figure 6-4-(b), shows that the polymer adheres well to the MCM-48 silica particles and that no unselective voids are present around the mesoporous silica particles. The permeability and FESEM results suggest that the as-synthesized MCM-48 added to the polymer matrix behaves as an impermeable filler, lowering the permeability of gases, and hindering the diffusion of oxygen. Furthermore, the MCM-48/PSF MMMs show no evidence of unselective voids.

The FESEM images of 10 ~ 20 wt % of calcined MCM-48/PSF MMMs are shown in Figures 6-5 ~ 6. The FESEM results of 10 wt % of calcined MCM-48 loading are similar to that of the as-synthesized 10 wt % MCM-48/PSF MMMs. At 10 wt % of MCM-48 loading (Figure 6-5-(a)), mesoporous silica particles are well distributed throughout the PSF matrix. Figure 6-5-(b) does not show any unselective voids around calcined MCM-48 particles, suggesting better wetting properties with the polymer matrix than is exhibited by zeolites.^{6,26} The FESEM images of unmodified zeolites loaded in a glassy polymer matrix revealed the presence of unselective voids surrounding zeolites particles. In contrast to zeolite crystals, mesoporous MCM-48 silica particles are covered with weakly acidic surface silanol groups showing favorable interactions with organic molecules.²⁷ A reported concentration of the surface SiOH groups is about 1.8 SiOH/nm² on the MCM-48 surface.²⁸ Although this value includes both reactive single SiOH groups

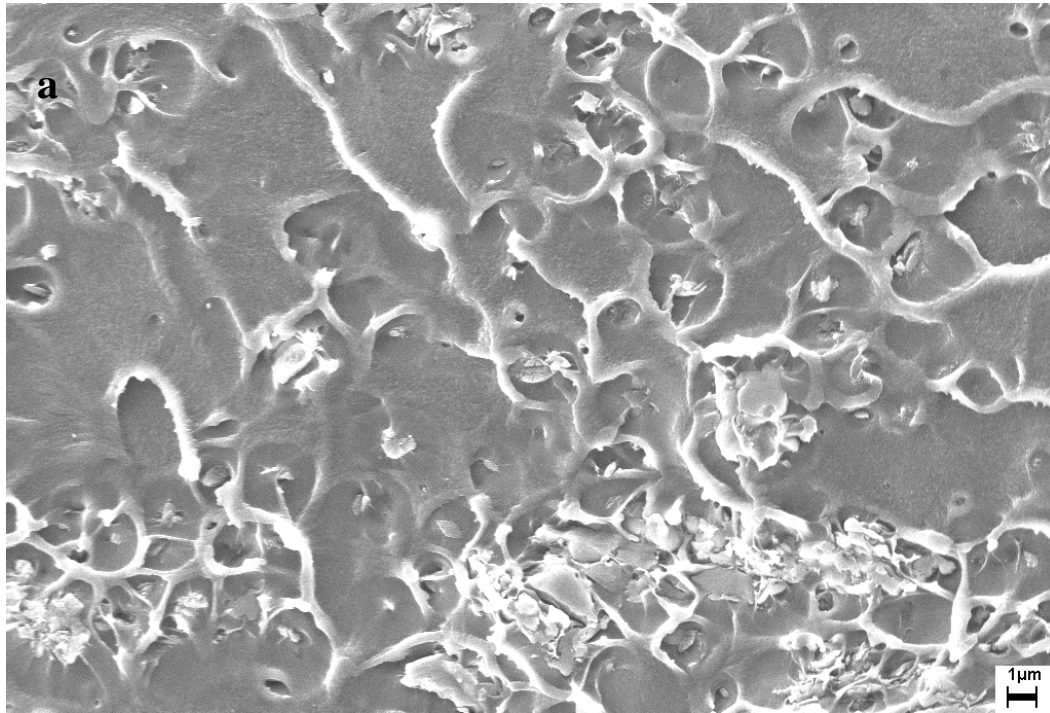


Figure 6-5. Cross-sectional FESEM images of 10 wt % calcined MCM-48/PSF MMMs at (a) lower and (b) higher magnification.

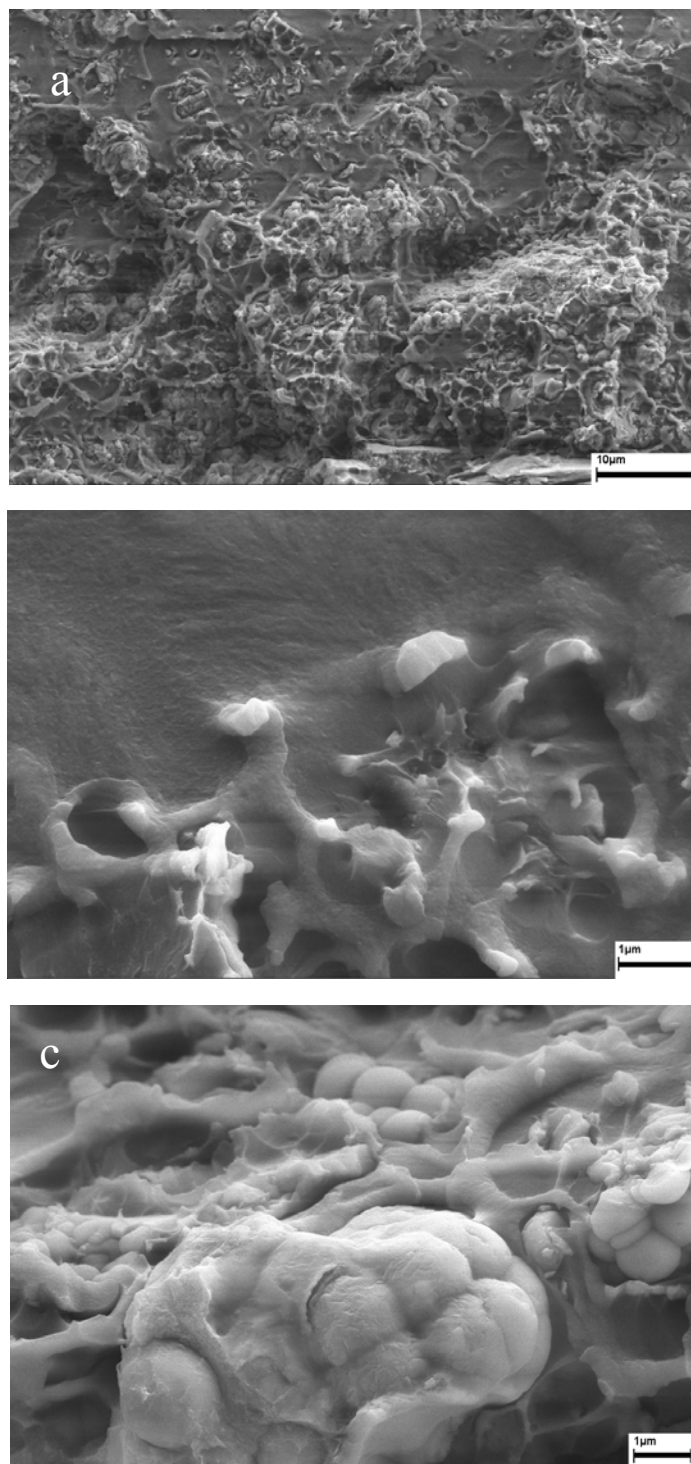


Figure 6-6. FESEM images of 20 wt % calcined MCM-48/PSF MMMs. (a) cross sectional view (lower magnification), (b) discontinuous phase, and (c) continuous silica phase (higher magnification).

and also unreactive hydrogen-bonded SiOH groups, approximately one SiOH/nm² can be a primary adsorption site for other molecules.¹⁷ In an ATR-FTIR spectroscopy study, Reid *et al.* suggested that the phenyl oxygens of PSF interact with surface silanol groups of MCM-41 silica through hydrogen bonding.²⁰ Therefore, it is possible that similar hydrogen bonding interaction occurs between PSF and surface silanol groups of MCM-48, thus providing good wetting properties of MCM-48/PSF MMMs. At the 20 wt % of MCM-48 loadings, unlike 10 wt % of loading, not all MCM-48 particles are well distributed through matrix and some MCM-48 silica particles form small domains in a polymer matrix as shown in Figure 6-6-(a). Although some MCM-48 particles aggregate and form silica domains, higher magnification of the FESEM image in Figures 6-6-(b) and (c) shows that isolated silica particles and the small domains of silica particles are well coated with the polymer.

Table 6-2. Gas permeabilities (Barrer) of various gases in the pure polysulfone and MCM-48 MMMs

Membrane	MCM-48 wt %	He	CO ₂	O ₂	N ₂	CH ₄
PSF	0	8.02±0.19	4.46±0.10	0.98±0.07	0.18±0.01	0.17±0.01
MCM48/PSF	10	15.75±0.53 (96.38%) ^a	8.45±0.13 (89.46%)	1.84±0.10 (87.76%)	0.32±0.02 (77.78%)	0.33±0.02 (94.12%)
MCM48/PSF	20	32.10±0.83 (300.25%)	18.21±0.41 (308.30%)	4.14±0.01 (322.45%)	0.77±0.02 (327.78%)	0.77±0.02 (352.94%)

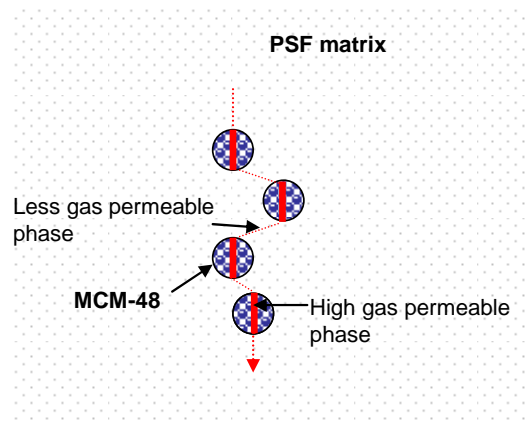
^a () increment from pure polymer

Table 6-3. Selectivity for polysulfone and MCM-48 MMMs

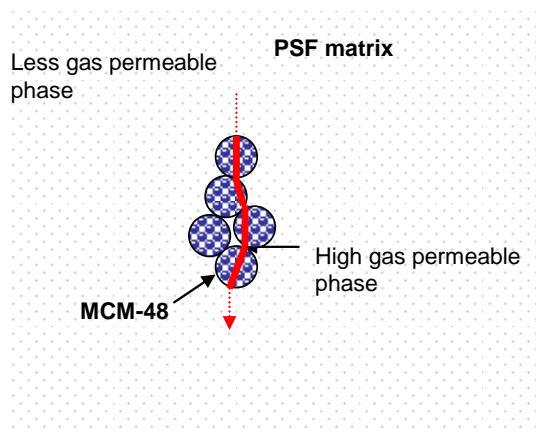
Membrane	MCM-48 wt %	He/CH ₄	CO ₂ /CH ₄	O ₂ / N ₂
PSF	0	46.52	25.88	5.47
MCM48/PSF	10	47.78	25.47	5.75
MCM48/PSF	20	41.56	23.58	5.38

The permeability results and ideal separation factors for the mesoporous MCM-48 silica and PSF MMMs are shown in Tables 6-2 and 6-3, respectively. Because of different polymer processing and film preparation history, our permeability values for pure PSF membranes are somewhat lower than those previously reported by other research groups.^{20,29} For all tested gases (He, CO₂, O₂, N₂, and CH₄), the permeability values increased in proportion to the amount of MCM-48 silica in the polymer matrix. Addition of 10 wt % of MCM-48 to PSF resulted in ~85 % increase in the permeability of all gases tested. These overall increases in permeability maintained the selectivity constant or only slightly changed as shown in Table 6-3. At 20 wt % of MCM-48 silica loading, the permeability increased dramatically by ~300 % for He and CO₂, and ~320% for O₂, N₂, and CH₄, respectively. Despite these increases in permeability, the separation factor decreased only slightly or remained virtually unchanged. From the FESEM images at 20 wt % MCM-48 loading, MCM-48 silica particles form small domains throughout the polymer matrix. Koros *et al.* suggested that higher membrane performance can be achieved if the mixed matrix membrane morphology forms some continuous pathways through the filler component.³⁰ Some semblance of silica domain continuity can be seen

in Figure 6-6 for the MCM48/PSF MMMs. Figure 6-7 illustrates simplistic, discontinuous and continuous penetrant pathways through the molecular sieving phase of MMMs. The continuous pathways present in the polymer matrix with the addition of 20 wt % of MCM-48 allow the gas molecules to diffuse solely through the molecular sieve phase such that high gas permeation performance results, while in discontinuous phase as in the case of 10 wt % of silica loading, gas molecules are forced to diffuse through less permeable PSF region.



(a)



(b)

Figure 6-7. Simple illustration for (a) discontinuous pathway through MCM-48 (10 wt % of MCM-48 loading), and (b) continuous pathway through MCM-48 (20 wt % of MCM-48 loading).

Table 6-4. Diffusivity (D) and solubility(S) of various gases in the pure polysulfone and MCM-48 MMMs

Sample	CO ₂		O ₂		N ₂		CH ₄	
	D	S	D	S	D	S	D	S
PSF	1.11±0.01	3.06±0.07	3.33±0.17	0.22±0.02	1.05±0.12	0.13±0.01	0.26±0.01	0.50±0.03
10 wt % MCM48 /PSF	2.06±0.04	3.11±0.07	5.03±0.34	0.28±0.00	1.35±0.04	0.18±0.01	0.44±0.03	0.57±0.03
20 wt % MCM48 /PSF	3.00±0.03	4.61±0.06	6.75±0.11	0.47±0.01	1.40±0.25	0.42±0.06	0.48±0.02	1.21±0.06

$$D = 10^{-8}, \text{ cm}^2/\text{sec}$$

$$S = \text{cm}^3 @ \text{STP} / (\text{cm}^3_{\text{polymer}} \text{ atm})$$

The differences in permeabilities of each MMMs can be better understood by analyzing the contributions of diffusivity and solubility coefficients to the overall permeabilities. The diffusivity and solubility coefficients for the tested gases are shown in Table 6-4. Similar to the observed increase in permeability, after the incorporation of MCM-48 silica to the polymer, diffusivity and solubility coefficients for all tested gases increased monotonically. Increases in gas permeability have been reported for polymer/silica MMMs.^{20,31-33} The increases in the O₂/N₂ selectivity and oxygen permeability compared to those in a pristine polymer were observed for the polymer/silica composites by Koros *et al.*³³ The increase in permeability was attributed to the disruption of polymer chain packing in the presence of the silica particles.³³ Also, Freeman *et al.* suggested that nanometer-sized fumed silica (FS) particles are able to disrupt packing of rigid polymer chains, thereby subtly increasing the free volume available for molecular transport.³¹ For example, at 20 wt % of FS loading, methane permeability in FS-filled glassy polymer is

approximately 140 % higher than that in the pure polymer membrane. The increase in permeability of MCM-48/PSF MMMs observed here is more than twice that of the FS-filled polymer membrane system suggesting that some permeation also occurs through the MCM-48 pores. The pore size of the tested MCM-48 silica is 2.0 nm by the BJH method. However, the BJH method overpredicts the pressures of the capillary condensation/desorption, and thus underestimates the calculated pore size in typical mesoporous silica materials by ca. 1.0 nm, or by 25 -30 % as the pore size approaches 2.0 nm.^{23,34,35} Thus, the MCM-48 silica pore size should be near 3.0 nm. While this may enhance gas diffusion, the pore openings may not be large enough to enable penetration of the high molecular weight polymer. Therefore, the monotonic increase in diffusivity could be a consequence of the presence of high diffusivity tunnels and redistribution of rigid polymer chain near the pore entrance. As shown in Table 6-4, the solubility coefficients also increase with the addition of MCM-48 silica. To better explain the increases in solubility in the MCM-48/PSF MMMs system, separate sorption studies for MCM-48, PSF, and MMMs were carried out. These gas sorption isotherms are shown in Figure 6-8. As shown in Figures 6-8-(a) and (b), mesoporous MCM-48 silica has a higher adsorption capacity than PSF because of its high coverage of silanol groups on silica surface.^{17,27,28} For porous filler particles dispersed in a continuous polymer matrix, the solubility of the composite can be modeled by³²

$$S = \phi_{\text{MCM48}} S_{\text{MCM48}} + (1 - \phi_{\text{MCM48}}) S_{\text{PSF}} \quad (1)$$

where S_{MCM48} and S_{PSF} are the intrinsic solubilities of MCM-48 and PSF. The volume fraction of MCM-48 (ϕ_{MCM48}) has been estimated using pure component densities as follows:³²

$$\phi_{MCM\ 48} = \frac{w_{MCM\ 48}}{w_{MCM\ 48} + \frac{\rho_{MCM\ 48}}{\rho_{PSF}}(1 - w_{MCM\ 48})} \quad (2)$$

Here, ρ_{MCM48} and ρ_{PSF} denote the MCM-48 silica and pure polymer densities, respectively, and w_{MCM48} is the silica weight fraction. The densities of MCM-48 and PSF used here were 1.64 and 1.24 g/cm³, respectively.³⁶ The calculated and experimental value of the solubility coefficients of N₂ at 4 bar and 308 K are shown in Table 6-5. Addition of 20 wt % of MCM-48 silica resulted in a 255 % increase in the solubility of N₂ (0.20 to 0.71 cm³@ STP / (cm³ polymer atm)). In Figure 6-8-(c), the predicted N₂ uptake for PSF containing 20 wt % MCM-48 based on the pure material sorption capacities and the additive model are expressed by eq 1. The measured uptake by 20 wt % of MCM-48/PSF MMM shows a very similar trend with the gas sorption values predicted by the additive model. Table 6-5 shows that the experimental solubility coefficient of MMM containing 20 wt % of MCM-48 (0.71 cm³@ STP / (cm³ polymer atm)) corresponds to the theoretical value (0.65 cm³@ STP / (cm³ polymer atm)). Therefore, the increase in permeability of MCM-48/PSF MMMs can be attributed to an increase in diffusivity as well as solubility.

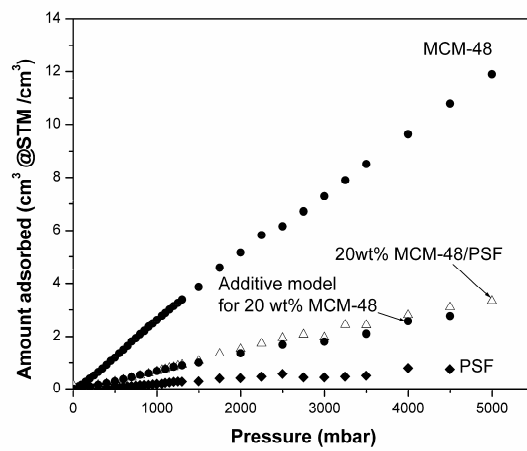
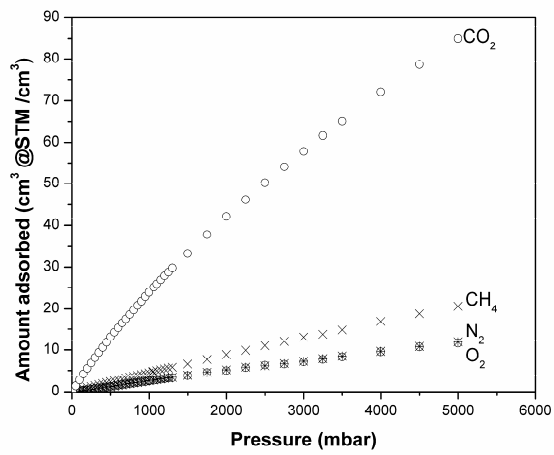
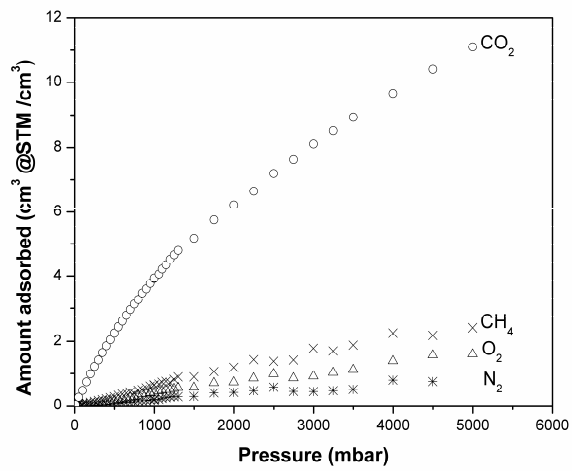


Figure 6-8. Gas adsorption isotherms for (a) PSF, (b) MCM-48 silica, and (c) 20 wt % MCM-48/PSF MMMs for N₂.

6.4. Conclusion

Mixed matrix membranes were prepared using a mesoporous MCM-48 silica synthesized by a templating method and a polysulfone as the polymer matrix. The high surface coverage of silanol groups on the MCM-48 provided good interaction with PSF matrix. Helium permeation data and SEM images of as-synthesized MCM-48/PSF MMMs suggest that MCM-48 silica particles adhered well to PSF and prepared MMMs were defect free. Mesoporous MCM-48 materials offer the favorable effect of large increase in gas permeability in MMMs without sacrificing selectivity. These dramatic increases in gas permeability resulted from increases in solubility as well as diffusivity. The continuous pathways present in the polymer matrix with the high loading of MCM-48 silica allowed the gas molecules to diffuse solely through the molecular sieve phase such that high gas permeation performance results. The measured uptake of MCM-48/PSF MMM showed a very similar increase in the gas sorption capacities predicted by a simple theoretical model. The observed increases in both the diffusivity and solubility make mesoporous MCM-48 silica an attractive additive for enhancing the gas permeability of MMMs without sacrificing selectivity.

6.5. References.

- [1] L. M. Robeson, Correlation of separation factor versus permeability for polymeric membranes, *J. Membr. Sci.*, 62 (1991) 165.
- [2] W. J. Koros and G. K. Fleming, Membrane-based gas separation, *J. Membr. Sci.*, 83 (1993) 1.
- [3] S. A. Stern, Polymers for gas separations: The next decade, *J. Membr. Sci.*, 94 (1994) 1.
- [4] B. D. Freeman, Basis of Permeability/Selectivity Tradeoff Relations in Polymeric Gas Separation Membranes, *Macromolecules*, 32 (1999) 375.
- [5] R. Mahajan and W. J. Koros, Factors controlling successful formation of mixed-matrix gas separation materials, *Ind. Eng. Chem. Res.*, 39 (2000) 2692.
- [6] R. Mahajan and W. J. Koros, Mixed matrix membrane materials with glassy polymers. Part 1, *Polym. Eng. Sci.*, 42 (2002) 1420.
- [7] R. Mahajan and W. J. Koros, Mixed matrix membrane materials with glassy polymers. Part 2, *Polym. Eng. Sci.*, 42 (2002) 1432.
- [8] S. Kulprathipanja, R. W. Neuzil and N. N. Li, Separation of fluids by means of mixed matrix membranes United States Patent 4,740,219 (1988)
- [9] T. W. Pechar, S. Kim, B. Vaughan, E. Marand, V. Baranauskas, J. Riffle, H. K. Jeong and M. Tsapatsis, Preparation and characterization of a poly(imide siloxane) and zeolite L mixed matrix membrane, *J. Membr. Sci.*, 277 (2006) 210.
- [10] T. W. Pechar, S. Kim, B. Vaughan, E. Marand, M. Tsapatsis, H. K. Jeong and C. J. Cornelius, Fabrication and characterization of polyimide-Zeolite L Mixed Matrix Membranes for Gas Separations, *J. Membr. Sci.*, 277 (2006) 195.
- [11] C. T. Kresge, M. E. Leonowicz, W. J. Roth, J. C. Vartuli and J. S. Beck, Ordered mesoporous molecular sieves synthesized by a liquid-crystal template mechanism, *Nature*, 359 (1992) 710.
- [12] J. S. Beck, J. C. Vartuli, W. J. Roth, M. E. Leonowicz, C. T. Kresge, K. D. Schmitt, C. T. W. Chu, D. H. Olson, E. W. Sheppard, S. B. McCullen, J. B. Higgins and J. L. Schlenker, A new family of mesoporous molecular sieves prepared with liquid crystal templates, *J. Am. Chem. Soc.*, 114 (1992) 10834.
- [13] G. Q. L. X. S. Zhao, Modification of MCM-41 by surface Silylation with trimethylchlorosilane and adsorption study, *J. Phys. Chem.B*, 102 (1998) 1556.
- [14] X. Feng, G. E. Fryxell, L. Wang, A. Y. Kim, J. Liu and K. M. Kemner, Functionalized monolayers on ordered mesoporous supports, *Science*, 276 (1997) 923.
- [15] X. Xu, C. Song, J. M. Andresen, B. G. Miller and A. W. Scaroni, Novel polyethylenimine-modified mesoporous molecular sieve of MCM-41 type as high-capacity adsorbent for CO₂ capture, *Energy and Fuels*, 16 (2002) 1463.
- [16] H. Y. Huang, R. T. Yang, D. Chinn and C. L. Munson, Amine-grafted MCM-48 and silica xerogel as superior sorbents for acidic gas removal from natural gas, *Ind. Eng. Chem. Res.*, 42 (2003) 2427.
- [17] S. Kim, J. Ida, V. V. Guliyants and J. Y. S. Lin, Tailoring pore properties of MCM-48 silica for selective adsorption of CO₂, *J. Phys. Chem.B*, 109 (2005) 6287.
- [18] N. Nishiyama, D. H. Park, A. Koide, Y. Egashira and K. Ueyama, A mesoporous silica (MCM-48) membrane: preparation and characterization, *J. Membr. Sci.*, 182 (2001) 235.

- [19] N. Nishiyama, D.-H. Park, Y. Egashira and K. Ueyama, Pore size distributions of silylated mesoporous silica MCM-48 membranes, *Separ. Pur. Tech.*, 32 (2003) 127.
- [20] B. D. Reid, F. A. Ruiz-Trevino, I. H. Musselman, J. Kenneth J. Balkus and J. P. Ferraris, Gas permeability properties of polysulfone membranes containing the mesoporous molecular sieve MCM-41, *Chem. Mater.*, 13 (2001) 2366.
- [21] A. D. M.S. Morey, G.D. Stucky Silica-Based, Cubic mesostructures: synthesis, characterization and relevance for catalysis, *J. Por. Mater.*, 5 (1998) 195.
- [22] J. Crank, *The Mathematics of Diffusion*, Oxford Press; London (1990)
- [23] M. Kruk, M. Jaroniec, Y. Sakamoto, O. Terasaki, R. Ryoo and C. H. Ko, Determination of pore size and pore wall structure of MCM-41 by using nitrogen adsorption, transmission electron microscopy, and X-ray diffraction, *J. Phys. Chem.B*, 104 (2000) 292.
- [24] A. Stein, B. J. Melde and R. C. Schrodin, Hybrid inorganic-organic mesoporous silicates - nanoscopic reactors coming of age, *Adv. Mater.*, 12 (2000) 1403.
- [25] F. d. Juan and E. Ruiz-Hitzky, Selective functionalization of mesoporous silica, *Adv. Mater.*, 12 (2000) 430.
- [26] J.-M. Duval, A. J. B. Kemperman, B. Folkers, M. H. V. Mulder, G. Desgrandchamps and C. A. Smolders, Preparation of zeolite filled glassy polymer membranes, *J. Appl. Polym. Sci.*, 54 (1994) 409.
- [27] K. K. a. H. V. A. Jentys, Concentration of surface hydroxyl groups on MCM-41, *Micro. Meso. Mater.*, 27 (1999) 321.
- [28] K. S. D. Kumar, C. du Fresne von Hohenesche, M. Grün, K. K. Unger, MCM-41, MCM-48 and related mesoporous adsorbents: their synthesis and characterisation, *Coll. Surf. A, Phys. Eng. Asp.*, 187-188 (2001) 109.
- [29] T. M. Gür, Permselectivity of zeolite filled polysulfone gas separation membranes *J. Membr. Sci.*, 93 (1994) 283.
- [30] C. M. Zimmerman, A. Singh and W. J. Koros, Tailoring mixed matrix composite membranes for gas separations, *J. Membr. Sci.*, 137 (1997) 145.
- [31] T. C. Merkel, B. D. Freeman, R. J. Spontak, I. P. Z. He, P. Meakin and A. J. Hill, Sorption, transport, and structural evidence for enhanced free volume in poly(4-methyl-2-pentyne)/fumed silica nanocomposite membranes, *Chem. Mater.*, 15 (2003) 109.
- [32] T. C. Merkel, Z. He, I. Pinnau, B. D. Freeman, P. Meakin and A. J. Hill, Sorption and transport in poly(2,2-bis(trifluoromethyl)-4,5-difluoro-1,3-dioxole-co-tetrafluoroethylene) containing nanoscale fumed silica, *Macromolecules*, 36 (2003) 8406
- [33] M. Moaddeb and W. J. Koros, Gas transport properties of thin polymeric membranes in the presence of silicon dioxide particles, *J. Membr. Sci.*, 125 (1997) 143.
- [34] D. W. P. I. Ravikovitch, W. T. Chueh, G. L. Haller, A. V. Neimark, Evaluation of pore structure parameters of MCM-41 catalyst supports and catalysts by means of nitrogen and argon adsorption, *J. Phys. Chem.B*, 101 (1997) 3671.
- [35] A. V. N. Peter I. Ravikovitch, Relations between structural parameters and adsorption characterization of templated nanoporous materials with cubic symmetry, *Langmuir*, 16 (2000) 2419.
- [36] A. M. Plinio Innocenzi, Massimo Guglielmi, Andrea Bearzotti, Enrico Traversa, Jean Claude Pivin, Mesoporous silica thin films for alcohol sensors, *J. Euro. Cer. Soc.* 21 (2001) 1985.

Chapter 7. Mesoporous Nanoparticles and Polymer Nano-composite Membranes: High Flux and Permeability

7.1. Introduction

Despite the limits of polymeric gas separation membranes, polymeric membranes have been widely used in industrial gas separation processes. There are many opportunities to extend membrane markets for gas separations, however, the existing polymeric membrane materials have been known to have a trade-off between permeability and selectivity as shown in upper bound curves developed by Robeson.¹ Therefore, there is a need for new membrane materials and the development of new membrane structures that exhibit both higher selectivity and intrinsic permeability to specific gases.

One potential strategy for fabricating high performance polymeric membranes involves organic-inorganic hybrid systems such as mixed matrix membranes (MMMs). MMMs have received a lot of attention in the past decade for enhancement of current gas separation membrane performance.²⁻⁶ Typically, fabrication of high gas separation performance MMM has involved the incorporation of various inorganic materials, such as zeolites,^{3,4} carbon molecular sieves,⁷ silica,^{5,6} carbon nanotubes,^{8,9} or mesoporous molecular sieves,^{10,11} into a polymer matrix. However, the application of zeolites is limited by poor interaction with the polymer matrix and the transport is limited by the modification of zeolites with silane coupling agents, which can block pore access.^{12,13} Recently, mesoporous molecular sieves have been used in MMMs to enhance permeability or selectivity.^{10,11,14} Reid *et al.* reported polysulfone (PSF) MMMs with mesoporous silica MCM-41 for gas separation.¹⁰ Kim *et al.* enhanced gas permeability of PSF by incorporating mesoporous MCM-48.¹¹ They showed that mesoporous materials

increased the permeability of the polysulfone MMMs without decreasing selectivity due to good compatibility with the polymer matrix. Shimizu *et al.* reported that the addition of amine functionalized SBA-15 was effective for enhancing CO₂/CH₄ selectivity.¹⁴ However, because the particles were micron sized, the composite membrane was extremely brittle and tended to crack at higher silica loading. Smaller inorganic particles would yield more polymer/particle interfacial area and provide more opportunity to synthesize higher loading of molecular sieves in the polymer matrix. In addition, nanoscale molecular sieves are more suitable for commercialization of MMMs with very thin selective layers than micro-sized zeolite or molecular sieves.

The main object of this study is to develop and characterize organic-inorganic nanocomposite membranes based on nanosized mesoporous silica dispersed inside a polymer matrix. We synthesized a MCM-41 mesoporous silica with ca. 50 nm of particle size and characterized it with X-ray diffraction (XRD), pore size analysis, and field emission scanning microscopes (FESEM). The structure, absence of defects, and properties of MCM-41/PSF MMMs were characterized by FESEM, sorption studies and gas permeation measurements.

7.2. Experimental and Characterization Method

7.2.1. Synthesis and Functionalization of Nano-sized Mesoporous MCM-41

Nano-sized mesoporous MCM-41 silica with particle size ~50 nm was synthesized according to a previously published procedure.^{15,16} In this method, the aqueous micellar solution containing 2 g of C₁₆H₃₃(CH₃)₃NBr (CTAB, Sigma-Aldrich), 0.57 g of NaOH, and 975 g of deionized water was prepared under stirring for 1 hour. Then,

tetraethylorthosilicate (TEOS, Alfa-Aesar Chemical) was slowly added to the solution at 353 K. The mixture was stirred for 2 hours. The MCM-41 silica was filtered, and washed with deionized water. At this stage, the as-synthesized MCM-48 still contained organic templates. Calcined MCM-41 silica used in the fabrication of MMMs was obtained after as-synthesized MCM-41 silica was calcined in air at 873 K for 3 hours with 1 K/min of heating rate. The MCM-41 silica was vacuum-dried overnight in order to be used in the fabrication of MMM.

The external surface of as-synthesized MCM-41 prior to CTAB removal was first silylated at room temperature for 72 h in a liquid phase of trimethylchlorosilane to avoid agglomeration of higher loading of nanosized silica particle. CTBA was removed by Soxhlet extraction in a mixture of methanol and HCl at 393 K.¹⁷ The modified mesoporous silica samples were filtered and washed in a soxhlet apparatus with n-hexane, and then dried at 323 K.

7.2.2. Fabrication of Membranes

Before fabrication of membranes, PSF (UDEL P-3500, Solvay) was degassed at 413 K for 3 hours under vacuum to remove adsorbed water. In order to fabricate pure PSF membrane, 0.6 g of the PSF was dissolved in 3 mL of chloroform and stirred for one day leading to a viscous solution. The membranes were cast onto a glass substrate using a doctor blade. The glass substrate was covered with a glass cover to slow down the evaporation of solvent, allowing for a film with a uniform thickness without curling. The solutions were given 1 day to dry at room temperature. Once dry, the films were placed under vacuum and the temperature was raised to its glass transition temperature, 458 K

for 1 hour and then cooled down to room temperature. A 6.35 cm diameter circular sample was cut from the film and used for permeation tests.

The fabrication procedure for the mixed matrix membranes was identical to the pure polymer membrane preparation with the additional step of incorporating MCM-41 silica. For a 40 vol % of MCM-41/PSF MMMs, approximately 0.68 g of the pure PSF was dissolved in 3 mL of chloroform and mixed for 24 hours. A predetermined mass of MCM-41 (0.078 g) was dissolved in 1 mL of chloroform with small amount of PSF solution (~5 drops) and sonicated for 30 minutes to enable the dilute polymer solution to coat the mesoporous silica. This MCM-41 solution was added to the polymer solution and the mixture was allowed to mix for 6 hours at room temperature. Following this time period, the mixture was sonicated for 10 minutes, after which it was allowed to mix for 10 minutes. This process was repeated several times. The membranes were cast onto a glass substrate using a Doctor Blade (Paul N. Gardner Company, FL). The evaporation and heat treatments for the mixed matrix membranes were identical to that of the pure polymer membrane.

7.2.3. Characterization

The powder XRD patterns of MCM-41 mesoporous silica were recorded on a Scintag Inc., XDS 2000 spectrometer using $\text{CuK}\alpha$ radiation with a step size of 0.02 °/s. The N_2 adsorption-desorption isotherms were collected at 77 K using Micromeritics ASAP 2010. The MCM-41 silica samples were outgassed prior to these measurements at 423 K overnight under N_2 flow. The surface areas were calculated using the Brunauer-Emmett-Teller (BET) method,¹⁸ and the pore volumes and pore diameters were calculated by the

Barret-Joyner-Halenda (BJH) method.¹⁹ FESEM (LEO 1550) was used to study the morphology of the membranes. Sorption studies were conducted by the gravimetric system (IGA-002, Hiden Isochema, UK). For each measurement, the samples were degassed at 403 K for 10 hours at $P \leq 10^{-6}$ mbar. All tubings and chambers were also degassed by applying vacuum ($P \leq 10^{-6}$ mbar). The degassed samples were then cooled down to the specified temperature (308 K) with a ramping rate of 1 K /minute. The gases used in this research were He, CO₂, O₂, N₂, and CH₄ with a reported purity of 99.99% and purified again by passing through a molecular sieve trap attached to the gravimetric system. The adsorption isotherms were measured by the small stepwise pressure (or concentration) change, i.e. 100 mbar ($P \leq 1.3$ bar) and 250 mbar ($P > 1.3$ bar). The gravimetric sorption studies in this research were conducted at a temperature of 308 ± 1 K and pressure range of 0.01 – 4 bar.

Permeabilities of the polymeric and composite membranes were measured using a constant volume varying pressure apparatus. Permeability was measured directly, and the Time Lag Method²⁰ was applied to the recorded data to determine the diffusivity coefficient. The solubility coefficient was taken as the ratio of the permeability to diffusivity coefficient.²⁰ The gases used in this research were He, CO₂, O₂, N₂, and CH₄. Each gas possessed a purity of 99.99% and was used as received from Air Products. The feed pressure and temperature were kept constant at 4 atm and 308 K, respectively, for all experiments. Each gas was run through a membrane six times and the average results and the standard deviations were recorded. Permeabilities are reported in units of Barrer ($1 \text{ Barrer} = 1 \times 10^{-10} \text{ cm}^3 \cdot (\text{STP}) \cdot \text{cm} / (\text{cm}^2 \cdot \text{sec} \cdot \text{cmHg})$).

7.3. Results and Discussion

The powder X-ray diffraction patterns (XRD) of the calcined MCM-41 nano particle are shown in Figure 7-1. The XRD patterns displayed Bragg peaks in the $2\theta = 1.5-8^\circ$ range, which can be indexed to different hkl reflections. The XRD patterns of the calcined mesoporous MCM-41 silica consisted of the typical reflection at 2.40° and weak reflections at 4.24° and 4.88° which correspond to (100), (110) and (210) of MCM-41, respectively, suggesting the hexagonal $p6$ space group.

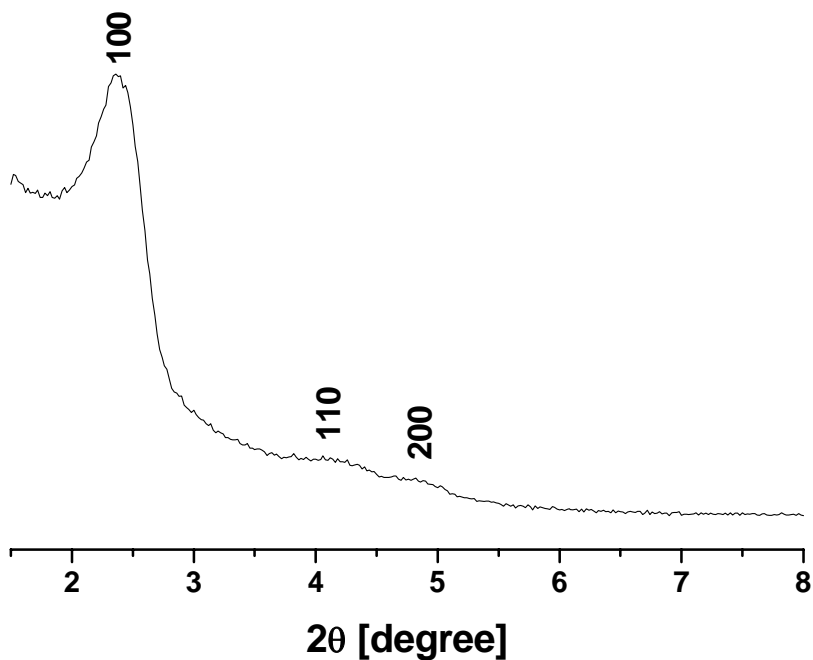


Figure 7-1. XRD pattern of MCM-41 silica

The N₂ adsorption-desorption isotherms at 77 K for the MCM-41 silica are shown in Figure 7-2. The N₂ adsorption isotherm of the MCM-41 is a typical reversible type IV adsorption isotherm characteristic of a mesoporous material. The MCM-41 silica has a very high surface area of around 921 m²/g, indicating its high quality. The unimodal pore size distribution is centered at 2.2 nm calculated by the BJH method. The TEM images of the calcined MCM-41 particles in Figure 7-3 show the existence of highly ordered hexagonal structures with particle size ~50 nm. These results are in agreement with previously published results on nano-sized mesoporous silica materials.^{15,16}

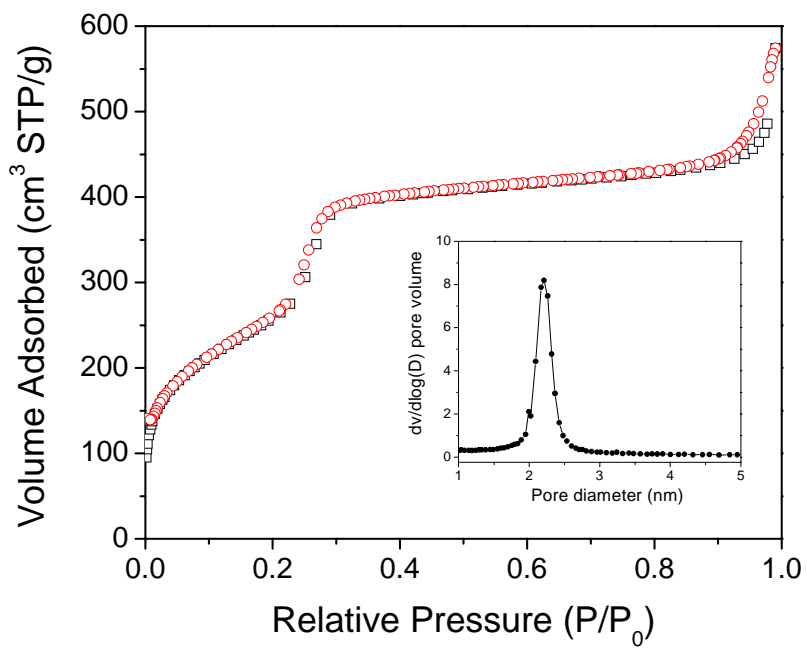


Figure 7-2. The N₂ adsorption-desorption isotherms of MCM-41 silica at 77 K.

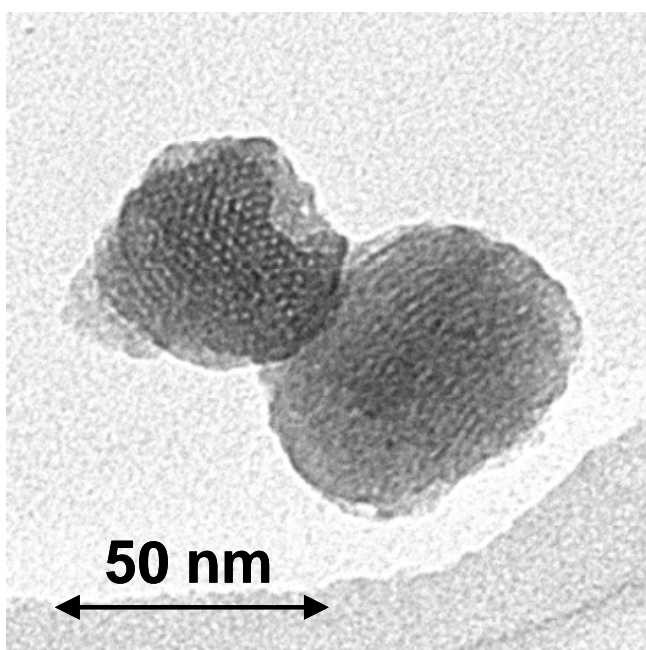


Figure 7-3. The TEM image of MCM-41 silica

Poor wetting properties between polymer and inorganic materials may lead to the formation of nonselective voids or agglomeration of inorganic particles in a polymer, resulting in loss of selectivity and mechanical properties of the membrane. In order to investigate the dispersion properties of mesoporous silica in a PSF matrix, we carefully inspected FESEM images for MMMs containing unmodified or silylated mesoporous silica. FESEM cross-sectional images of 60 vol % unmodified and modified MCM-41/PSF MMMs are shown in Figure 7-4. Figure 7-4-(a) shows that unmodified MCM-41 silica particles agglomerate and form micrometer scale void spaces (indicated by arrows) between polymer matrix and silica phases. However, modified mesoporous silica particles as shown in Figure 7-4-(b) appear to be well dispersed throughout the PSF matrix. The nano-sized mesoporous silica has a high surface area covered by hydrophilic silanol groups. Consequently, the silica particles easily adhere to each other via hydrogen bonding and form irregular agglomeration in polymer matrix.²¹ However, after modification of the silica with trimethyl silyl groups, the external hydrophilic surface is changed into a hydrophobic surface. This treatment can reduce silica-silica interaction and produce a composite with well-dispersed nano-sized mesoporous silica in the matrix.

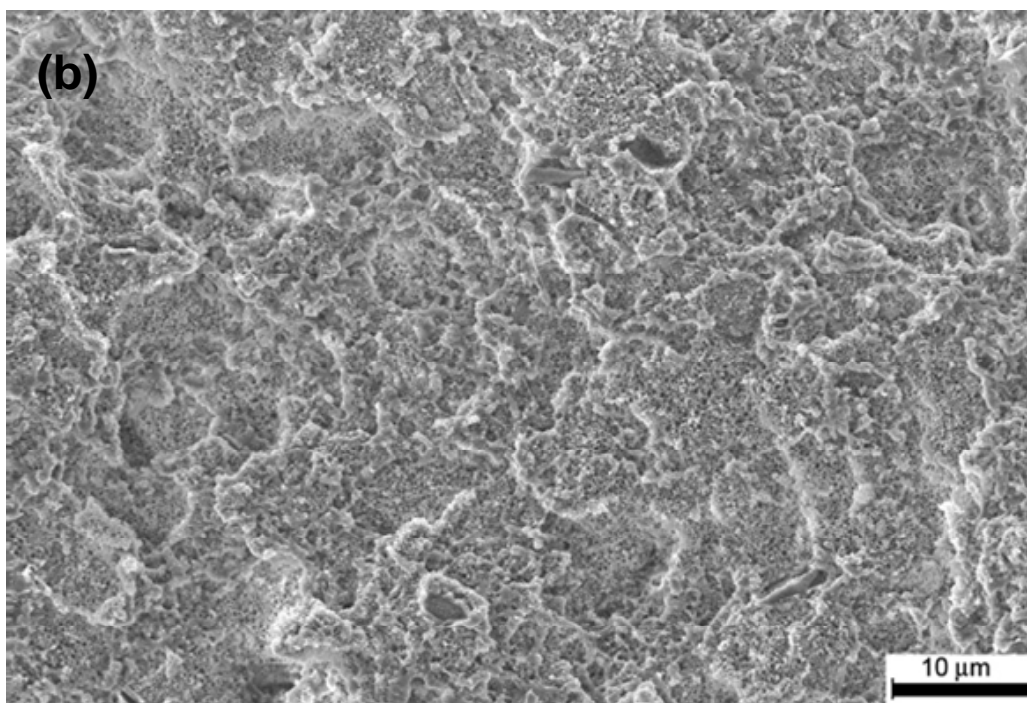
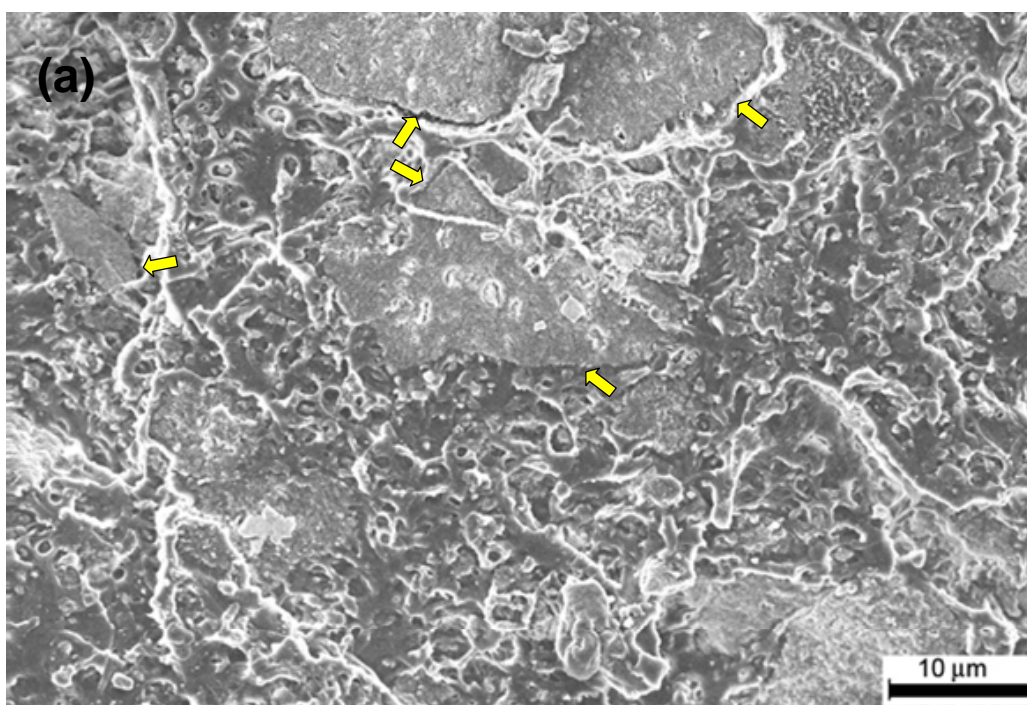


Figure 7-4. FESEM images of (a) unmodified MCM-41/PSF and (b) modified MCM-41/PSF.

The FESEM images of 80 vol % of modified MCM-41/PSF MMMs are shown in Figures 7-5. The FESEM results of 80 vol % modified MCM-41 are similar to that of the 60 vol % MCM-41/PSF MMMs. Even at a loading of 80 vol % (Figure 7-5-(a)), nano-sized silica particles are well dispersed throughout the polymer matrix. The resulting composites are free-standing films which can be used for measuring gas permeation. Higher magnification FESEM images of 80 vol% silica in PSF (Figure 7-5-(b)) show that nano particles have good interaction with the polymer matrix. Few empty cavities remain representing replicas of MCM-41 silica cleaved away from the liquid nitrogen fractured surface.

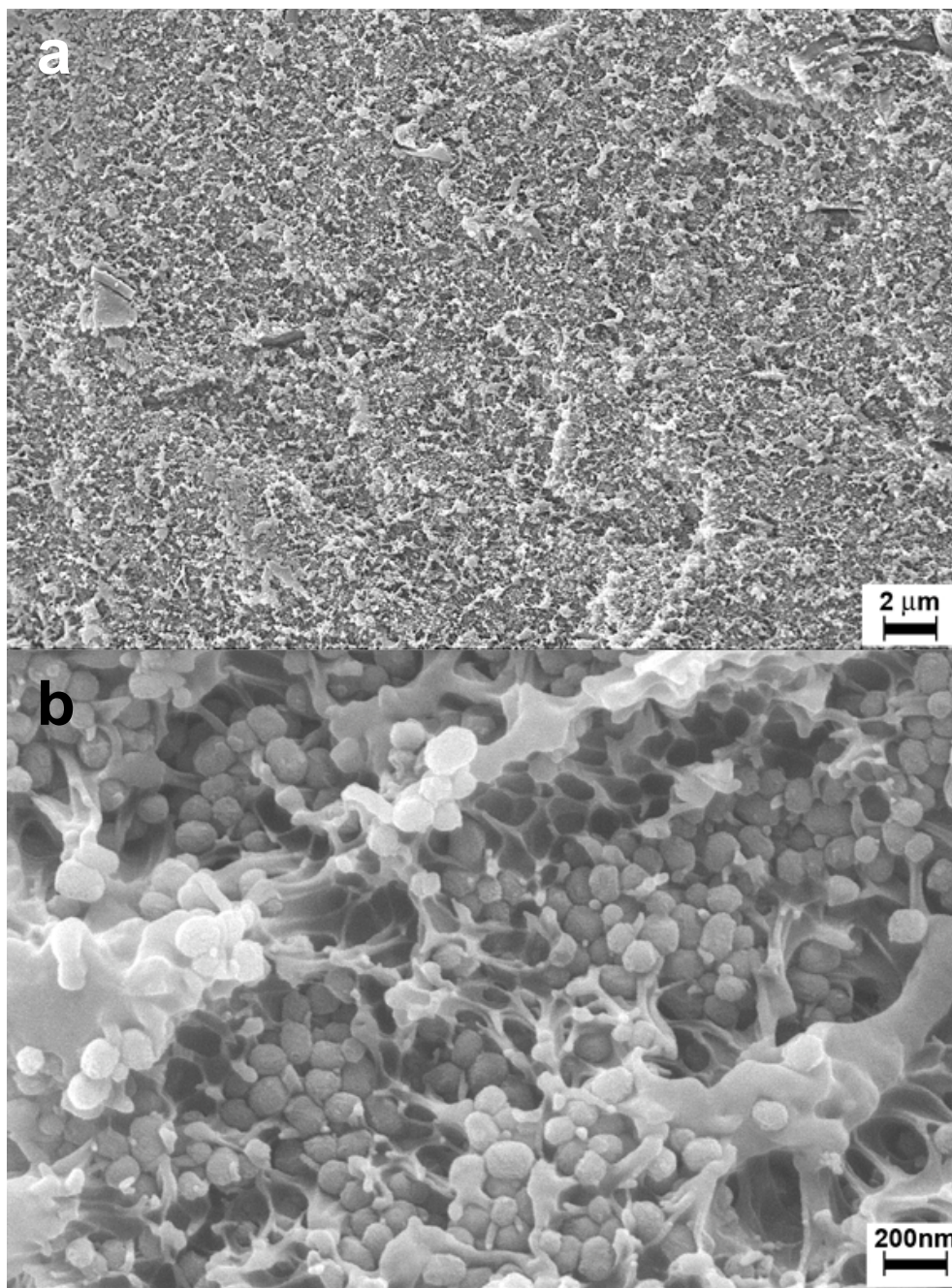


Figure 7-5. Cross-sectional FESEM images of 80 vol % functionalized MCM-41/PSF MMMs at (a) lower and (b) higher magnification.

The permeability results and ideal separation factors for the modified MCM-41 silica and PSF MMMs are shown in Tables 7-1 and 7-2, respectively. Because of different polymer processing and film preparation history, our permeability values for pure PSF membranes are somewhat lower than those previously reported by other research groups. For all tested gases (He, CO₂, O₂, N₂, and CH₄), the permeability values increased in proportion to the amount of MCM-41 silica in the PSF matrix. The addition of 40 vol % and 60 vol % MCM-41 to PSF resulted in ~50% and ~75 % increases in the permeability of all gases tested, respectively. However, there are only slight changes in the selectivity. At a MCM-41 loading of 80 vol%, permeability increased according to mass of gas molecules except helium. The increases in permeability of lighter gas (CH₄ and N₂) are much larger than those of heavier gas (CO₂ and O₂). Gas transport properties through mesoporous silica membranes are governed by the Knusen diffusion model.²² According to Knudsen diffusion model, permeance is inversely proportional to the square root of molecular weight. Addition of higher loading of mesoporous silica into the polymer matrix forms silica rich inorganic phases and its transport properties start to deviate from pristine polymer gas transport properties. For helium, the increase in permeability is smaller than CH₄ because the permeability of helium in the polymer matrix is already high due to its small size. These different increases in permeability at 80 vol % of silica loading cause changes in selectivities. However, those values are much higher than ideal selectivity predicted by the Knusen model and can still be useful in practice gas separations.

Table 7-1. Gas permeabilities (Barrer) of various gases in the pure polysulfone and MCM-41 MMMs

Membrane	MCM-41 vol %	He	CO ₂	O ₂	N ₂	CH ₄
PSF	0	8.02±0.19	4.46±0.10	0.98±0.07	0.18±0.01	0.17±0.01
MCM41/PSF	40	11.81±1.12 (47.25%)	6.58±0.02 (47.53%)	1.40±0.08 (42.86%)	0.28±0.00 (55.56%)	0.29±0.00 (70.59%)
MCM41/PSF	60	14.23±1.33 (77.43%)	7.82±0.38 (75.33%)	1.68±0.09 (71.43%)	0.32±0.01 (77.78%)	0.34±0.00 (100.00%)
MCM41/PSF	80	30.06±0.12 (274.81%)	14.82±0.24 (232.29%)	3.42±0.01 (248.98%)	0.90±0.01 (400.00%)	1.00±0.01 (488%)

^a () increment from pure polymer**Table 7-2.** Selectivity for polysulfone and MCM-41 MMMs

Membrane	MCM-48 wt %	He/CH ₄	CO ₂ /CH ₄	O ₂ / N ₂
PSF	0	46.52	22.97	5.07
MCM41/PSF	40	40.97	22.82	4.99
MCM41/PSF	60	42.00	23.07	5.20
MCM41/PSF	80	30.14	14.85	3.79

The differences in permeabilities of each MMMs can be better understood by analyzing the contributions of diffusivity and solubility coefficients to the overall permeabilities. In order to evaluate the solubility from permeation data, gravimetric sorption isotherms were measured. As shown in Figures 7-6a and b, mesoporous MCM-41 silica has a higher adsorption capacity than PSF because silanol groups cover the inner surface of mesoporous silica. For porous filler particles dispersed in a continuous polymer matrix, the solubility of the composite can be modeled by

$$S = \phi_{\text{MCM41}} S_{\text{MCM41}} + (1 - \phi_{\text{MCM41}}) S_{\text{PSF}} \quad (1)$$

where S_{MCM41} and S_{PSF} are the intrinsic solubilities of MCM-41 and PSF, and ϕ_{MCM41} is the volume fraction of MCM-41. The calculated values of the solubility coefficients of N_2 and CO_2 at 308 K as a function of pressure are represented as dotted lines in Figure 7-6. The addition of nanosized MCM-41 silica resulted in increases in the solubility of N_2 and CO_2 in the membrane. However, the measured N_2 uptake by 80 vol % of MCM-41/PSF MMM shows a lower value than the gas sorption values predicted by the additive model. For CO_2 adsorption uptake, the difference between the experimental and the predicted value is much larger than in the case of N_2 adsorption. Hydrogen-bonding interactions between the surface silanol groups on the external/internal surfaces of the mesoporous silica and the aryl ether groups of PSF have been reported.¹⁰ Although polymer molecules cannot fully penetrate into the mesoporous silica channels, some of silanol groups near the pore entrance are able to interact with the aryl ether groups of PSF. There is a competition for silanol groups by the polysulfone and the penetrant. This results in a decrease in the number of surface silanol groups for interaction with other molecules. However, the addition model assumes an intrinsic solubility of MCM-41, which has

higher reactive silanol number than the modified MCM-41 in composites. Therefore, in composites, lower number of silanol groups for gas adsorption result in lower gas adsorption uptake than predicted by the mixing model.

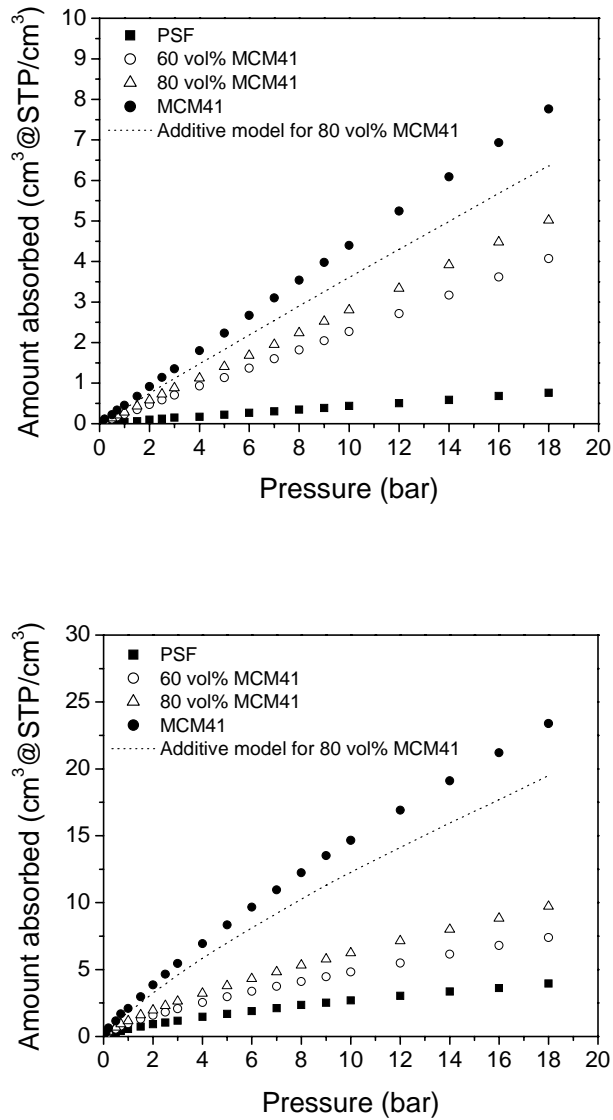


Figure 7-6. Gas adsorption isotherms for (a) N₂ and (b) CO₂ on MMMs and additive model for 80 vol% MCM41.

The solubility coefficients calculated from time-lag method as well as sorption measurements for CO₂, O₂, N₂, and CH₄ are shown in Figure 7-7. Although, the absolute values of the solubility coefficients calculated from the time-lag and gravimetric sorption method are different, the solubilities are increased with the addition of mesoporous MCM-41 silica. This is consistent with the observed increases in permeability. These results are also consistent with the separate gravimetric sorption measurements shown in Figures 7-6, which demonstrate increases in sorption capacity at 4 atm with the addition of nanosized MCM-41.

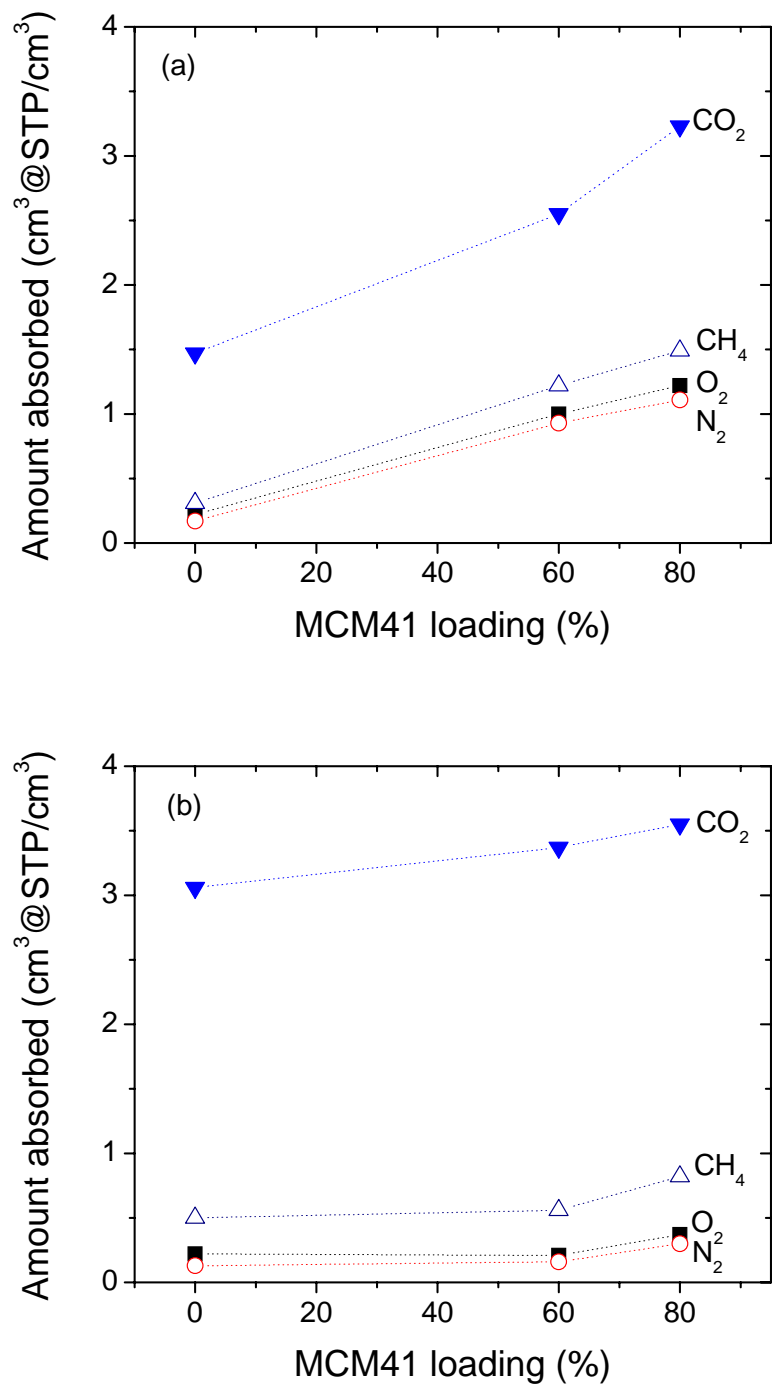


Figure 7-7. Solubility coefficient of 0 wt%, 60 vol%, and 80 vol% MCM41/PSF MMMs at 308 K and 4 bar (a) adsorption isotherm, and (b) time-lag method.

In addition to steady-state diffusion coefficients calculated using permeability data and time-lag method, kinetic diffusion coefficients were also calculated from sorption data. Figure 7-8 presents CO₂ kinetic sorption fractional uptake curves in pure PSF and MMMs containing 60 vol % and 80 vol % nanosized silica. Since the CO₂ diffusivity is strongly dependent on concentration, uptake curves were carried out only at very low concentration, 0.1 bar. As shown in these CO₂ uptake curves for PSF and composite films, the CO₂ sorption equilibrium is attained more rapidly as mesoporous silica loading increases. This implies that addition of mesoporous silica result in faster diffusion in the MCM-41 composite samples. Kinetic diffusion coefficients were calculated from the mass uptake curves (M_t/M_∞) by data-fitting the Fick's second law for the sorption of a penetrant in film as described by Crank:²⁰

$$\frac{M_t}{M_\infty} = 1 - \frac{8}{\pi^2} \sum_{n=0}^{\infty} \frac{1}{(2n+1)^2} \exp\left[-\frac{D(2n+1)^2 \pi^2 t}{l^2}\right] \quad (2)$$

where M_t and M_∞ represent the amount of gas absorbed by the membrane film at time t and the equilibrium sorption after infinite time, respectively. D is the kinetic (transport) diffusion coefficient, t is the time required to attain M_t and l is the thickness of the sample.

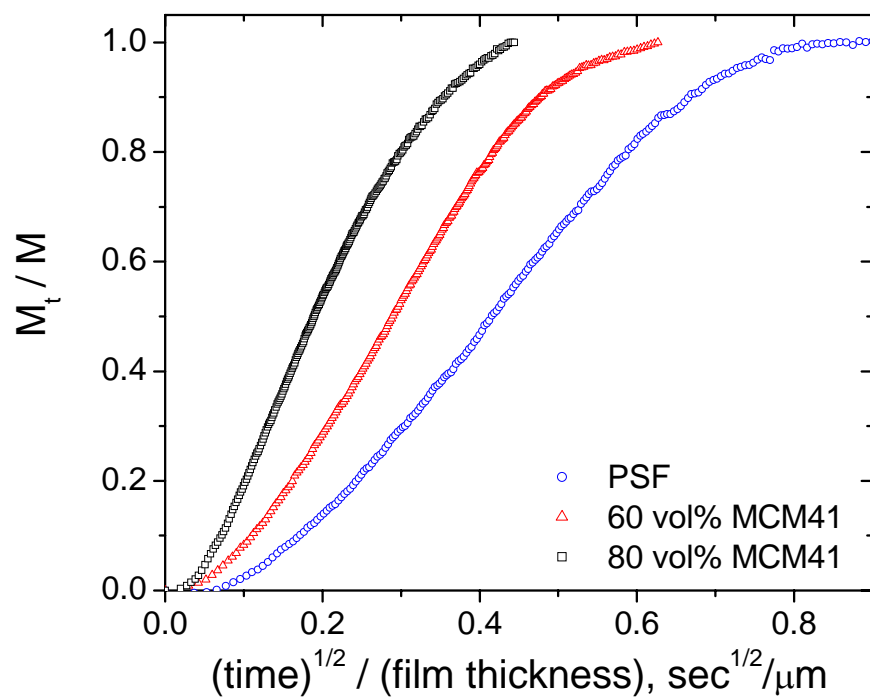


Figure 7-8. CO₂ kinetic uptake curves in 0 wt%, 60 vol%, and 80 vol% MCM41/PSF MMMs at 308 K and 0.1 bar. M_t is permeate mass uptake at time t and M_∞ is the mass uptake at equilibrium state.

Figure 7-9 shows CO₂ diffusion coefficients in PSF and MCM41/PSF composite films determined from the kinetic sorption studies. Also included in this figure are the diffusion coefficients calculated from time-lag method for comparison. Although the absolute values of the diffusion coefficients obtained by the time-lag and kinetic sorption methods are different,²³ qualitatively the changes are consistent. Consistent with permeation data, both of diffusion coefficients increases with the addition of nanosized mesoporous silica. Typically, kinetic diffusion coefficients measured by the gravimetric sorption method are lower than those obtained by the time-lag method. This discrepancy results because kinetic uptake experiments involve additional diffusion into the dead-end pores, while transport through dead-end pores does not play a role in steady-state permeation (time-lag) experiments.²⁴ From solubility and diffusivity data, therefore, it is suggested that the increase in permeability of MCM-41/PSF MMMs can be attributed to an increase in diffusivity as well as solubility.

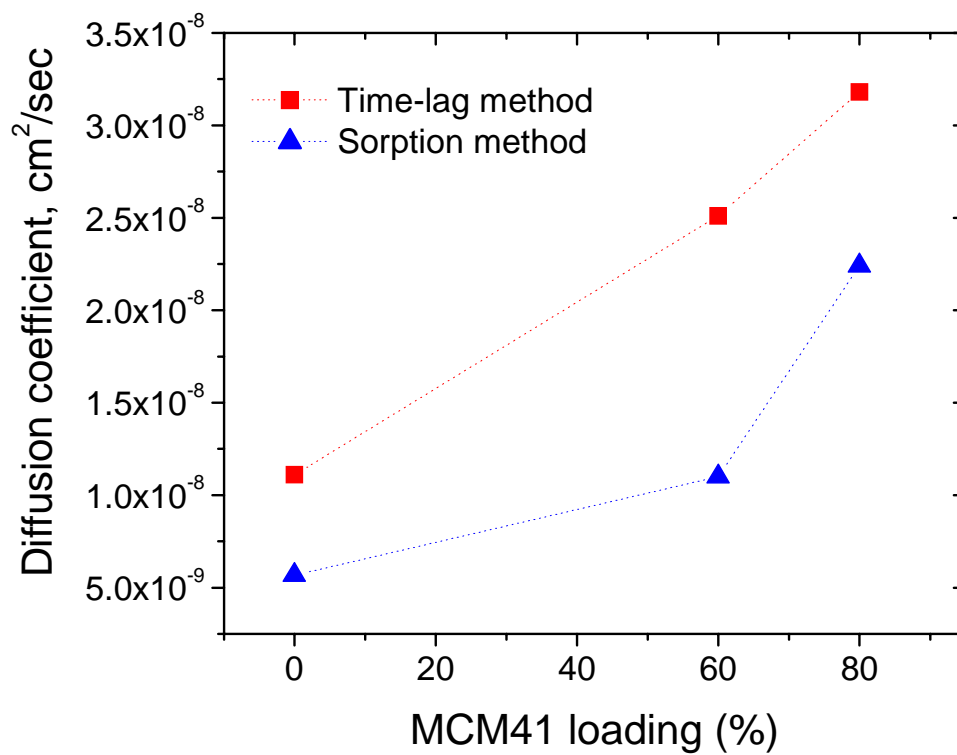


Figure 7-9. CO₂ diffusion coefficients in 0 wt%, 60 vol%, and 80 vol% MCM41/PSF MMMs at 308 K and 0.1 bar.

7.4. Conclusion

Nanosized mesoporous MCM-41 silica was used for the fabrication of MMMs to increase silica loading in a polysulfone matrix. In order to avoid agglomeration of nanosized silica particles at higher loadings, the external surface of mesoporous silica was modified hydrophobic trimethylsilyl group and composite membrane containing mesoporous silica up to 80 vol%. MMM made with mesoporous MCM-41 materials result in large increase in gas permeability. These dramatic increases in gas permeability resulted from an increases in solubility as well as diffusivity. The measured uptake of MCM-41/PSF MMM showed an increase in the gas sorption capacities with the addition of mesoporous silica. In addition, diffusivities calculated from steady-state permeation data and kinetic uptake curves, demonstrated that the diffusion coefficients increased with increasing nanosized mesoporous silica content in PSF. The observed increases in both the diffusivity and solubility make mesoporous MCM-41 silica an attractive additive for enhancing the gas permeability of MMMs without sacrificing selectivity.

However, the true potential of these nanocomposite membranes will be realized when mesoporous silica channels are functionalized to enhance facilitated transport of penetrant gases. Currently, efforts are underway to enhance the nanosized mesoporous silica and penetrant (e.g CO₂) interaction via chemical functionalization of the channel surface with amine groups. Then the combination of selectivity and high permeability will propel the performance of these mesoporous silica/polymer nanocomposite membranes above Robeson's upper bound.¹

7. 5. References

- [1] L. M. Robeson, Correlation of separation factor versus permeability for polymeric membranes, *J. Membr. Sci.*, 62 (1991) 165.
- [2] R. Mahajan and W. J. Koros, Factors controlling successful formation of mixed-matrix gas separation materials, *Ind. Eng. Chem. Res.*, 39 (2000) 2692.
- [3] R. Mahajan and W. J. Koros, Mixed matrix membrane materials with glassy polymers. Part 1, *Polym. Eng. Sci.*, 42 (2002) 1420.
- [4] R. Mahajan and W. J. Koros, Mixed matrix membrane materials with glassy polymers. Part 2, *Polym. Eng. Sci.*, 42 (2002) 1432.
- [5] T. C. Merkel, B. D. Freeman, R. J. Spontak, Z. He, I. Pinnau, P. Meakin and A. J. Hill, Ultrapermeable, reverse-selective nanocomposite membranes, *Science*, 296 (2002) 519.
- [6] T. C. Merkel, B. D. Freeman, R. J. Spontak, I. P. Z. He, P. Meakin and A. J. Hill, Sorption, transport, and structural evidence for enhanced free volume in poly(4-methyl-2-pentyne)/fumed silica nanocomposite membranes, *Chem. Mater.*, 15 (2003) 109.
- [7] D. Vu, W. J. Koros and S. J. Miller, Effect of condensable impurity in CO₂/CH₄ gas feeds on performance of mixed matrix membranes using carbon molecular sieves, *J. Membr. Sci.*, 221 (2003) 233.
- [8] S. Kim, T. W. Pechar and E. Marand, Poly(imide siloxane) and carbon nanotube mixed matrix membranes for gas separation, *Desalination*, 192 (2006) 330.
- [9] S. Kim, L. Chen, J. K. Johnson and E. Marand, Polysulfone and functionalized carbon nanotube mixed matrix membranes for gas separation: theory and experiment, *J. Membr. Sci.*, in print (2007)
- [10] B. D. Reid, F. A. Ruiz-Trevino, I. H. Musselman, J. Kenneth J. Balkus and J. P. Ferraris, Gas permeability properties of polysulfone membranes containing the mesoporous molecular sieve MCM-41, *Chem. Mater.*, 13 (2001) 2366.
- [11] S. Kim, E. Marand, J. Ida and V. V. Gulians, Polysulfone and mesoporous molecular sieve MCM-48 mixed matrix membranes for gas separation, *Chem. Mater.*, 18 (2006) 1149.
- [12] T. W. Pechar, S. Kim, B. Vaughan, E. Marand, V. Baranauskas, J. Riffle, H. K. Jeong and M. Tsapatsis, Preparation and characterization of a poly(imide siloxane) and zeolite L mixed matrix membrane, *J. Membr. Sci.*, 277 (2006) 210.
- [13] T. W. Pechar, S. Kim, B. Vaughan, E. Marand, M. Tsapatsis, H. K. Jeong and C. J. Cornelius, Fabrication and characterization of polyimide-Zeolite L Mixed Matrix Membranes for Gas Separations, *Journal of Membrane Science*, 277 (2006) 195.
- [14] S. Shimizu, H. Matsuyama and M. Teramoto, Gas separation properties of polyimide membrane containing mesoporous material, *International Congress on Membranes and Membrane Processes*, August 21-26 (2005) SW.
- [15] Q. Cai, Z. S. Luo, W. Q. Pang, Y. W. Fan, X. H. Chen and F. Z. Cui, Dilute solution routes to various controllable morphologies of MCM-41 silica with a basic medium, *Chem. Mater.*, 13 (2001) 258.
- [16] J. H. Park, S. Kim, Y. C. Kim and O. O. Park, Polymer/nanoporous silica nanocomposite blue-light-emitting diodes, *Nanotechnology*, 16 (2005) 1793.
- [17] S. Kim, J. Ida, V. V. Gulians and J. Y. S. Lin, Tailoring pore properties of MCM-48 silica for selective adsorption of CO₂, *J. Phys. Chem.B*, 109 (2005) 6287.

- [18] S. Brunauer, P. H. Emmett and E. Teller, Adsorption of gases in multimolecular layers, *J. Am. Chem. Soc.*, 60 (1938) 309.
- [19] E. P. Barrett, L. G. Joyner and P. P. Halenda, The determination of pore volume and area distributions in porous substances. I. computations from nitrogen isotherms, *J. Amer. Chem. Soc.*, 73 (1951) 373.
- [20] J. Crank, *The Mathematics of Diffusion*, Oxford Press; London (1990).
- [21] Y. Sun, Z. Zhang and C. P. Wong, Study on mono-dispersed nano-size silica by surface modification for underfill applications, *J. Coll. Interf. Sci.* 292 (2005) 436.
- [22] N. Nishiyama, D. H. Park, A. Koide, Y. Egashira and K. Ueyama, A mesoporous silica (MCM-48) membrane: preparation and characterization, *J. Membr. Sci.*, 182 (2001) 235.
- [23] T. C. Merkel, Z. He, I. Pinnau, B. D. Freeman, P. Meakin and A. J. Hill, Sorption and transport in poly(2,2-bis(trifluoromethyl)-4,5-difluoro-1,3-dioxole-co-tetrafluoroethylene) containing nanoscale fumed silica, *Macromolecules*, 36 (2003) 8406.
- [24] S. Lagorsse, F. D. Magalhães and A. Mendes, Carbon molecular sieve membranes: Sorption, kinetic and structural characterization *J. Membr. Sci.*, 241 (2004) 275.

Chapter 8. Conclusions and Future Work

The primary objective of this research was to develop new methods for fabrication of mixed matrix membranes consisting of either carbon nanotubes or mesoporous silica in a polymer matrix membrane without the presence of unselective voids at their interfaces. As a first goal we fabricated a polymer/CNT mixed matrix membrane. Closed-ended CNTs were mixed with a poly(imide siloxane) copolymer. The He permeability dropped and there was no change in N₂ permeability. This was taken as an indication of good contact between the CNTs and copolymer. Nano-composite membranes were fabricated by incorporating open-ended CNTs in a copolymer matrix and it was demonstrated that the rise in permeability with the addition of CNTs is primarily due to the increase in the diffusion. Given the results of CNT/poly(imide siloxane) copolymer system, nano-composite membranes were fabricated by incorporating CNTs functionalized with ODA in a commercial polymeric membrane material, PSF. The modified nanotubes dispersed well in the polymer matrix as well as in chloroform. The FESEM for the cross sectional area images of the MMM films indicated that SWNTs were well dispersed in the polymer matrix at a loading of 5 and 10 wt% SWNTs. At 15 wt% the tubes formed two domains in the copolymer matrix: a well dispersed SWNTs region and a dense SWNTs region. Overall increases in permeance and diffusivity for all tested gases suggested that carbon nanotubes can provide high diffusivity tunnels in the SWNTs within the PSF matrix. In addition, the observed decreases in He/CH₄ selectivity agree well with H₂/CH₄ selectivities in SWNTs predicted by atomistic simulations.¹

However, at higher loading of CNTs, the increase in permeability was offset by increased tortuosity around the agglomerated CNTs domains in both case of

SWNT/poly(imide siloxane) and functionalized SWNT/polysulfone MMMs. Even though purified CNTs were cut by a chemical oxidation method, they still have high aspect ratio, ~800. Due to their high aspect ratio and the strong van der Waals attraction between nanotubes, long-length CNTs tend to aggregate into a dense, and robust network of nanotube ropes. 4:1 (vol/vol 96% H₂SO₄:30% H₂O₂) piranha reactions have been previously shown to create short nanotubes (~100 nm) from long SWNTs. These aggressive solutions are good at creating short length CNTs, however, they typically result in significant losses of nanotubes due to fast etch rates.² For example, there was 90 % weight loss when 100 nm length nanotubes were made from a nanotube sample with 1000 nm length. Clearly this is not an efficient way to achieve short length CNTs. Recently, a fluorination method has been developed, leading to the cutting of SWNTs into short length.³ The overall CNTs yield for the fluorination cutting method is typically 70 -80%, and the final average length of the nanotube is less than 100 nm.³ Therefore, to fully exploit the potential of SWNTs in nano-composites and to overcome the critical issues of limited solubility, dispersity and processibility of nanotubes, one must prepare a new composite system containing short functionalized CNTs. In addition, more enhancements in dispersity of nanotubes in polymer can be synergistically achieved by combining the in-situ polymerization of CNTs/polymer nanocomposites.

A second goal of this research was to develop a fabrication method for oriented CNT nanocomposite membranes to maximize the performance of the CNTs/polymer MMMs. We developed a simple, fast, and practical route to vertically align carbon nanotubes on a porous support using a combination of self-assembly and filtration methods. The advantage of this approach is that it can be easily scaled up to large surface areas,

allowing for fabrication of membranes with practical gas separation applications. The gas transport properties of the constructed carbon nanotube/polymer nanocomposite membranes were analogous to those of carbon nanotube membranes grown by chemical vapor deposition. As a result of functionalization, the high gas permeation rates through the carbon nanotubes were coupled with a “gatekeeper” mechanism which leads to an enhancement of selectivity observed when separating gas mixtures.

However, in order to apply these CNT nanocomposites to practical gas separation processes, further increases in selectivity are expected. As chemically grown CNT membranes, the gas transport properties through the CNT membranes prepared by the filtration method followed the inverse-square-root scaling to molecular mass so that no significant selectivity was observed. The application of the Knudsen diffusion model to gas separation is highly uneconomical and is only utilized to effect separations in which economics is not a primary factor.⁴ Although the nanocomposite membrane showed higher selectivity for CO₂ over other gas molecules, the selectivity of CNT membranes is far below the DOE requirement of $P_{CO_2} > 3 \times 10^{-7}$ mol/m²·s·Pa, and $\alpha_{CO_2 / N_2} > 100$.

Carbon molecular sieve (CMS) membranes have shown a wide range of high α_{CO_2 / CH_4} (35-85)⁵ and α_{O_2 / N_2} (3-30)⁶ values depending on the polymer precursor, the pyrolysis condition, and other factor. The high gas separation performance of CMS membranes is due to a combination of entropic effects arising from the difference in size of gas molecules and enthalpic effects that primarily depends on the adsorbate-adsorbent interactions. Recent theoretical simulation studies pointed out that the smoothness of the interaction between the adsorbate molecules and the carbon nanotube walls results in the high gas transport properties, but plays little role in the gas separation selectivity.⁷ They

suggested that a small pore size constriction in CNTs (0.365 nm) can lead to a high sieving resistance for N₂ but not for O₂, resulting high O₂/N₂ separation selectivities.⁷ This is in agreement with the current consensus that a pore size of about 0.4 nm or less is required in carbon membranes for the separation of similar size of gas molecules, such as N₂ and O₂. Consequently, there is need for new CNT membranes having tube diameters less than 5 Å that is average pore size of CMS membrane.^{6,8}

Recently, CNTs, whose inner core diameter can be as low as 4 Å, have been fabricated by several research groups.⁹⁻¹¹ Tang *et al.* reported that simple improvements in the electric-arc technique can create a CNTs with a diameter of 5 Å.¹² Ijima *et al.* produced metal-free high-quality MWNTs, in which the innermost nanotubes have a diameter of 4 Å. Endo *et al.* reported 4.3 Å free-standing SWNTs grown on small catalyst particles deposited on a porous material.¹³ Also, 4 Å SWNTs have been successfully produced inside the 1-nm-sized channels of AlPO₄-5 (AFI) zeolite single crystals.^{10,14} These SWNTs are perfectly aligned, uniform in size, and isolated from each other. These aligned small size CNTs can be easily applied to the fabrication of membranes. Therefore, the true potential of the CNTs membranes will be realized when nanocomposite membranes are fabricated using aligned CNT having tube diameters less than 5 Å.

In this investigation, another mixed matrix membrane system was developed using a mesoporous MCM-48 silica and a polysulfone as the polymer matrix. The high surface coverage of silanol groups on the MCM-48 provided good interaction with PSF matrix. Helium permeation data and SEM images of as-synthesized MCM-48/PSF MMMs suggest that MCM-48 silica particles adhered well to PSF and the prepared MMMs were defect free. Mesoporous MCM-48 materials offer the favorable effect of large increases

in gas permeability in MMMs without sacrificing selectivity. The continuous pathways present in the polymer matrix with high loading of MCM-48 silica allowed the gas molecules to diffuse solely through the molecular sieve phase resulting in high gas permeation. However, the highest loading of MCM-48 (~ 60 vol %) in the composites resulted in membranes that tended to be brittle and crack even under lower pressure on the upstream side of permeation test. Smaller inorganic particles would yield more polymer/particle interfacial area and provide more opportunity to synthesize higher loading of molecular sieves in the polymer matrix. In addition, nanoscale molecular sieves are more suitable than micro-sized zeolite or molecular sieves for commercialization of MMMs with very thin selective layers.

In order to overcome the disadvantages of MMMs containing micro-sized mesoporous silica, we have developed and characterized organic-inorganic nanocomposite membranes based on nanosized mesoporous silica dispersed inside a polymer matrix. The external surface of mesoporous silica was modified with hydrophobic trimethylsilyl groups to avoid agglomeration of nanosized silica particles at higher loadings. Composite membranes containing mesoporous silica up to 80 vol% have been successfully fabricated and these MMM showed large increase in gas permeability. These dramatic increases in gas permeability resulted from an increase in solubility as well as diffusivity. The measured uptake of MCM-41/PSF MMM showed an increase in the gas sorption capacities with the addition of mesoporous silica. In addition, diffusivities calculated from steady-state permeation data and kinetic uptake curves, showed diffusion coefficients increased with increasing nanosized mesoporous silica content in PSF. The observed increases in both the diffusivity and solubility make mesoporous MCM-41

silica an attractive additive for enhancing the gas permeability of MMMs without sacrificing selectivity.

However, the true potential of these nanocomposite membranes will be realized when the mesoporous silica channels are functionalized to enhance facilitated transport of penetrant gases. Currently, efforts are underway to enhance the nanosized mesoporous silica and penetrant (e.g CO₂) interaction via chemical functionalization of the channel surface with amine groups. Then the combination of selectivity and high permeability will propel the performance of these higher loading of mesoporous silica/polymer nanocomposite membranes above Robeson's upper bound.¹⁵

References

- [1] H. Chen and D. S. Sholl, Predictions of selectivity and flux for CH₄/H₂ separations using single walled carbon nanotubes as membranes, *J. Membr. Sci.*, 269 (2006) 152.
- [2] K. J. Ziegler, Z. Gu, H. Peng, E. L. Flor, R. H. Hauge and R. E. Smalley, Controlled oxidative cutting of single-walled carbon nanotubes, *J. Am. Chem. Soc.*, 127 (2005) 1541.
- [3] K. J. Ziegler, Z. Gu, J. Shaver, Z. Chen, E. L. Flor, D. J. Schmidt, C. Chan, R. H. Hauge and R. E. Smalley, Cutting single-walled carbon nanotubes, *Nanotechnology*, 16 (2005) S539.
- [4] R. E. Kesting and A. K. Fritzsche, *Polymeric Gas Separation Membranes*, John Wiley and Sons, Inc. (1993)
- [5] D. Q. Vu, W. J. Koros and S. J. Miller, High Pressure CO₂/CH₄ Separation Using Carbon Molecular Sieve Hollow Fiber Membranes, *Ind. Eng. Chem. Res.*, 41 (2002) 367.
- [6] M. B. Shiflett and H. C. Foley, Ultrasonic deposition of high-selectivity nanoporous carbon membranes, *Science*, 285 (1999) 1902.
- [7] G. Arora and S. I. Sandler, Molecular sieving using single wall carbon nanotubes, *Nano Lett.*, (2007)
- [8] K. M. Steel and W. J. Koros, Investigation of porosity of carbon materials and related effects on gas separation properties, *Carbon*, 41 (2003) 253.
- [9] L.-C. Qin, X. Zhao, K. Hirahara, Y. Miyamoto, Y. Ando and S. Iijima, The smallest carbon nanotube, *Nature*, 408 (2000) 50.
- [10] N. Wang, Z. K. Tang, G. D. Li and J. S. Chen, Materials science: Single-walled 4 Å carbon nanotube arrays, *Nature*, 408 (2000) 50.
- [11] A. Koshio, M. Yudasaka and S. Iijima, Metal-free production of high-quality multi-wall carbon nanotubes, in which the innermost nanotubes have a diameter of 0.4 nm, *Chem. Phys. Lett.*, 356 (2002) 595.
- [12] L. F. Sun, S. S. Xie, W. Liu, W. Y. Zhou, Z. Q. Liu, D. S. Tang, G. Wang and L. X. Qian, Materials: Creating the narrowest carbon nanotubes, *Nature*, 403 (2000) 384.
- [13] T. Hayashi, Y. A. Kim, T. Matoba, M. Esaka, K. Nishimura, T. Tsukada, M. Endo and M. S. Dresselhaus, Smallest Freestanding Single-Walled Carbon Nanotube, *Nano Lett.*, 3 (2003) 887.
- [14] Z. K. Tang, H. D. Sun, J. Wang, J. Chen and G. Li, Mono-sized single-wall carbon nanotubes formed in channels of AlPO₄-5 single crystal, *Appl. Phys. Lett.*, 73 (1998) 2287.
- [15] L. M. Robeson, Correlation of separation factor versus permeability for polymeric membranes, *J. Membr. Sci.*, 62 (1991) 165.